Poster Katalogo Digitala · Catálogo Digital de Posters

Catalogue Numérique de Posters · Posters' Digital Catalogue

EHU **Euskampus** Bordeaux Eguna 2024

Haut Carré, Talence

Université de Bordeaux

Urr **14-15** Oct

euskampus FUNDAZIOA

Universidad del País Vasco · Euskal Herriko Unibertsitatea

dipc

tecnalia

université de BORDEAUX

EUSKO JAURLARITZA GOBIERNO VASCO

EUROREGION EUROESKUALDEA EUROREGIÓN

Nouvelle-Aquitaine

Ville de BORDEAUX

Index

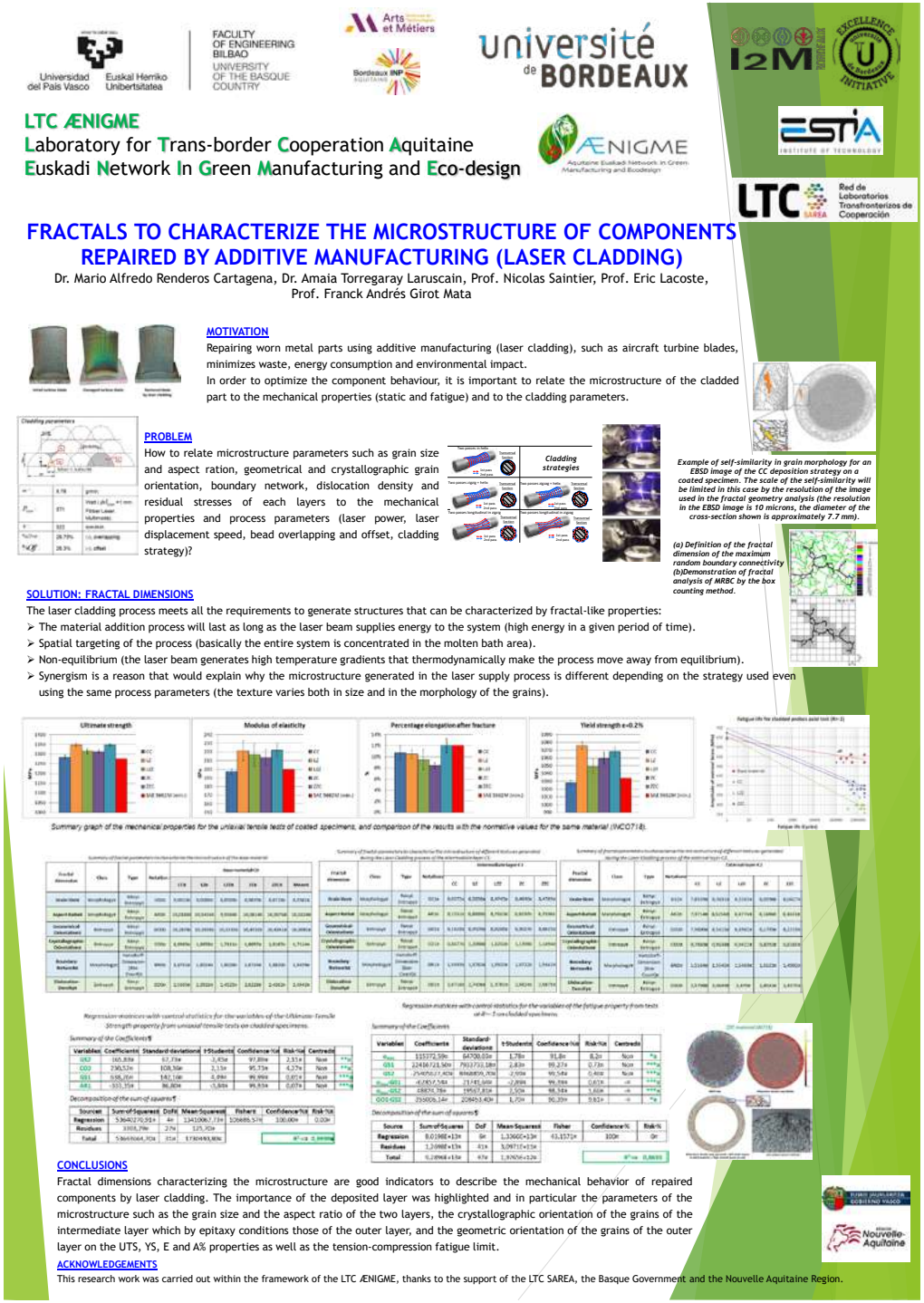

Aenigme LTC

Fractals to Characterize the Microstructure of Components Repaired by Additive Manufacturing (laser cladding)

Mario Alfredo Renderos Cartagena
Amaia Torregaray Laruscain
Nicolas Saintier
Eric Lacoste
Franck Andrés Girot Mata

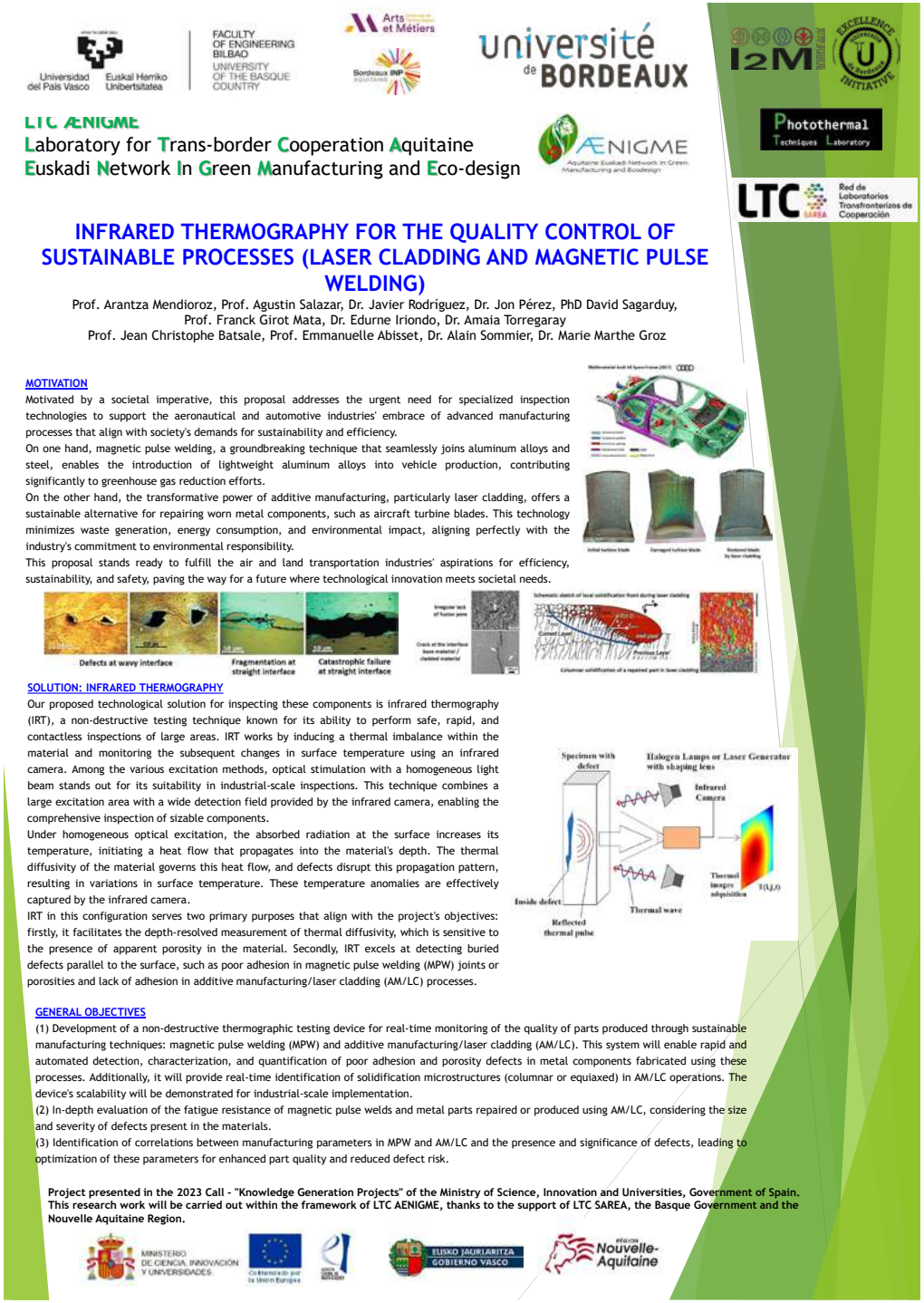

Aenigme LTC

Infrared Thermography for the Quality Control of Sustainable Processes (laser cladding and magnetic pulse welding)

Arantza Mendioroz
Agustin Salazar
Javier Rodríguez
Jon Pérez
David Sagarduy
Franck Girot Mata
Edurne Iriondo
Amaia Torregaray,
Jean Christophe Batsale
Emmanuelle Abisset
Alain Sommier
Marie Marthe Groz

Laser powder bed fusion of Ni-based alloy components: Reused powder effects on surface/structural integrity and reproducibility of thin-walled structures

2024 EHU Euskampus Bordeaux Eguna
Bordeaux, France, October 14-15, 2024

Post-doc fellow: Dr. Dmytro Lesyk*
Supervisor: Prof. Aitzol Lamikiz

Aeronautics Advanced Manufacturing Center (CFAA) of the University of the Basque Country (UPV/EHU), Zamudio, Spain
**dmytro.lesyk@ehu.eus, lesyk_d@ukr.net*

Introduction

Laser powder bed fusion (LPBF) is an emerging technology for the additive manufacturing of metal/composite products with complex shapes using powder materials. At the same time, the LPBF technology is a good tool to produce the Inconel superalloys with high precision, expanding manufacturing capabilities. Heat-resistance superalloys with favorable mechanical and physical properties are crucial materials for various relevant applications.

Despite the enormous potential of LPBF, this technology still has many challenges to use it for the manufacture of appropriate aircraft parts that work in extreme environments. The optimization of the LPBF parameters, powder reuse/recycling evaluation, and post-processing are required to achieve high-quality manufactured superalloy products for a critical manufacturing sector.

This work focused on the effects of reused powder on the porosity and surface texture of the LPBF-built IN 718 alloy parts. The reproducibility of thin-walled structures is also under consideration.

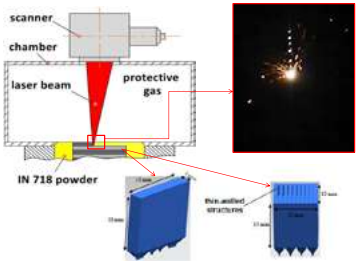

Fig. 1. Schematic illustration of the LPBF process

EXPERIMENTAL RESULTS

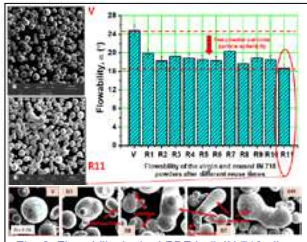

Fig. 2. Flowability in the LPBF-built IN 718 alloy after different reuse times

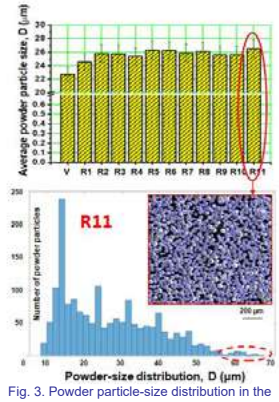

Fig. 3. Powder particle-size distribution in the LPBF-built IN 718 alloy after different reuse times

Fig. 4. Schematic representation of the powder reuse cycle: 1) LPBF process; 2) remove build plate; 3) sieve unmelted powder; 4) replace sieved powder into silo [1]

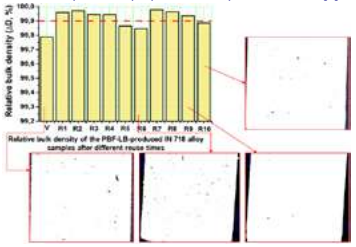

Fig. 5. Material density of the LPBF-produced IN 718 alloy parts after different reuse times

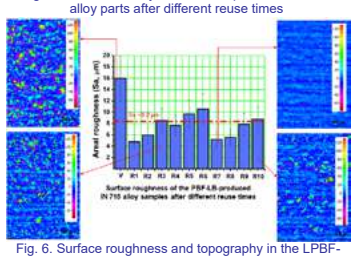

Fig. 6. Surface roughness and topography in the LPBF-produced IN 718 alloy parts after different reuse times

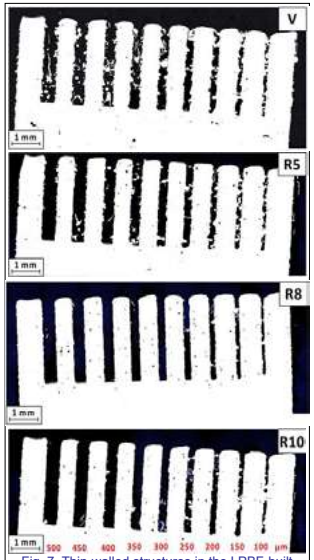

Fig. 7. Thin-walled structures in the LPBF-built IN 718 alloy parts using virgin powder (V) and reused powders (R) after the R5, R8, and R10 reuse times

REFERENCES

[1] https://issuu.com/inovar-communications/docs/magazine_metal_am_autumn_2017_app_-/11?fr=sYml1MzEyMDA5MDQ

ACKNOWLEDGMENT

The authors acknowledge the European Union's HORIZON 2020 research and innovation programme under the Marie Sklodowska-Curie Grant (agreement No. 101034379) and TED2021-130543B-I00 Grant funded by the MCIN/AEI/10.13039/501100011033 and the European Union Next Generation EU/PRTR.

Summary:

The powder reuse 10th iterations showed negligible effect on the material density (~99.9%) and surface roughness (Sa ~8.2 μm) of the LPBF-built IN 718 alloy parts.

Characterization of the reused powder showed a reduction in the number of smaller powder particles and an increasing number of irregular particles (powder particle size of irregular particles L = 100–120 μm, R6–R10).

LPBF-built thin-walled structures are characterized by better quality and repeatability using the reused powder.

Aenigme LTC

Laser powder bed fusion of Ni-based alloy components: Reused powder effects on surface/structural integrity and reproducibility of thin-walled structures

Dmytro Lesyk[1,3]
Silvia Martinez[1]
Aitzol Lamikiz[1,2]

[1] Aeronautics Advanced Manufacturing Center, University of the Basque Country, 202 Bizkaia Science and Technology Park, Zamudio 48170, Spain.

[2] Mechanical Engineering Department, University of the Basque Country,1 Plaza Ingeniero Torres Quevedo, Bilbao 48013, Spain.

[3] Laser Systems and Advanced Technologies Department, National Technical University of Ukraine; Igor Sikorsky Kyiv Polytechnic Institute, 37 Beresteiskyi Avenue, Kyiv 03056, Ukraine.

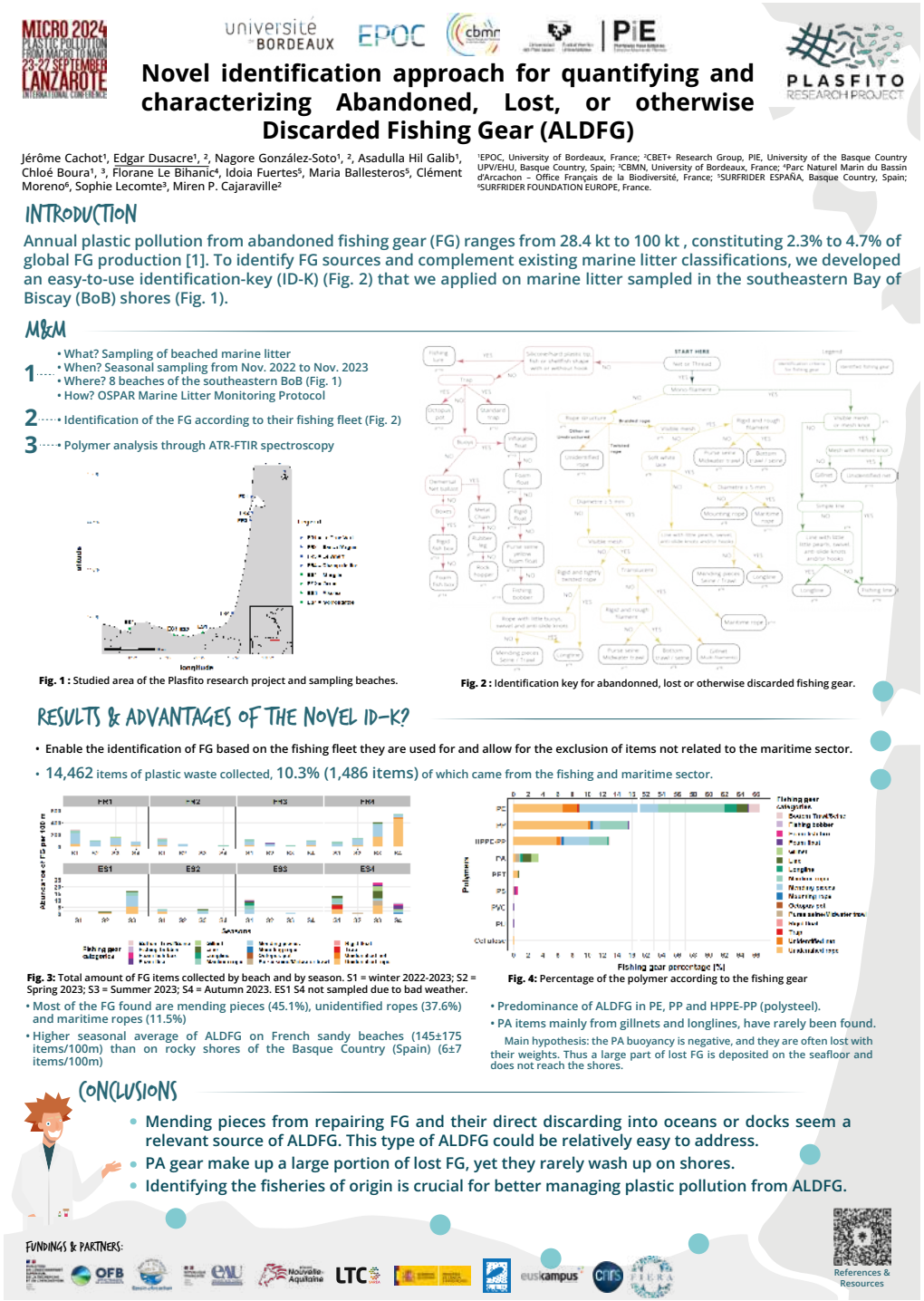

AquEUS LTC

Novel Identification Approach for quantifying and characterizing Abandoned, Lost, or Otherwise Discarded Fishing Gear

Jérôme Cachot[1]
Edgar Dusacre[1,2]
Nagore González-Soto[1,2]
Asadulla Hil Galib[1]
Chloé Boura[1,3]
Florane Le Bihanic[4]
Idoia Fuertes[5]
Maria Ballesteros[5]
Clément Moreno[6]
Sophie Lecomte[3]
Miren P. Cajaraville[2]

[1] EPOC, University of Bordeaux, CNRS, INP Bordeaux, UMR 5805, 33600 Pessac, France.

[2] CBET+ Research Group, Dept. Zoology and Animal Cell Biology; Faculty of Science and Technology and Research Centre for Experimental Marine Biology and Biotechnology PIE, University of the Basque Country UPV/EHU, Basque Country, Spain.

[3] CBMN, University of Bordeaux, CNRS, Bordeaux INP, UMR 5248, 33600, Pessac, France.

[4] Parc Naturel Marin du Bassin d'Arcachon (PNM-BA) – Office Français de la Biodiversité (OFB), 4 Rue Copernic, 33470 Le Teich, France.

[5] SURFRIDER ESPAÑA, Edificio Tabakalera, Plaza Cigarreras 1, 20012 Donostia/San Sebastián, Basque Country, Spain.

[6] SURFRIDER FOUNDATION EUROPE, 33 allée du Moura, 64200, Biarritz.

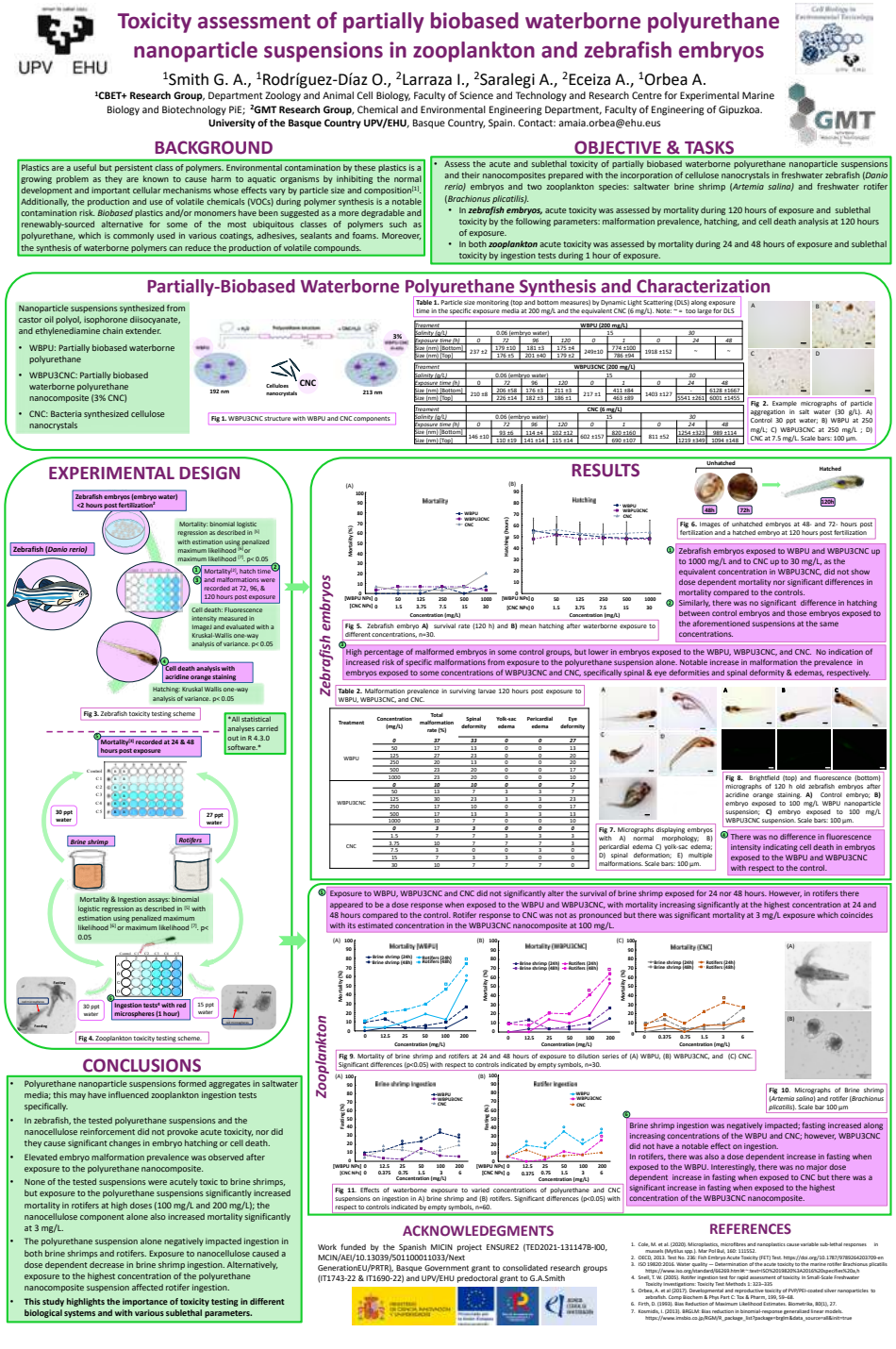
Toxicity assessment of partially biobased waterborne polyurethane nanoparticle suspensions in zooplankton and zebrafish embryos
[1]Smith G. A., [1]Rodríguez-Díaz O., [2]Larraza I., [2]Saralegi A., [2]Eceiza A., [1]Orbea A.
[1]CBET+ Research Group, Department Zoology and Animal Cell Biology, Faculty of Science and Technology and Research Centre for Experimental Marine Biology and Biotechnology PiE; [2]GMT Research Group, Chemical and Environmental Engineering Department, Faculty of Engineering of Gipuzkoa.
University of the Basque Country UPV/EHU, Basque Country, Spain. Contact: amaia.orbea@ehu.eus
BACKGROUND
Plastics are a useful but persistent class of polymers. Environmental contamination by these plastics is a growing problem as they are known to cause harm to aquatic organisms by inhibiting the normal development and important cellular mechanisms whose effects vary by particle size and composition[11]. Additionally, the production and use of volatile chemicals (VOCs) during polymer synthesis is a notable contamination risk. Biobased plastics and/or monomers have been suggested as a more degradable and renewably-sourced alternative for some of the most ubiquitous classes of polymers such as polyurethane, which is commonly used in various coatings, adhesives, sealants and foams. Moreover, the synthesis of waterborne polymers can reduce the production of volatile compounds.
OBJECTIVE & TASKS
Assess the acute and sublethal toxicity of partially biobased waterborne polyurethane nanoparticle suspensions and their nanocomposites prepared with the incorporation of cellulose nanocrystals in freshwater zebrafish (Danio rerio) embryos and two zooplankton species: saltwater brine shrimp (Artemia salina) and freshwater rotifer (Brachionus plicatilis).
In zebrafish embryos, acute toxicity was assessed by mortality during 120 hours of exposure and sublethal toxicity by the following parameters: malformation prevalence, hatching, and cell death analysis at 120 hours of exposure.
In both zooplankton acute toxicity was assessed by mortality during 24 and 48 hours of exposure and sublethal toxicity by ingestion tests during 1 hour of exposure.
Partially-Biobased Waterborne Polyurethane Synthesis and Characterization
Nanoparticle suspensions synthesized from castor oil polyol, isophorone diisocyanate, and ethylenediamine chain extender.
WBPU: Partially biobased waterborne polyurethane
WBPU3CNC: Partially biobased waterborne polyurethane nanocomposite (3% CNC)
CNC: Bacteria synthesized cellulose nanocrystals
3%
192 nm
Cellulose nanocrystals
CNC
213 nm
Fig 1. WBPU3CNC structure with WBPU and CNC components
Table 1. Particle size monitoring (top and bottom measures) by Dynamic Light Scattering (DLS) along exposure time in the specific exposure media at 200 mg/L and the equivalent CNC (6 mg/L). Note: ~ = too large for DLS
Fig 2. Example micrographs of particle aggregation in salt water (30 g/L). A) Control 30 ppt water; B) WBPU at 250 mg/L; C) WBPU3CNC at 250 mg/L ; D) CNC at 7.5 mg/L. Scale bars: 100 µm.
EXPERIMENTAL DESIGN
Zebrafish embryos (embryo water) <2 hours post fertilization2
Zebrafish (Danio rerio)
Mortality: binomial logistic regression as described in [9] with estimation using penalized maximum likelihood [10] or maximum likelihood [7]. p< 0.05
Mortality[2], hatch time and malformations were recorded at 72, 96, & 120 hours post exposure
Cell death: Fluorescence intensity measured in ImageJ and evaluated with a Kruskal-Wallis one-way analysis of variance. p< 0.05
Cell death analysis with acridine orange staining
Hatching: Kruskal Wallis one-way analysis of variance. p< 0.05
Fig 3. Zebrafish toxicity testing scheme
All statistical analyses carried out in R 4.3.0 software.
Mortality[2] recorded at 24 & 48 hours post exposure
30 ppt water
27 ppt water
Brine shrimp
Rotifers
Mortality & Ingestion assays: binomial logistic regression as described in [9] with estimation using penalized maximum likelihood [10] or maximum likelihood [7]. p< 0.05
30 ppt water
Ingestion tests[3] with red microspheres (1 hour)
15 ppt water
Fig 4. Zooplankton toxicity testing scheme.
RESULTS
Zebrafish embryos
Mortality
Hatching
Fig 5. Zebrafish embryos A) survival rate (120 h) and B) mean hatching after waterborne exposure to different concentrations, n=30.
Unhatched
Hatched
48h
72h
120h
Fig 6. Images of unhatched embryos at 48- and 72- hours post fertilization and a hatched embryo at 120 hours post fertilization
Zebrafish embryos exposed to WBPU and WBPU3CNC up to 1000 mg/L and to CNC up to 30 mg/L, as the equivalent concentration in WBPU3CNC, did not show dose dependent mortality nor significant differences in mortality compared to the controls.
Similarly, there was no significant difference in hatching between control embryos and those embryos exposed to the aforementioned suspensions at the same concentrations.
High percentage of malformed embryos in some control groups, but lower in embryos exposed to the WBPU, WBPU3CNC, and CNC. No indication of increased risk of specific malformations from exposure to the polyurethane suspension alone. Notable increase in malformation the prevalence in embryos exposed to some concentrations of WBPU3CNC and CNC, specifically spinal & eye deformities and spinal deformity & edemas, respectively.
Table 2. Malformation prevalence in surviving larvae 120 hours post exposure to WBPU, WBPU3CNC, and CNC.
Fig 7. Micrographs displaying embryos with A) normal morphology; B) pericardial edema C) yolk-sac edema; D) spinal deformation; E) multiple malformations. Scale bars: 100 µm.
Fig 8. Brightfield (top) and fluorescence (bottom) micrographs of 120 h old zebrafish embryos after acridine orange staining. A) Control embryos; B) embryo exposed to 100 mg/L WBPU nanoparticle suspension; C) embryo exposed to 100 mg/L WBPU3CNC suspension. Scale bars: 100 µm.
There was no difference in fluorescence intensity indicating cell death in embryos exposed to the WBPU and WBPU3CNC with respect to the control.
Zooplankton
Exposure to WBPU, WBPU3CNC and CNC did not significantly alter the survival of brine shrimp exposed for 24 nor 48 hours. However, in rotifers there appeared to be a dose response when exposed to the WBPU and WBPU3CNC, with mortality increasing significantly at the highest concentration at 24 and 48 hours compared to the control. Rotifer response to CNC was not as pronounced but there was significant mortality at 3 mg/L exposure which coincides with its estimated concentration in the WBPU3CNC nanocomposite at 100 mg/L.
Mortality [WBPU]
Mortality [WBPU3CNC]
Mortality [CNC]
Brine shrimp (24h)
Brine shrimp (48h)
Rotifers (24h)
Rotifers (48h)
Fig 9. Mortality of brine shrimp and rotifers at 24 and 48 hours of exposure to dilution series of (A) WBPU, (B) WBPU3CNC, and (C) CNC. Significant differences (p<0.05) with respect to controls indicated by empty symbols, n=30.
Fig 10. Micrographs of Brine shrimp (Artemia salina) and rotifer (Brachionus plicatilis). Scale bar 100 µm
Brine shrimp Ingestion
Rotifer Ingestion
Fig 11. Effects of waterborne exposure to varied concentrations of polyurethane and CNC suspensions on ingestion in A) brine shrimp and (B) rotifers. Significant differences (p<0.05) with respect to controls indicated by empty symbols, n=60.
Brine shrimp ingestion was negatively impacted; fasting increased along increasing concentrations of the WBPU and CNC; however, WBPU3CNC did not have a notable effect on ingestion.
In rotifers, there was also a dose dependent increase in fasting when exposed to the WBPU. Interestingly, there was no major dose dependent increase in fasting when exposed to CNC but there was a significant increase in fasting when exposed to the highest concentration of the WBPU3CNC nanocomposite.
CONCLUSIONS
Polyurethane nanoparticle suspensions formed aggregates in saltwater media; this may have influenced zooplankton ingestion tests specifically.
In zebrafish, the tested polyurethane suspensions and the nanocellulose reinforcement did not provoke acute toxicity, nor did they cause significant changes in embryo hatching or cell death.
Elevated embryo malformation prevalence was observed after exposure to the polyurethane nanocomposite.
None of the tested suspensions were acutely toxic to brine shrimps, but exposure to the polyurethane suspensions significantly increased mortality in rotifers at high doses (100 mg/L and 200 mg/L); the nanocellulose component alone also increased mortality significantly at 3 mg/L.
The polyurethane suspension alone negatively impacted ingestion in both brine shrimps and rotifers. Exposure to nanocellulose caused a dose dependent decrease in brine shrimp ingestion. Alternatively, exposure to the highest concentration of the polyurethane nanocomposite suspension affected rotifer ingestion.
This study highlights the importance of toxicity testing in different biological systems and with various sublethal parameters.
ACKNOWLEDGMENTS
Work funded by the Spanish MICIN project ENSURE2 (TED2021-131147B-I00, MCIN/AEI/10.13039/501100011033/Next GenerationEU/PRTR), Basque Government grant to consolidated research groups (IT1743-22 & IT1690-22) and UPV/EHU predoctoral grant to G.A.Smith
REFERENCES
1. Cole, M. et al. (2020). Microplastics, microfibres and nanoplastics cause variable sub-lethal responses in mussels (Mytilus spp.). Mar Pol Bul, 160. 111552.
2. OECD, 2013. Test No. 236: Fish Embryo Acute Toxicity (FET) Test. https://doi.org/10.1787/9789264203709-en
3. ISO 10820:2016. Water quality — Determination of the acute toxicity to the marine rotifer Brachionus plicatilis https://www.iso.org/standard/64269.html#:~:text=ISO%2010820%3A2016%20specifies%20a,h
4. Snell, T. W. (2005). Rotifer ingestion test for rapid assessment of toxicity. In Small-Scale Freshwater Toxicity Investigations: Toxicity Test Methods 1: 323–335
5. Orbea, A. et al (2017). Developmental and reproductive toxicity of PVP/PEI-coated silver nanoparticles to zebrafish. Comp Biochem & Phys Part C: Tox & Pharm, 195, 59–68.
6. Firth, D. (1993). Bias Reduction of Maximum Likelihood Estimates. Biometrika, 80(1), 27.
7. Kosmidis, I. (2013). BRGLM: Bias reduction in binomial-response generalized linear models. https://www.imsbio.co.jp/RGM/R_package_list?package=brglm&data_source=all&init=true
AquEUS LTC
Toxicity assessment of partially biobased waterborne polyurethane nanoparticle suspensions in zooplankton and zebrafish embryos

Gaybrielle A Smith[1]
Olga Rodríguez-Díaz[1]
Izaskun Larraza[2]
Ainara Saralegi[2]
Arantxa Eceiza[2]
Amaia Orbea[1]
[1] UCBET+ Research Group, Department Zoology and Animal Cell Biology, Faculty of Science and Technology and Research Centre for Experimental Marine Biology and Biotechnology PiE.
[2] GMT Research Group, Chemical and Environmental Engineering Department, Faculty of Engineering of Gipuzkoa. University of the Basque Country UPV/EHU, Basque Country, Spain.

Toxicity to a fish liver cell line of leachates and extracts from micronized plastic items collected at different beaches of the Bay of Biscay

Nagore González-Soto[1,2*], Christelle Clérandeau[2], Bénédicte Morin[2], Jérôme Cachot[2] and Miren P. Cajaraville[1]

[1]CBET+ Research Group, Department Zoology and Animal Cell Biology, Faculty of Science and Technology and Research Centre for Experimental Marine Biology and Biotechnology PiE, University of the Basque Country UPV/EHU, Basque Country, Spain.

[2]EPOC UMR 5805, University of Bordeaux, CNRS, Bordeaux INP, 33600 Pessac, France.

*nagore.gonzalez@ehu.eus

Introduction

Despite increasing micro and nanoplastic (MNPs) research, limited information on toxicity of realistic environmental MNPs (eMNPs) exists. This study aims to compare the toxicity to the rainbow trout liver cell line (RTL-W1) of leachates and DMSO and methanol extracts of micronized plastic items collected at different beaches of the Bay of Biscay.

Materials and Methods

Plastics were collected on 3 beaches of the Spanish Basque Country (Gorrondatxe,Orrua and Murgita), in winter and spring 2023, and 1 beach in the French Basque Country (Tarnos) in spring 2021

Establishment of plastic polymer proportions

Micronization of the plastic items

Obtention of micronized mix (polymer proportions in mass):

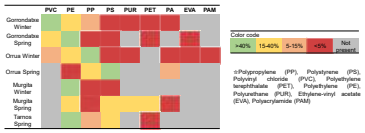

Polypropylene (PP), Polystyrene (PS), Polyvinyl chloride (PVC), Polyethylene terephthalate (PET), Polyethylene (PE), Polyurethane (PUR), Ethylene-vinyl acetate (EVA), Polyacrylamide (PAM)

Protocols selected to produce extracts and leachates

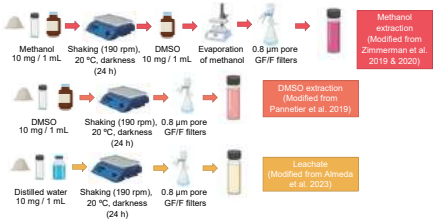

Cell exposure

Liver fibroblasts from the rainbow trout cell line RTL-W1 were selected for toxicity testing

1. Cell viability assay (Alamar Blue)
- Leachates: 0.1-100% dilutions
- DMSO and Methanol extracts: 0.01-1% dilutions

(Exposure: 24 hours at 20 °C)

2. Data analysis
- Differences among groups: Kruskal–Wallis test & Dunn's post-hoc test
- LC50, LC25, LC10, LOEC and NOEC: Probit analysis

3. Sublethal endpoints
The first dilution <LC25
3.1. ROS production
(4 hours at 20 °C)
3.2. EROD activity
(24 hours at 20 °C)
For comparison purposed 1% of leachates was also tested

4. Data analysis
Differences with controls: Mann–Whitney's U test

*A minimum of 3 replicates of each treatment were used in all tests and tests were performed three times each.

Results

LC50, LC25, LC10, LOEC and NOEC after Alamar Blue cytotoxicity assay

Leachate	LC50	LC25	LC10	LOEC	NOEC
Gorrondatxe Winter	98,21 %	37,31 %	12,91 %	20%	10%
Gorrondatxe Spring	>100 %	24,85 %	4,78 %	20%	10%
Orrua Winter	>100 %	35,41 %	8,83 %	20%	10%
Orrua Spring	>100 %	36,04 %	10,84 %	20%	10%
Murgita Winter	>100 %	> 100 %	8,20 %	20%	10%
Murgita Spring	>100 %	98,72 %	20,27 %	40%	20%
Tarnos Spring	73,64 %	23,15 %	8,17 %	20%	10%

DMSO extract	LC50	LC25	LC10	LOEC	NOEC
Gorrondatxe Winter	X	X	X	0,1%	0,05%
Gorrondatxe Spring	X	X	X	0,01%	X
Orrua Winter	X	X	X	0,05%	0,01%
Orrua Spring	30,49%	4,29%	0,73%	0,5%	0,1%
Murgita Winter	X	X	X	X	1%
Murgita Spring	>100%	>100%	3%	0,05%	0,01%
Tarnos Spring	X	X	X	0,05%	0,01%

Methanol extract	LC50	LC25	LC10	LOEC	NOEC
Gorrondatxe Winter	X	X	X	0,1%	0,05%
Gorrondatxe Spring	X	X	X	0,01%	X
Orrua Winter	X	X	X	0,01%	X
Orrua Spring	>100%	>100%	6,57%	0,01%	X
Murgita Winter	X	X	X	0,05%	0,01%
Murgita Spring	>100%	>100%	0,16%	0,01%	X
Tarnos Spring	X	X	X	0,01%	X

ROS production:

	Leachate (20%)	Leachate (1%)	DMSO extract (1%)	Methanol extract (1%)
Gorrondatxe Winter	↑	↑	↑	↑
Gorrondatxe Spring	↑	↑	↑	-
Orrua Winter	↑	↓	↑	-
Orrua Spring	↑	↓	↑	-
Murgita Winter	↑	↑	-	-
Murgita Spring	↑	↑	-	-
Tarnos Spring	↑	↑	-	-

↑: significant increase in ROS production in comparison to controls
↓: significant decrease in ROS production in comparison to controls
-: no significant difference observed in comparison to controls
Tested concentration: Leachates: 20% & 1%, DMSO extract: 1%, Methanol extract: 1%

EROD activity:

	Leachate (20%)	Leachate (1%)	DMSO extract (1%)	Methanol extract (1%)
Gorrondatxe Winter	-	-	-	-
Gorrondatxe Spring	↑	↑	↑	↑
Orrua Winter	-	-	↑	↑
Orrua Spring	-	↑	-	-
Murgita Winter	↑	-	-	-
Murgita Spring	↑	↑	↑	↑
Tarnos Spring	↑	↑	-	↑

↑: significant increase in EROD activity in comparison to controls
-: no significant difference observed in comparison to controls
Tested concentration: Leachates: 20% & 1%, DMSO extract: 1%, Methanol extract: 1%

Conclusions

- **All leachates caused cytotoxicity at dilutions higher than 40% and almost all extracts at dilutions ≤1% on RTL-W1 cell line**
- **ROS production increased in cells exposed to all leachates at 20%, while different responses were observed for 1% dilution of leachates, DMSO and methanol extracts**
- **Similarly, EROD activity was induced in cells exposed to leachates and extracts of several tested samples**
- **Overall for leachates, Tarnos Spring was the most toxic mix. It showed the lowest LC50 and it increased ROS production and EROD activity even at 1% dilution. However, no clear trend was observed for DMSO and methanol extracts.**
- **These results highlight the complexity of analyzing toxicity of eMNPs due to differences in polymer types and proportions, additives, sorbed pollutants and aging degree**

References
Almeda et al. 2023. A protocol for bioisolation of microplastics for aquatic toxicity testing. Chemosphere 333, 138894
Pannetier et al. 2019. Toxicity assessment of pollutants sorbed on environmental sample microplastics collected on beaches: Part I-adverse effects on fish cell line. Environmental Pollution 248, 1098e1097
Zimmerman et al 2019 Benchmarking the in Vitro Toxicity and Chemical Composition of Plastic Consumer Products Environ. Sci. Technol., 53, 19, 11467–11477
Zimmerman et al. 2020 What are the drivers of microplastic toxicity? Comparing the toxicity of plastic chemicals and particles to *Daphnia magna* Environmental Pollution 267, 115392

Acknowledgements
Work funded by the Spanish MICIN project FIERA (PID2021-128600OB-I00, MCIN/AEI/10.13039/501100011033 and "ERDF A way of making Europe"), the Basque Government through a grant to the consolidated research group IT1743-22 and a postdoctoral fellowship to NGS and the Laboratory for Transborder Cooperation LTC AquEus (Euskampus and Basque Government).

AquEUS LTC

Toxicity to fish liver cell line of leachates and extracts from micro and nanoplastics produced from plastic items collected at different beaches of the Bay of Biscay

Nagore González-Soto[1,2]
Christelle Clérandeau[2]
Bénédicte Morin[2]
Jérôme Cachot[2]
Miren P. Cajaraville[1]

[1] 1CBET+ Research Group, Department Zoology and Animal Cell Biology, Faculty of Science and Technology and Research Centre for Experimental Marine Biology and Biotechnology PiE, University of the Basque Country UPV/EHU, Basque Country, Spain.

[2] EPOC UMR 5805, University of Bordeaux, CNRS, Bordeaux INP, 33600 Pessac, France.

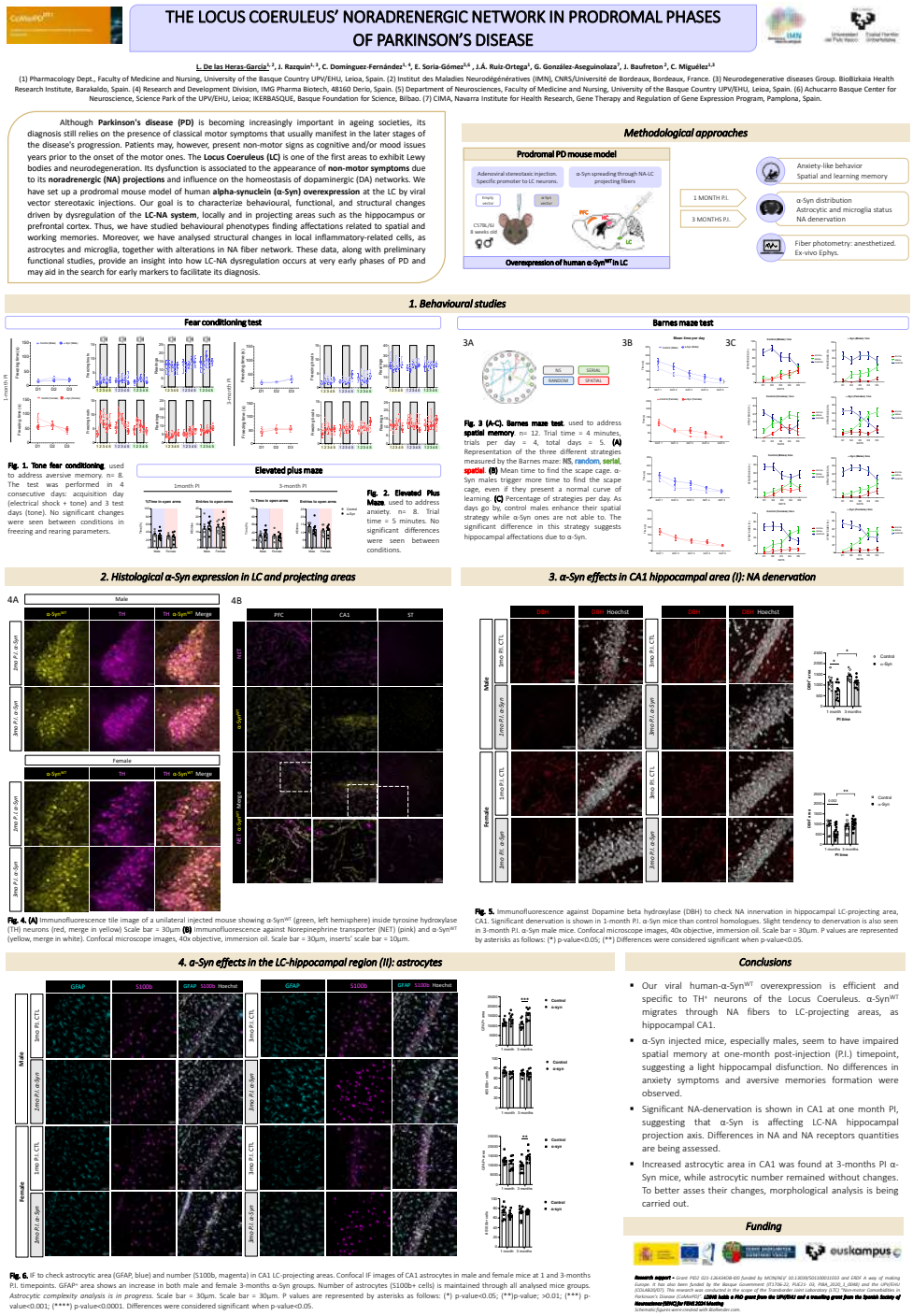

ComorPD LTC

The Locus Coeruleus-Hippocampus axis in prodromal phases of Parkinson's disease

L. De las Heras-García[1,2]
J. Razquin[1, 3]
C. Domínguez-Fernández[1,4]
E. Soria-Gómez[5, 6]
J.A. Ruiz-Ortega[1]
G. Gonzalez-Aseguinolaza[7]
J. Baufreton[2]
C. Miguélez-Palomo[1,3]

[1] Department of Pharmacology, Faculty of Medicine and Nursing, University of the Basque Country UPV/EHU, Leioa, Spain.

[2] Institut des Maladies Neurodégénératives (IMN), CNRS/Université de Bordeaux, Bordeaux, France.

[3] Neurodegenerative diseases Group. Biocruces Bizkaia Health Research Institute, Barakaldo, Spain.

[4] Research and Development Division, IMG Pharma Biotech, 48160 Derio, Spain.

[5] Department of Neurosciences, Faculty of Medicine and Nursing, University of the Basque Country UPV/EHU, Leioa, Spain.

[6] Achucarro Basque Center for Neuroscience, Science Park of the UPV/EHU, Leioa; IKERBASQUE, Basque Foundation for Science, Bilbao.

[7] CIMA, Navarra Institute for Health Research, Gene Therapy and Regulation of Gene Expression Program, Pamplona, Spain.

Green Concrete LTC

Developement of Ultra High Performance Geopolymer Smart Concrete

Youssef SLEIMAN[1]
Nadia SAIYOURI[1]
Mehdi Sbartaï[1]

[1] Université de Bordeaux, UMR 5295, Institut de Mécanique et d'Ingénierie (I2M), CNRS, Esplanade des Arts et Métiers, 33405 Talence, France.

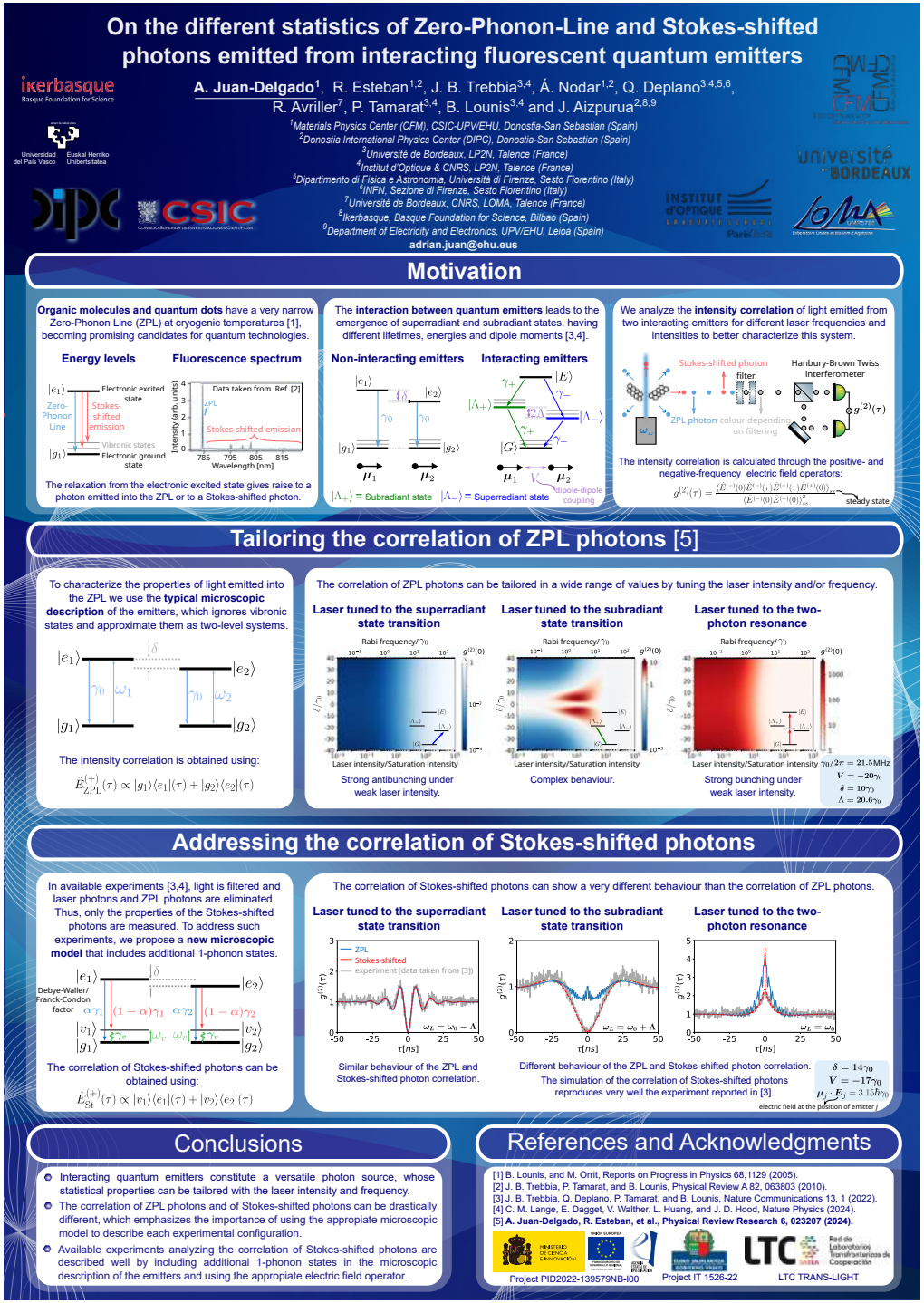

Translight LTC

On the different statistics of Zero-Phonon-Line and Stokes-shifted photons emitted from interacting fluorescent quantum emitters

A. Juan-Delgado[1]
R. Esteban[1,2]
J. B. Trebbia[3,4]
Á. Nodar[1,2]
Q. Deplano[3,4,5,6]
R. Avriller[7]
P. Tamarat[3,4]
B. Lounis[3,4,]
J. Aizpurua[2,8,9]

[1] Centro de Física de Materiales (CFM-MPC), CSIC-UPV/EHU, Donostia-San Sebastián, Spain.

[2] Donostia International Physics Center DIPC, Donostia-San Sebastián, Spain.

[3] Université de Bordeaux, LP2N, Talence, France.

[4] Institut d'Optique & CNRS, LP2N, Talence, France.

[5] Dipartimento di Fisica e Astronomia, Università di Firenze, Sesto Fiorentino, Italy.

[6] INFN, Sezione di Firenze, Sesto Fiorentino, Italy.

[7] Université de Bordeaux, CNRS, LOMA, Talence, France.

[8] IKERBASQUE, Basque Foundation for Science, Bilbao, Spain.

[9] Department of Electricity and Electronics, University of the Basque Country, Leioa, Spain.

HYDROGEN INTERACTION WITH W(110) SURFACE

RAÚL BOMBÍN[1], JEAN-CHRISTOPHE TREMBLAY[1], DANIEL PÉLAEZ[1], CÉDRIC CRESPOS[1], OIHANA GALPARSORO[4] AND PASCAL LARREGARAY[1]
[1]Institut des Science Moléculaires - Université de Bordeaux
[2]Université de Lorraine [3]Université Paris-Sarclay
[4]Universidad el Pais Vasco - Euskalherriko Universitatea

ABSTRACT

An understanding of the dynamics of hydrogen atom scattering on metal surfaces is of great importance for a number of applications, including catalysis and material science. Of particular interest is the case of tungsten surfaces, as it will be the material employed for facing components in future fusion reactors. In this study, we investigate the scattering of hydrogen atoms on the W(110) surface, employing both classical and quantum dynamics approaches to elucidate the importance of quantum effects in this system. The focus of this study is on several key observables, including the sticking probability and diffraction channels, which are used to characterise the scattering process. Furthermore, the vibrational excitation spectra of H atom adsorbed on the tungsten surface is studied at both the semiclassical and quantum levels.

POTENTIAL ENERGY SURFACE

We make classical and quantum dynamics for **hydrogen on W(110)** using an accurate Potential energy surface (PES) calculated with PW91 functional.

$$V = V(x, y, z) \quad (1)$$

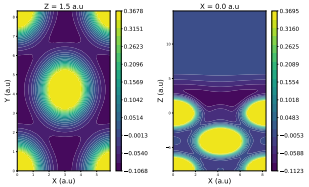

Fig. 1: Left (right) XY (XZ) cuts of the potential energy surface in the (2×1 cell). The hydrogen atom adsorption on hollow and bridge positions is energetically favorable.

MCTDH PARAMETERS

- Spatial grid with spacing $\Delta \approx 0.15$ a.u.
- The number of natural potentials chosen so that the fitting error < 1 meV
- We use ftt SFPs basis with X and Y ones being periodic. The number of SFPs is chosen to converge stickingn probabilities.

	X	Y	Z
Spatial-grid	41	55	155
Natpots	20	27	155
SPFs	24	32	64

Table: 1. Spatial grid, number of natutal potentials (Natpots) used in the fit of the PES and number of SPFs per degree of freedom.

Initial Wave packet: We chose a product of plane waves for X and Y and a localized Gaussian in Z as the initial state. The initial position and momentum are x_0 and p_0 in normal incidence.

$$\psi_0 \sim e^{-ik_x x} e^{-ik_y y} e^{-((z-z_0)/2\sigma)^2} e^{-ip_i(z-z_0)} \quad (2)$$

STICKING PROBABILITY AFTER SCATTERING

- In the classical case, many trajectories are trapped in the surfce at low energy, **traping at the surface** has a shorter lifetime and is almost negligible after 1 ps when quantum dynamics are done.
- The latter differences are more pronounced at low energy resulting in a large quantum **reflection probability.**
- **Bulk absorption** is enhanced in the quantum dynamical case due to tunneling effect, probably.

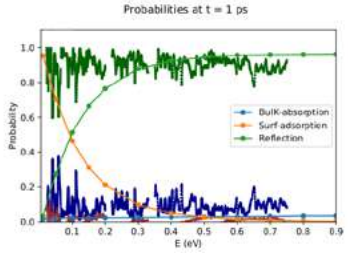

Fig. 2: Reflection (green), adsorption (red) and absorption (blue) probatilities of Hidrogen on W(110) under normal incidence conditions. Dark (light) lines correspond to quantum (classical calculations.)

VIBRATIONAL SPECTRA

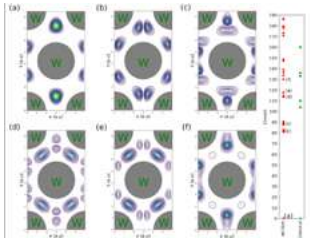

Fig. 3. Left: From (a) to (f) squared wave-funcionts for different vibrational states of Hydrogen adsorbed on W(110) surface. Right: vibrational spectra computed with MCTDH and a 1D quasiclassical approach.

DIFFRACTION

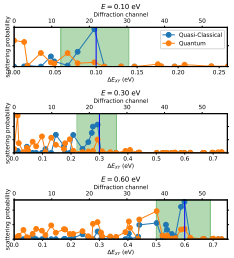

Fig. 4. Classical (blue) and quantum (orange) diffraction probabilities for H scattering from W(110) with normal incidence as a function of energy transfer to transversal directions.

ONGOING WORK

It is known that electronic friction plays a crucial role for atoms scattering on metals.
We plan to use the the stochastic version of MCTD to include this energy dissipation channels

CONTACT INFORMATION

raul.bombin@u-bordeaux.fr Group THEO - https://www.ism.u-bordeaux.fr/

ACKNOWLEDGMENTS - FINALCIAL SUPPORT

QuantumChemPhys LTC

Hydhyrogen Interaction with W(110) Surface

Raúl Bombín[1]
Jean-Christophe Tremblay[1]
Daniel Pélaez[1]
Cédric Crespos[1]
Oihana Galparsoro[4]
Pascal Larregaray[1]

[1] Institut des Science Moléculaires - Université de Bordeaux.
[2] Université de Lorraine.
[3] Université Paris-Sarclay.
[4] Euskal Herriko Unibersitatea - Universidad del Pais Vasco (UPV/EHU).

BioMolecular Interactions Platform

Cross-border Cooperation Laboratory Network San Sebastian - Bordeaux

BIOMINT

Carmelo Di Primo, Fernando Cossío, Iván Rivilla, Leire San José, Iliane Rafaniello, Thomas Schäfer

Molecular Biophysics, (Bio)Organic Chemistry, Sensor Technology, Materials Science, (Bio)Chemical Engineering

Our Motivation

Biomolecular Interactions are at the core of designing and employing advanced and functional materials in biotechnology, bionanotechnology, health, and biosensors as well as separation and purification processes in, for example, fine chemicals and pharmaceutical manufacturing. Yet, **their measurement and characterization often pose a challenge.**

What is BIOMINT about?

- **Trans-border technological platform** that offers its expertise on biomolecular interactions to both the scientific community and industry in the area of **bio/materials/health**.
- Vibrant collaboration network in both applied and fundamental research, promoting best laboratory practices when it comes to determining biomolecular interactions.

How BIOMINT works

Example: Insights into binding mechanisms for the design of sensors for the detection of SARS-CoV-2

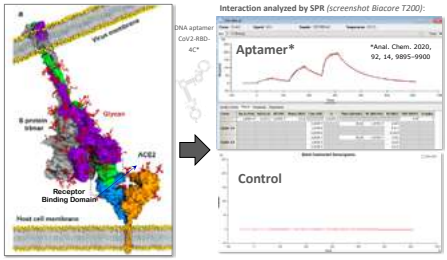

Image: Taka et al. 2021, J Phys Chem.

Aptamers can rival antibodies for recognizing the RBD of the spike protein. Within an international consortium, we have observed that some supposed RBD-aptamers actually do not interact specifically and that some literature data lack rigour or are based on measuring artefacts. This demonstrates how crucial it is to investigate molecular interactions with effective and straightforward methods prior to potential health applications.

Available Technologies

Quartz-Crystal Microbalance with Dissipation Monitoring (**QCM-D**, Biolin)

Multi-Parameter Surface Plasmon Resonance (**MP-SPR**, Bionavis)

Surface Plasmon Resonance (**SPR**, Biacore T200)

Bio-Layer Interferometry (**BLI**, Sartorius Octet)

The use of complementary techniques warrants robustness of the interaction data obtained and avoids interpreting artefacts. During our varied research activity we have learnt that thermodynamic constants of biomolecular interactions not only vary with the characterization technique but also depend on the particular application and environment.

BIOMINT Activities

- Hands-on workshop (Univ. Bordeaux annual summer school) on the use of surface-sensitive techniques for elucidating biomolecular interaction on surfaces
- Training of young researchers within collaborative projects
- Seminar series between Bordeaux and San Sebastián
- Joint projects in the bio/materials and health interface

What is in for me?

- BIOMINT is an **open platform** that welcomes partners from **both academia** and **industry**.
- Access to expertise on characterizing biomolecular/materials interactions with a set of complementary techniques that are not widely accessible.
- Unique opportunity for **young researchers** to be trained in state-of-the-art characterization techniques.

Additional support from…

Institutions:

Private companies:

***Contacts:** Carmelo Di Primo (Bordeaux) – carmelo.diprimo@inserm.fr ; Thomas Schäfer (San Sebastián-Donostia) - thomas.schafer@ehu.eus

BioMINT LTC incubator

BioMolecular Interactions Platform

Carmelo Di Primo[1]
Fernando Cossío[2]
Iván Rivilla[3]
Leire San José[5]
Iliane Rafaniello[4,5]
Thomas Schäfer[5]

[1] INSEM.
[2] UPV/EHU.
[3] DIPC.
[4] SURPHASE.
[5] POLYMAT UPV/EHU.

Imaging astrocyte-neuron lactate supply in multiple sclerosis

AM Baraibar[1,2,3], A Bernal-Chico[1,2,3], Y Nasu[4], I Fernández-Moncada[5,6], G Marsicano[5,6], S Mato[1,2,3]

[1]Department of Neurosciences, University of the Basque Country UPV/EHU and [2]Achucarro Basque Center for Neuroscience, E-48940 Leioa, Spain; [3]Neuroinmunology Unit, ISS Biocruces, Bizkaia, E-48903 Barakaldo, Spain; [4]Department of Chemistry, School of Science, The University of Tokyo, 113-0033 Tokyo, Japan; [5]INSERM U1215, Neurocentre Magendie and [6]Université de Bordeaux, E-33000 Bordeaux France

Introduction

Astrocytes are primarily glycolytic cells that produce and release lactate to support neuronal aerobic metabolism during neurotransmission. This so called astrocyte-neuron lactate shuttle is tightly regulated by neuronal signals that trigger aerobic glycolysis in astrocytes and regarded as an essential mechanism underlying astrocytic modulation of brain performance.

Multiple sclerosis (MS) is a chronic demyelinating disease initiated by pathogenic immune responses against myelin followed by a broader inflammatory and neurodegenerative process. Astrocytes undergo a pronounced transformation in MS whereby they acquire a variety of disease-promoting functions. In particular, accumulating evidence suggests that deficits in astrocyte glycolytic activity encompass the pathogenic activation of these cells during neuroinflammation and contribute to neurodegenerative processes. However, the specific features of astrocytic lactate supply to neurons in multiple sclerosis (MS) remain unknown.

Here we used newly generated, genetically coded lactate biosensors to investigate **astrocyte lactate efflux** induced by physiological stimuli associated with neuronal activity. *Ex vivo* two-photon imaging of extracellular lactate using eLACCO2.9 targeted to astrocytes of the mouse somatosensory cortex showed positive responses to extracellular K^+, $NH4^+$ and to thus confirming previous observations in culture systems. Cortical astrocytes also displayed eLACCO2.9 fluorescence increases in response to the cannabinoid agonist WIN55,212-2 that were prevented by the selective CB_1 antagonist AM251. Our preliminary results in cortical slices suggest decreased lactate efflux induced by extracellular WIN55,212-2 in cells activated with pro-inflammatory stimuli (IL-1α, TNFα and C1q). *Ex vivo* astrocyte lactate imaging in the experimental autoimmune encephalomyelitis (EAE) model of MS showed a decreased lactate efflux induced by K^+ and CB_1R activation. These observations support the utility of eLACCO2.9c as novel imaging tool to explore the features of astrocyte-neuron lactate supply *ex vivo* and suggest aberrant astrocyte-neuron communication in terms of lactate supply during neuroinflammation.

1 Lactate biosensors for fluorescence ex vivo imaging of cortical astrocytes

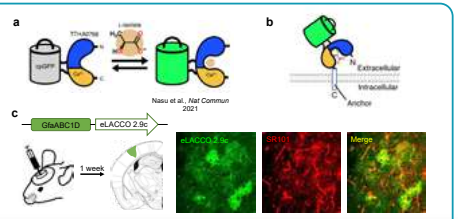

Figure 1. Mechanism of operation of eLACCO2.9c and expression of the biosensor in astrocytes of the mouse somatosensory cortex. (**a**) Diagram depicting the mechanism of action of TTHA0766-based eLACCO in response to L-lactate and (**b**) sensor expression within the cellular membrane. (**c**) Viral vector injected in the somatosensory cortex (S1) and fluorescence images showing co-localization between eLacco2.9c and the astrocytic marker sulforhodamine (SR101).

2 Astrocytic lactate efflux in response to extracellular stimuli

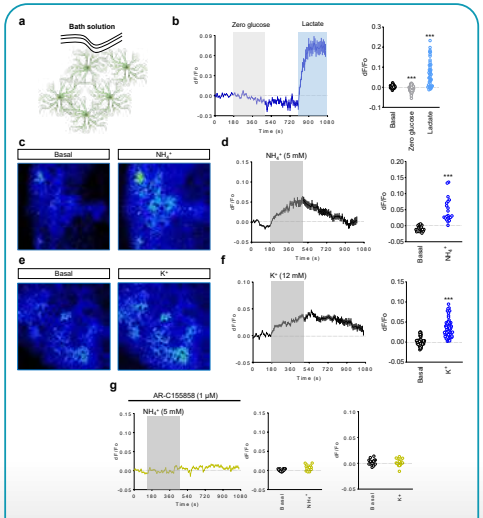

Figure 2. Extracellular K^+ and $NH4^+$ induce astrocytic lactate efflux *ex vivo*. (**a**) Experimental approach. Bath application of extracellular stimuli in cortical slices from mice injected with eLACCO2.9c. (**b**) Two-photon imaging of eLACCO2.9c in response to zero-glucose and lactate (10 mM) (grey bars). Pseudocolor images from cortical astrocytes before and after (**c**) $NH4^+$ and (**e**) K^+ application. (**e**) Time course of eLACCO2.9c fluorescence responses to (**d**) $NH4^+$ or (**f**) K^+ application in basal conditions. (**g**) eLACCO2.9c fluorescence responses to $NH4^+$ or K^+ application in the presence of the monocarboxylate transporter (MCT) inhibitor AR-C155858. Data are expressed as mean ± SEM. *** p < 0.001.

3 CB_1R activation increases lactate efflux

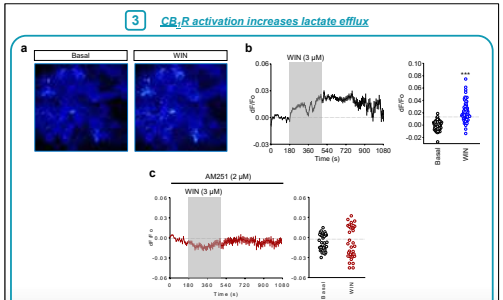

Figure 3. CB_1R activation increases astrocyte lactate efflux. (**a**) Pseudocolor images from cortical astrocytes before and after application of the cannabinoid agonist WIN55,212-2 (WIN). (**b-c**) Two-photon imaging of extracellular L-lactate surrounding astrocytes in response to WIN (grey bar). Time course and quantitative analysis of eLACCO2.9c fluorescence responses to WIN in (**b**) control conditions and (**c**) in presence of the CB_1R antagonist (AM251). Data are expressed as mean ± SEM. **$p < 0.01$ and ***$p < 0.001$.

4 G_q protein-mediated signaling promotes astrocyte lactate efflux

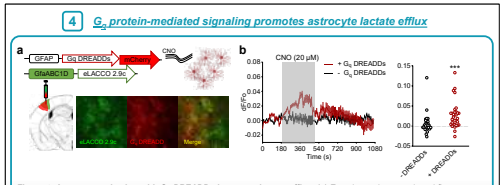

Figure 4. Astrocyte activation with G_q-DREADDs increases lactate efflux. (**a**) Experimental approach and fluorescence images showing co-localization between eLACCO2.9c and mCherry. (**b**) Two-photon imaging of extracellular L-lactate around astrocytes in response to CNO (grey bar) in mice injected with and without G_q-DREADDs. Data are expressed as mean ± SEM. ***$p < 0.001$.

5 Aberrant astrocyte-neuron lactate supply during neuroinflammation

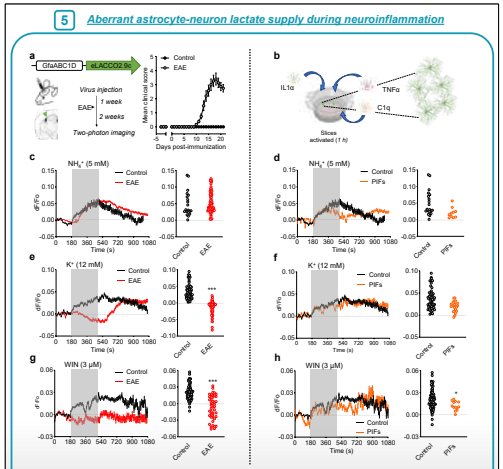

Figure 5. Deregulation of astrocyte lactate efflux during EAE. (**a**, **b**) Experimental approaches for the *ex vivo* analysis of astrocyte lactate efflux during neuroinflammation. (**c-h**) Two-photon imaging of extracellular L-lactate responses to $NH4^+$, K^+ and WIN in control and EAE slices (**c**, **e** and **g**) or following incubation with pro-inflammatory factors (**d**, **f** and **h**). Data are expressed as mean ± SEM. *$p < 0.05$, ***$p < 0.001$. Pro-inflammatory factors (PIFs) TNFα (30 ng/ml), IL1α (3 ng/ml) and C1q (3 ng/ml).

Summary

1. Viral targeting of cortical astrocytes with eLACCO2.9c allows real-time measurement of extracellular lactate fluctuations *ex vivo*.
2. Cortical astrocytes display positive eLACCO2.9c fluorescence responses to extracellular K^+, $NH4^+$ and CB_1R activation that are sensitive to the pharmacological blockade of lactate transport.
3. Activation of G_q protein-mediated signaling promotes astrocyte lactate efflux in the mouse cortex.
4. Inflammatory activation of cortical astrocytes *ex vivo* and *in vivo* deregulates lactate supply.

Acknowledgements

This study was supported by Instituto de Salud Carlos III (ISCIII) through the project (PI21/00629) and co-funded by the European Union, the Basque Government (PIBA_2023_1_0046) and ARSEP Foundation (ARSEP-1310).

CannaMetHD LTC incubator

Imaging astrocyte-neuron lactate supply in multiple sclerosis

AM Baraibar[1,2,3]
A Bernal-Chico[1,2,3]
Y Nasu[4]
Fernández-Moncada[5,6]
G Marsicano[5,6]
S Mato[1,2,3]

[1] Department of Neurosciences, University of the Basque Country UPV/EHU.

[2] Achucarro Basque Center for Neuroscience, E-48940 Leioa, Spain.

[3] Neuroinmunology Unit, ISS Biocruces, Bizkaia, E-48903 Barakaldo, Spain.

[4] Department of Chemistry, School of Science, The University of Tokyo, 113-0033 Tokyo, Japan.

[5] INSERM U1215, Neurocentre Magendie.

[6] Université de Bordeaux, E-33000 Bordeaux France.

CannaMetHD LTC incubator

In vivo imaging of CB1-dependent modulation of brain metabolism

Dalla-Tor T.[1,2,3]
Gómez-Sotres P.[1,2]
Bellocchio L.[1,2]
Rodrigues R.[1,2]
Delcasso S.[1,2]
Gisquet D.[1,2]
Cannich A.[1,2]
Drago F.[3]
Fernández-Moncada I.[1,2]
*Marsicano G.[*1,2]*

[1] Inserm U1215 Neurocentre Magendie, Endocannabinoids and neuroadaptation, Bordeaux, France.

[2] Université de Bordeaux, Bordeaux, France.

[3] Università di Catania, Catania, Italy.

CannaMetHD LTC

In vivo imaging of CB1-dependent modulation of brain metabolism

Dalla-Tor T.[1,2,3], Gómez-Sotres P.[1,2], Bellocchio L.[1,2], Rodrigues R.[1,2] Delcasso S.[1,2], Gisquet D.[1,2] Cannich A.[1,2], Drago F.[3], Fernández-Moncada I.[1,2], Marsicano G.*[1,2]

[1]Inserm U1215 Neurocentre Magendie, Endocannabinoids and neuroadaptation, Bordeaux, France,

[2]Université de Bordeaux, Bordeaux, France

[3]Università di Catania, Catania, Italy

INTRODUCTION

Despite representing only the 2% of the body weight, the brain consumes up to 20% of the body energy. Most of the brain energy comes from the full oxidation of glucose. However, a sizeable amount of glucose is partially oxidized and transformed into Lactate via a process called aerobic glycolysis. Most current data point indicate that astrocytes are the main producers of Lactate, which is in turn used by neurons to fulfil their energy requirements. Interestingly, Lactate does not only play a metabolic role, but it is also a fundamental brain signaling molecule. The mechanisms regulating Lactate production and release in the brain are, however, scantly known. Cannabinoid receptors type 1 (CB1R) has recently emerged as an important factor playing a complex role in these processes. Whereas persistent (24h) activation of astroglial CB1R leads to a reduction of Lactate1, our recent data show that their transient stimulation (5 min) triggers an increase of Lactate levels2. These data, however, were obtained mainly in cultured astrocytes, and the impact of CB1R activity on Lactate levels in vivo has never been directly measured. By combining a novel Lactate fluorescent biosensor (eLacco2.1)3 and fiber photometry (FP), I carried out for the first time high resolution recordings of brain Lactate dynamics in freely moving animals. Interestingly, I observed that the levels of Lactate correlate with locomotor activity and that Lactate administration blocks hypolocomotor effects of cannabinoids. Current experiments aim at addressing the potential mechanistic link between locomotor effects of cannabinoids and Lactate levels regulation.

1) CHARACTERIZATION OF eLACCO2.1

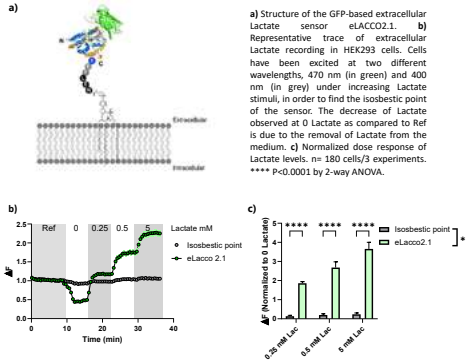

a) Structure of the GFP-based extracellular Lactate sensor eLACCO2.1. **b)** Representative trace of extracellular Lactate recording in HEK293 cells. Cells have been excited at two different wavelengths, 470 nm (in green) and 400 nm (in grey) under increasing Lactate stimuli, in order to find the isosbestic point of the sensor. The decrease of Lactate observed at 0 Lactate as compared to Ref is due to the removal of Lactate from the medium. **c)** Normalized dose response of Lactate levels. n= 180 cells/3 experiments. **** P<0.0001 by 2-way ANOVA.

2) IN VIVO LACTATE RECORDINGS

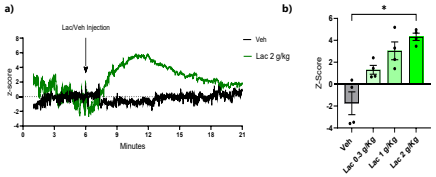

a) Representative trace of FP extracellular lactate changes detected by the eLacco2.1 sensor in a freely moving mouse treated with vehicle (Veh) or 2g/kg Lactate by IP injection. **b)** Dose response quantification of Lactate changes induced by increasing doses of exogenously administered Lactate. Baseline Z-Score (0) is the averaged signal for the last 3 minutes before injections. n=4 mice. * P<0.05 by 1-way ANOVA.

3) IMPACT OF LACTATE LEVELS ON LOCOMOTION

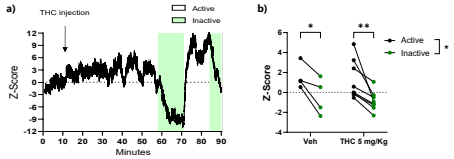

The hypolocomotive effect of THC is correlated with a reduction of Lactate levels in the brain.
a) Representative trace of FP extracellular Lactate changes detected by the eLacco2.1 sensor in a freely moving mouse. Arrow indicates the IP injection of 5 mg/Kg THC. Green areas indicate inactive behavioral phase. Recordings lasted 90 minutes, with injection after 11 minutes. **b)** Quantification of Lactate. changes during the shift from active to inactive phases under vehicle or 5 mg/Kg THC. n= 8 mice. 2-Way Anova. **, P<0.01 (General effect of activity).

4) ROLE OF LACTATE IN LOCOMOTOR EFFECTS OF CANNABINOIDS

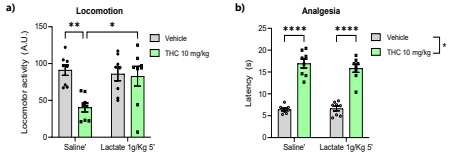

The hypolocomotor, but not antinociceptive, effect of THC is blocked by Lactate injection.
a) Locomotor activity (activity cages) and **(b)** Thermal antinociception (hot-plate) of mice treated with vehicle or THC 10 mg/Kg, followed by saline or Lactate 1 g/kg 5 min after. 2-way ANOVA: **(a)** Interaction (p=0.0175); * P<0.05, ** P<0.01; **(b)** Main effect of THC, **** P<0.0001

CONCLUSIONS AND FUTURE DIRECTIONS

In the first part of this PhD project we effectively proved that:

- The isosbestic point of eLacco2.1 is at 400 nm (fundamental for fiber photometry recordings).
- It is possible to measure lactate changes in freely moving mice with fiber photometry.
- The best lactate dose in order to observe a lactate increase without saturating the sensor is 2g/Kg.
- The hypolocomotive effect of THC is correlated with a reduction of Lactate levels in the brain.
- The hypolocomotor, but not antinociceptive, effect of THC is blocked by Lactate injection.

In the future, we are planning to:

- Analyze different behaviors related to Lactate changes during locomotion (DeepOF).
- Explore CB1-dependent modulation of Lactate on locomotion.
- Study the impact of locomotion on brain Lactate levels in basal ganglia (Striatum, Substantia nigra and globus pallidus).
- Confirming the blocking effect of Lactate on THC-induced hypolocomotion by local injections into these brain regions, and by intracerebroventricular injections.
- Explore the cellular and molecular mechanisms of the relationship between cannabinoids, Lactate and locomotion.

PARTENAIRES

Oligodendrocyte energy metabolism: modulation by CB_1 receptors

E Sanchez-Martin[1,2,3], AM Baraibar[1,2,3], T Colomer[1,2,3], A Bernal-Chico[1,2,3] A Ruiz[1,2,4], I Fernández-Moncada[5,6], G Marsicano[5,6], S Mato[1,2,3]

[1]Department of Neurosciences, University of the Basque Country UPV/EHU and [2]Achucarro Basque Center for Neuroscience, E-48940 Leioa, Spain; [3]Neuroinmunology Unit, ISS Biocruces, Bizkaia, E-48903 Barakaldo, Spain; [4]Centro de Investigación Biomédica en Red sobre Enfermedades Neurodegenerativas (CIBERNED), E-28031 Madrid, Spain; [5]INSERM U1215, Neurocentre Magendie and [6]Université de Bordeaux, E-33000 Bordeaux France

ABSTRACT

Oligodendrocytes (OLs) produce central nervous system myelin thus providing protection and metabolic support to axons. Myelin formation and repair are energetically expensive and oligodendrocyte metabolic defects have been postulated as a cause of neurodegeneration. Endocannabinoids modulate neuroglial metabolism through the activation of CB_1 receptors (CB_1Rs). Myelinating OLs and precursor cells (OPCs) express CB_1Rs promote lineage progression but the metabolic implications of these effects in health and disease remains uncertain. Here we investigated the energy metabolism of oligodendroglial linage and the role of CB1Rs in oligodendrocyte energy metabolism *in vitro.*

Seahorse analysis revealed that OLs exhibited a higher glycolysis metabolism compared to OPCs. Additionally, lactate extracellular biosensor eLACCO2.9 revealed differences in lactate release between OLs and OPCs. Seahorse analysis showed inhibitory effects of the CB_1R agonist ACEA on mitochondrial respiration in OLs cultures. The antagonist AM251 prevented the inhibitory effect of ACEA on maximal OCR. These results suggest that oligodendrocyte differentiation is associated with changes in energy metabolism *in vitro* and CB_1Rs modulate mitochondrial respiration in OLs, possibly mediated by mitochondrial CB_1R.

Methods: Oligodendrocyte cultures

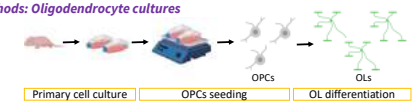

Figure 1. Experimental procedure for oligodendrocyte cultures. Cells were isolated from the cortex of postnatal rats and maintained as mixed glial cell cultures for 10-15 days. OPCs were plated and maintained as OPCs or differenciated to OLs.

Mature oligodendrocytes are more glycolytic than OPCs in vitro

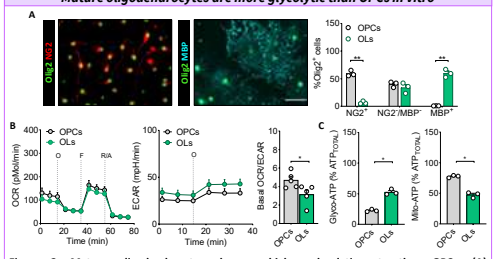

Figure 2. Mature oligodendrocytes show a higher glycolytic rate than OPCs. (A) Immunofluorescence images of OPC-enriched cultures (left) and OLs cultures (right). **(B)** Mitostress Seahorse analysis of oxygen consumption rate (OCR), extracellular acidification rate (ECAR) and ratio between basal OCR and basal ECAR. **(C)** ATP rate Seahorse analysis of ATP produced from glycolisis or mitochondrial respiration. **p < 0.05; ** p < 0.01. Student's t-test.* Scale bar: 50 µm.

Lactate biosensor for fluorescence in vitro imaging of oligodendroglia

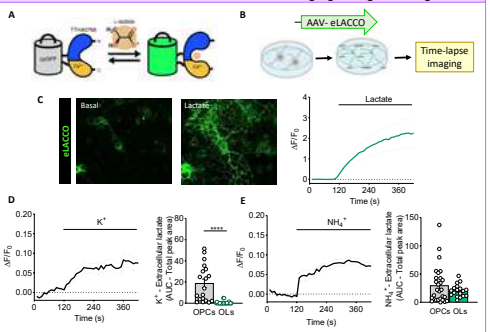

Figure 3. Extracellular K^+ and NH_4^+ induce oligodendroglial lactate efflux *in vitro* . (A-B) Diagram of the mechanism of action eLACCO in response to L-lactate and expression in oligodendroglial cells. **(C)** eLACCO fluorescence response to lactate (10 mM). **(D-E)** Time course of eLACCO fluorescence responses to K^+ and NH_4^+ in OPCs and OLs. **** p < 0.001. Student's t-test.* Scale bar: 50 µm.

CB_1Rs modulate mitochondrial metabolism in oligodendrocytes

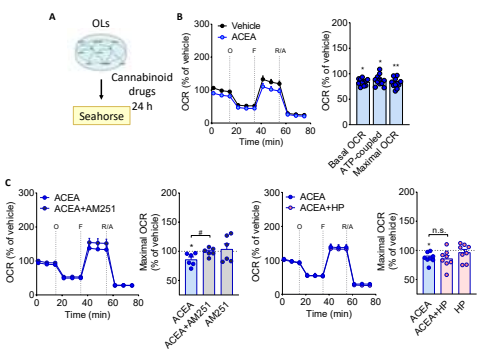

Figure 4. Agonist activation of CB_1Rs inhibits mitochondrial energy metabolism in oligodendrocyte cultures. (A) Diagram of OLs treatment**. (B)** ACEA (25 nM) reduced OCR in OLs. **(C)** AM251 treatment blocked maximal inhibition of OCR triggered by ACEA in OLs **(C).** Hemopressin (HP; 25 nM) did not blocked maximal inhibition of OCR triggered by ACEA. ** p < 0.05; ** p < 0.01; *** p < 0.001; ****p < 0.0001 Student's t-test and One-way ANOVA.*

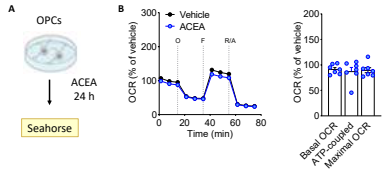

Figure 5. CB_1R does not modulate mitochondrial metabolism in OPCs. (A) Diagram of OPCs treatment with ACEA (25 nM). **(B)** ACEA did not modulate OCR in OPCs. *Student's t-test.*

CB_1Rs do not modulate glycolysis in oligodendrocytes

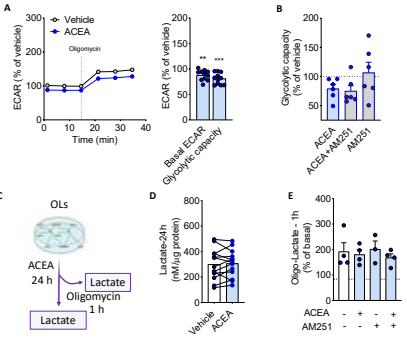

Figure 6. Agonist activation of CB_1Rs does not modulate glycolysis in oligodendrocytes. Treatment with ACEA (25 nM) reduces ECAR in OLs but AM251 **(B)** did not blocked this effect. **(C)** Diagram of the experimental procedure for extracellular lactate assay. **(D)** Extracellular lactate realeased after 1 hour by cells treated with ACEA during 24 hours. **(E)** Measurment of extracellular lactate under 1 hour oligomycin treatment. **p < 0.05; ** p < 0.01. Student's t-test.*

CONCLUSIONS

- **OPC differenciation** involves the modulation of bioenergetic profiles.
- CB_1R agonism **inhibits mitochondrial respiration** in oligodendrocytes via mitochondrial CB_1R.
- Oligodendrocyte CB_1Rs do **not modulate glycolysis**.

Acknowledgements

This study was supported by grants from the FEDER and ISCIII (PI21/00629), Basque Government (PIBA19-0059), CIBERNED (CB06/0005/0076) and ARSEP Foundation

CannaMetHD LTC incubator

Oligodendrocytes energetic metabolism: modulation by CB1 receptors

E Sanchez-Martin[1,2,3],
AM Baraibar[1,2,3],
T Colomer[1,2,3],
A Bernal-Chico[1,2,3],
A Ruiz[1,2,4]
I Fernández-Moncada[5,6]
G Marsicano[5,6]
S Mato[1,2,3]

[1] Department of Neurosciences, University of the Basque Country UPV/EHU.

[2] Achucarro Basque Center for Neuroscience, E-48940 Leioa, Spain.

[3] Neuroinmunology Unit, ISS Biocruces, Bizkaia, E-48903 Barakaldo, Spain.

[4] Centro de Investigación Biomédica en Red sobre Enfermedades Neurodegenerativas (CIBERNED), E-28031 Madrid, Spain.

[5] INSERM U1215, Neurocentre Magendie and 6Université de Bordeaux, E-33000 Bordeaux France.

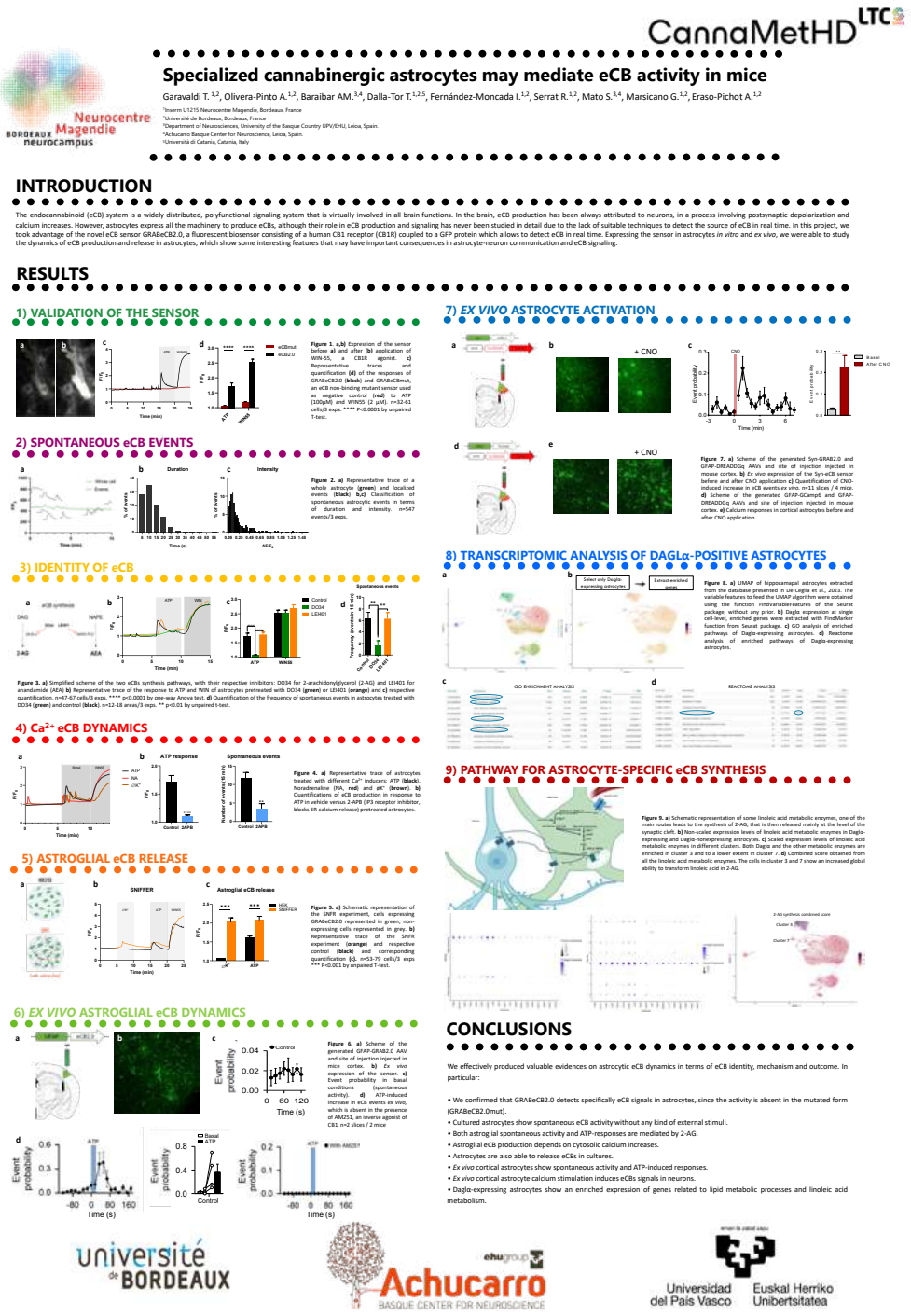

CannaMetHD LTC incubator

Specialized cannabinergic astrocytes may mediate eCB activity in mice

Garavaldi T. [1,2]
Olivera-Pinto A.[1,2]
Baraibar AM.[3,4]
Dalla-Tor T.1,[2,5]
Fernández-Moncada I.[1,2]
Serrat R.[1,2]
Mato S.[3,4]
Marsicano G.[1,2]
Eraso-Pichot A.[1,2]

[1] Inserm U1215 Neurocentre Magendie, Bordeaux, France.

[2] Université de Bordeaux, Bordeaux, France.

[3] Department of Neurosciences, University of the Basque Country UPV/EHU, Leioa, Spain.

[4] Achucarro Basque Center for Neuroscience, Leioa, Spain.

[5] Università di Catania, Catania, Italy.

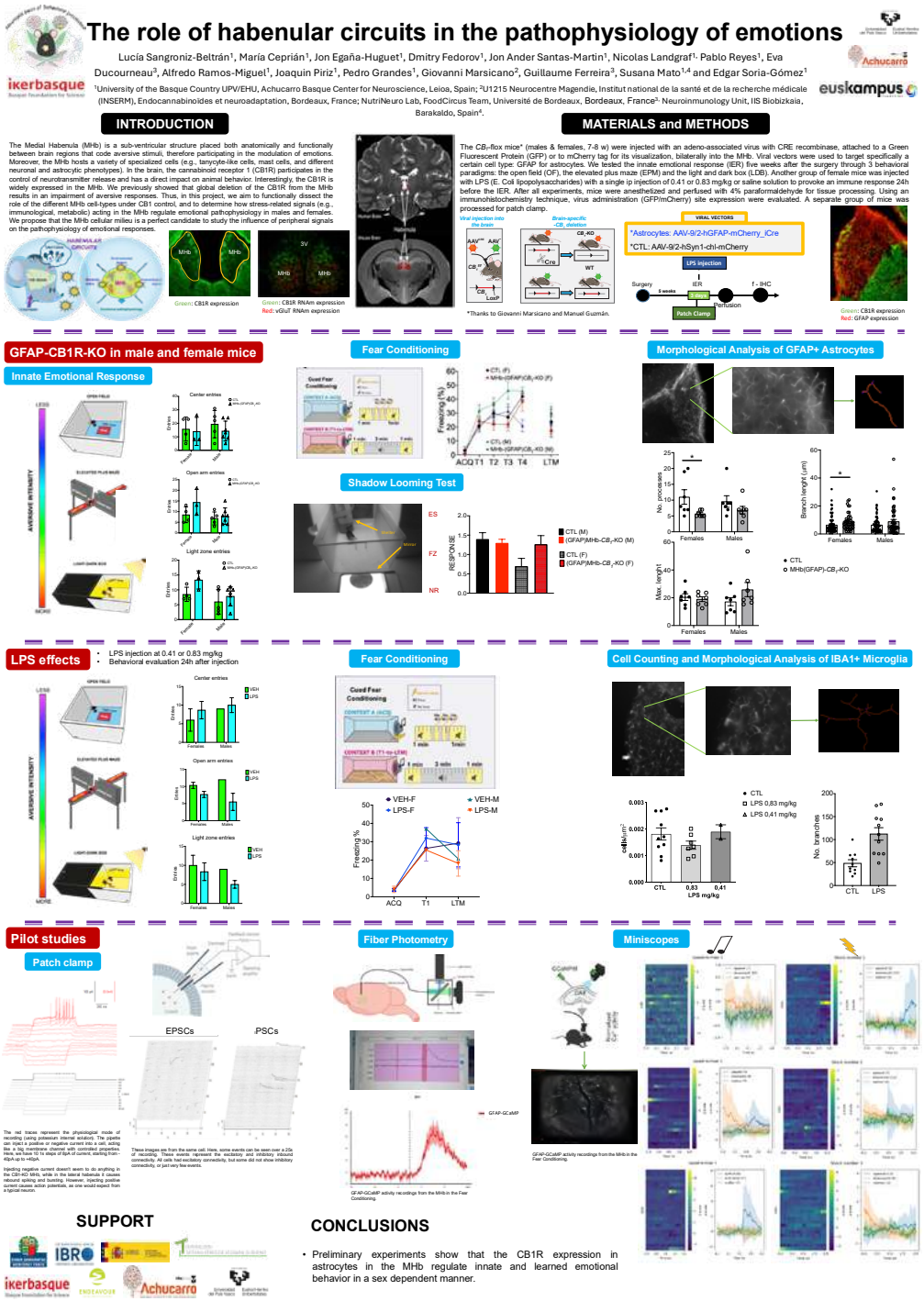

CannaMetHD LTC incubator

The role of habenular circuits in the pathophysiology of emotions

Lucía Sangroniz-Beltrán[1]
María Ceprián[1]
Jon Egaña-Huguet[1]
Dmitry Fedorov[1]
Jon Ander Santas-Martin[1]
Nicolas Landgraf[1]
Pablo Reyes[1]
Eva Ducourneau[3]
Alfredo Ramos-Miguel[1]
Joaquin Piriz[1]
Pedro Grandes[1]
Giovanni Marsicano[2]
Guillaume Ferreira[3]
Susana Mato[1,4]
Edgar Soria-Gómez[1]

[1] University of the Basque Country UPV/EHU, AchucarroBasque Center for Neuroscience, Leioa, Spain.

[2] U1215 Neurocentre Magendie, Institut national de la santé et de la recherche médicale (INSERM), Endocannabinoïdes et neuroadaptation, Bordeaux, France.

[3] NutriNeuro Lab,FoodCircus Team, Université de Bordeaux, Bordeaux, France.

[4] Neuroinmunology Unit, IIS Biobizkaia, Barakaldo, Spain.

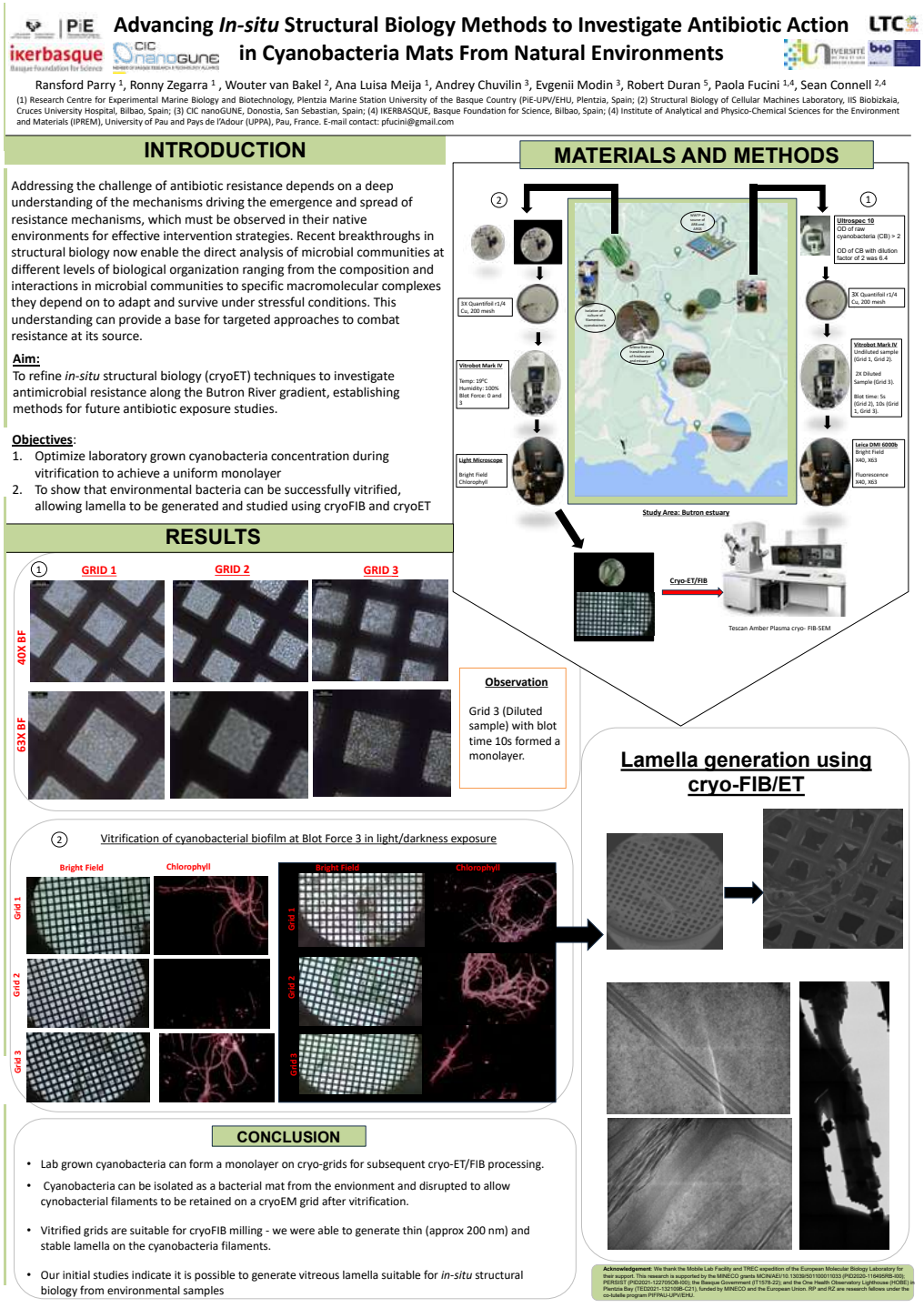

EAR LTC incubator

Advancing In-situ Structural Biology Methods to Investigate Antibiotic Action in Cyanobacteria Mats From Natural Environments

Ransford Parry[1]
Ronny Zegarra[1]
Wouter van Bakel[2]
Ana Luisa Meija[1]
Andrey Chuvilin[3]
Evgenii Modin[3]
Robert Duran[4]
Paola Fucini[1]
Sean Connell[2]

[1] Research Centre for Experimental Marine Biology and Biotechnology, Plentzia Marine Station University of the Basque Country (PiE-UPV/EHU), Plentzia, Spain.

[2] Structural Biology of Cellular Machines Laboratory, IIS Biobizkaia, Cruces University Hospital, Bilbao, Spain.

[3] CIC nanoGUNE, Donostia, San Sebastian, Spain.

[4] Institute of Analytical and Physico-Chemical Sciences for the Environment and Materials (IPREM), University of Pau and Pays de l'Adour (UPPA), Pau, France.

EXPLORING ENVIRONMENTAL RESERVOIRS OF ANTIBIOTIC-RESISTANT BACTERIA: A CASE STUDY IN THE BUTRON RIVER OF PLENTZIA

Ronny Zegarra,[1] Ana Luisa Mejía,[1] Ransford Parry,[1] Itziar Alkorta,[2] Lucia Gallego,[3] Robert Duran,[4] Sean Connell,[5,6] Paola Fucini[1,6]

(1) Research Centre for Experimental Marine Biology and Biotechnology, Plentzia Marine Station University of the Basque Country (PiE-UPV/EHU, Plentzia, Spain.
(2) Department of Molecular Biology and Biochemistry, Faculty of Science and Technology University of the Basque Country (UPV-EHU), Leioa, Spain.
(3) Department of Immunology, Microbiology and Parasitology, Faculty of Medicine and Nursing University of the Basque Country (UPV-EHU), Leioa, Spain.
(4) Institute of Analytical and Physico-Chemical Sciences for the Environment and Materials (IPREM), University of Pau and Pays de l'Adour (UPPA), Pau, France.
(5) Structural Biology of Cellular Machines Laboratory, IIS Biobizkaia, Cruces University Hospital, Bilbao, Spain; (6) IKERBASQUE, Basque Foundation for Science, Bilbao, Spain.

INTRODUCTION

The widespread of antibiotics in nearly all environments combined with microorganisms' ability to adapt and survive stress, has led to the emergence of antimicrobial resistance (AMR) [1], which is considered a silent pandemic projected to cause about 10 million deaths annually by 2050 [2]. In relation to clinical, veterinary and food-producing animal settings, AMR monitoring in the environment lack integration and standardization [3]. The identification of environmental AMR reservoirs, where resistant microorganisms can persist, proliferate, and potentially spread to humans and animals, is crucial for establishing routine monitoring and targeting intervention strategies to prevent the spread of resistance in a One Health context [4].

AIM:

Establish a suitable monitoring strategy within the One Health approach to identify ARB's potential sources and environmental reservoirs, understanding their dynamics and dispersal in the Butrón River. This under the context of wastewater effluents input in the river, has caused beach closures due to high levels of fecal bacteria indicators [5], while the bay is frequented year-round by locals for aquatic sports and attracts around 20,000 tourists during the summer [6].

OBJECTIVES:

1. Identification of potential environmental AMR reservoirs within the aquatic ecosystem of the Butrón River.
2. Develop a monitoring strategy to identify culturable ARB and evaluate the environmental levels of AMR.
3. Assess the potential of biotic (green algae) and abiotic (water, sediments, and sand) components as hosts of culturable ARB.

Only AST results with over 15 CFU were considered to avoid misleading AMR data. Plentzia beach and DOX excluded.

METHODS

Antibiotic	Class	Mode of Action	AST concentration (µg/mL)
Ampicillin (AMP)	Penicillin	Cell wall synthesis inhibitor	8
Doxycycline (DOX)	Tetracyclines	Protein synthesis inhibitor	16
Sulfamethoxazole (SMX)	Sulfonamides	Dihydropteroate synthase inhibitor	76
Trimethoprim (TMP)	Diaminopyrimidines	Dihydrofolate reductase inhibitor	4

RESULTS

Comparison between environmental reservoirs.
PER ANTIBIOTIC AND SAMPLING LOCATION.

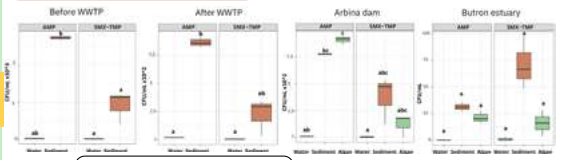

ARB colonies from freshwater extracts > estuarine samples – salinity-driven patterns and WWTP influence.

Comparison among sampling sites
FOR EACH RESERVOIR AND ANTIBIOTIC

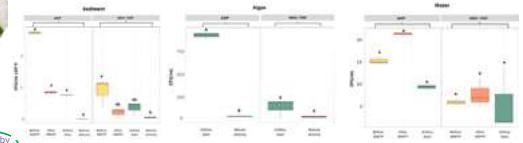

Reservoirs of ARB: Sediment > algae > water

Water use of 3 µm filter - targeting particle-associated bacteria only.

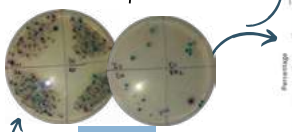

ARB composition by color colony
Relative concentration (CFU/mL) of each sample by sampling site.

Conclusions

These findings offer a first assessment of culturable ARBs relevant to human health and suggest the method for estuary samples may need refinement for better microbiome recovery.

Future work

- Improve microbiome extraction for a minimum of 50 µl of 10^7 CFU/mL*AST
- Narrow isolation of human colonizer/pathogenic bacteria using selective media.
- Monitor ARB seasonal dynamics to assess environmental impacts.
- Metagenomics for ARGs and antibiotic synthesis pathways identification

References

This work is funded by the MINECO grants MCIN/AEI/10.13039/501100011033 (PID2020-116495RB-I00); PERSIST (PID2021-122705OB-I00); Basque Government (IT1578-22) and the One Health Observatory Lighthouse (HOBE) in Plentzia Bay (TED2021-132109B- C21) by MINECO and the European Union.
RZ and RP are research fellows under the co-tutelle program PIFPAU-UPV/EHU.

EAR LTC incubator

Exploring environmental reservoirs of antibiotic-resistant bacteria: a case study in the Butron River, Plentzia

Ronny Zegarra[1]
Ana Luisa Mejía[1]
Ransford Parry[1]
Itziar Alkorta[2]
Lucia Gallego[3]
Robert Duran[4]
Sean Connell[5]
Paola Fucini[1,6]

[1] University of the Basque Country, Research Centre for Experimental Marine Biology and Biotechnology, Plentzia Marine Station (PiE-UPV/EHU), Plentzia, Spain.

[2] University of the Basque Country (UPV-EHU), Faculty of Science and Technology, Department of Molecular Biology and Biochemistry, Leioa, Spain.

[3] University of the Basque Country (UPV-EHU), Faculty of Medicine and Nursing, Department of Immunology, Microbiology and Parasitology, Leioa, Spain.

[4] Institute of Analytical and Physico-Chemical Sciences for the Environment and Materials (IPREM), University of Pau and Pays de l'Adour (UPPA), Pau, France.

[5] IIS Biobizkaia, Cruces University Hospital, Structural Biology of Cellular Machines Laboratory, Bilbao, Spain.

[6] Basque Foundation for Science, IKERBASQUE, Bilbao, Spain.

ICE COUPLING PROTEIN

Ruiz-Cruz, Sofía & Alkorta, Itziar.

Faculty of Science and Technology; Biochemistry and Molecular Biology Department; University of the Basque Country

EAR INCUBATOR

ABSTRACT

Antibiotic Resistance (AR) is one of the greatest threats to human health. The global overuse of antibiotics has resulted in the proliferation and dissemination of antibiotic resistant bacteria harboring a multitude of AR genes that can be mobilized by different Horizontal Gene Transfer (HGT) processes. Three types of self-transmissible mobile genetic elements participate in HGT: bacteriophages, conjugative plasmids, and Integrative Conjugative Elements (ICEs). Conjugative plasmids and ICEs rely on conjugation for its dissemination, a process that requires direct cell-to-cell contact to enable unidirectional translocation of DNA across the membranes of two mating cells. ICEs are typically found integrated in the host chromosome and encode the machinery for their conjugation, which consists of: (*i*) proteins that form the relaxosome; (*ii*) proteins that form the Type IV Secretion System (T4SS); and (*iii*) the Type IV Coupling Protein (T4CP) that links the relaxosome with the T4SS. To date, ICE coupling proteins have received little attention despite their indispensability in the transfer mechanism. **We are focused on the molecular and functional characterization of the coupling protein an ICE present in multiple *Enterobacteriaceae*, with the ultimate goal of finding ICE conjugation inhibitors to block or, at least, minimize the AR spread.**

BACKGROUND

Conjugative plasmids and ICEs constitute the main drivers of AR spread. Although ICEs outnumber conjugative plasmids, yet they still have been largely overlooked as vectors of AR[1]. Both elements encode their conjugation machinery, but conjugative plasmids replicate autonomously whereas ICEs integrate into and replicate along with the chromosome[2]. An integrated ICE remains quiescent, but under certain conditions, the ICE excises from the chromosome as a circular plasmid-like form, which is transferred by the conjugative transfer machinery. Then, is recircularized and integrated in the chromosome[3]. Additionally, in some cases, ICEs and conjugative plasmids transfer non-conjugative elements such as mobilizable plasmids or integrative mobile genetic elements to a new host.

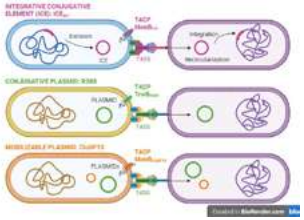

T4CPs are essential for conjugation, but only a few T4CPs (all plasmid-encoded) have been exhaustively studied, such as the archetype of the T4CP family , $TrwB_{R388}$, encoded by the conjugative plasmid R388 or $MobB_{CloDF13}$, which is one of the few T4CPs encoded by a mobilizable plasmid, CloDF13[4]. Mobilizable plasmids, which can encode AR genes as well, use the T4CPs and T4SS of co-resident conjugative elements, because they usually only encode the proteins needed for relaxosome formation. Given their **critical role in conjugation, T4CPs represent a promising drug target to block conjugation and, hence, AR dissemination among bacteria.**

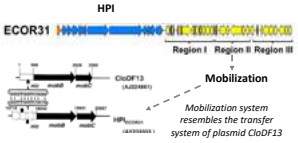

Figures adapted from 5 and 6.

A homologue of $mobB_{CloDF13}$, herein named ***mobB*$_{ICE}$**, was identified within **ICE*Ec1*** from *Escherichia coli* ECOR31[6], containing a wide distributed High-Pathogenicity Island (HPI) among *Enterobacteriaceae*. encodes a functional T4SS similar to the one described for the conjugative plasmid R6K, but its DNA-mobilization region is related to plasmid CloDF13**. The expected product of *mobB*$_{ICE}$, (629 amino acids) shows 31% of identity and 42% similarity with $MobB_{CloDF13}$.** It was shown that *mobB*$_{ICE}$ is involved in the transfer of a plasmid carrying the origin of transference (*oriT*) present on ICE*Ec1*[6].

$MobB_{ICE}$ is an ideal candidate to in-depth characterize an essential component of an ICE conjugative machinery, a T4CP, to find ICE conjugation inhibitors, with the aim of blocking/ minimizing AR spread.

OBJECTIVES

1. *In vitro* characterization of $MobB_{ICE}$

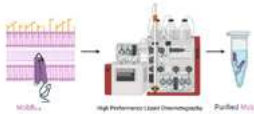

1.1. Protein purification.
1.2. Determination of oligomerization state.
1.3. Effect of the ionic strength, detergent concentration, and pH on $MobB_{ICE}$ stability
1.4. Secondary structure and thermal stability.
1.5. DNA-binding properties.
1.6. ATPase activity determination.

2. *In vivo* activity of $MobB_{ICE}$

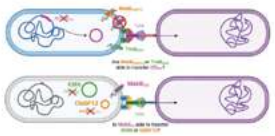

2.1. *mobB*$_{ICE}$ deletion on self-transmission.
2.2. Effect of $MobB_{ICE}$ in plasmid conjugation.
2.3. Mobilization of CloDF13 by $MobB_{ICE}$.

3. *In vitro* and *in vivo* validation of potential $MobB_{ICE}$ inhibitors

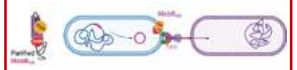

3.1. *In vitro* effect of potential inhibitors of $MobB_{ICE}$
3.2. Effect of inhibitors on the transfer of ICE_{EC1}.
3.3. Effect of inhibitors on the transfer frequency of plasmids R388 and CloDF13

REFERENCES

1. Botelho J & Schulenburg H. Trends Microbiol (2021) 29(1):8-18
2. Burrus V. Curr Opin Microbiol (2017), 38:44-50
3. Johnson CM & Grossman AD. Annu Rev Genet (2015) 49:577-601
4. Álvarez-Rodríguez I. et al. Front Mol Biosci (2020) 12;7:201
5. Auvray F. et al. Microb Genom (2021) 7:000579
6. Schubert, S. et al. Mol Microbiol (2004) 51: 837-848

ACKNOWLEDGEMENTS

Sofía Ruiz-Cruz is a beneficiary of a MSCA-2022-PF-01-Postdoctoral Fellowships. Project ICECOUP-101107037.
The group is supported by MCIN/AEI/10.13039/501100011033 (PID2020-116495RB-I00), Gobierno Vasco (IT1578-22) and LTC EAR Incubator: EUSKAMPUS 2023 (EUSK23/01) y EUSKAMPUS 2022 (EUSK22/23

EAR LTC incubator

ICE coupling protein

Sofía Ruiz-Cruz[1]
Itziar Alkorta[1]

[1] Faculty of Science and Technology; Biochemistry and Molecular Biology Department; University of the Basque Country (UPV/EHU).

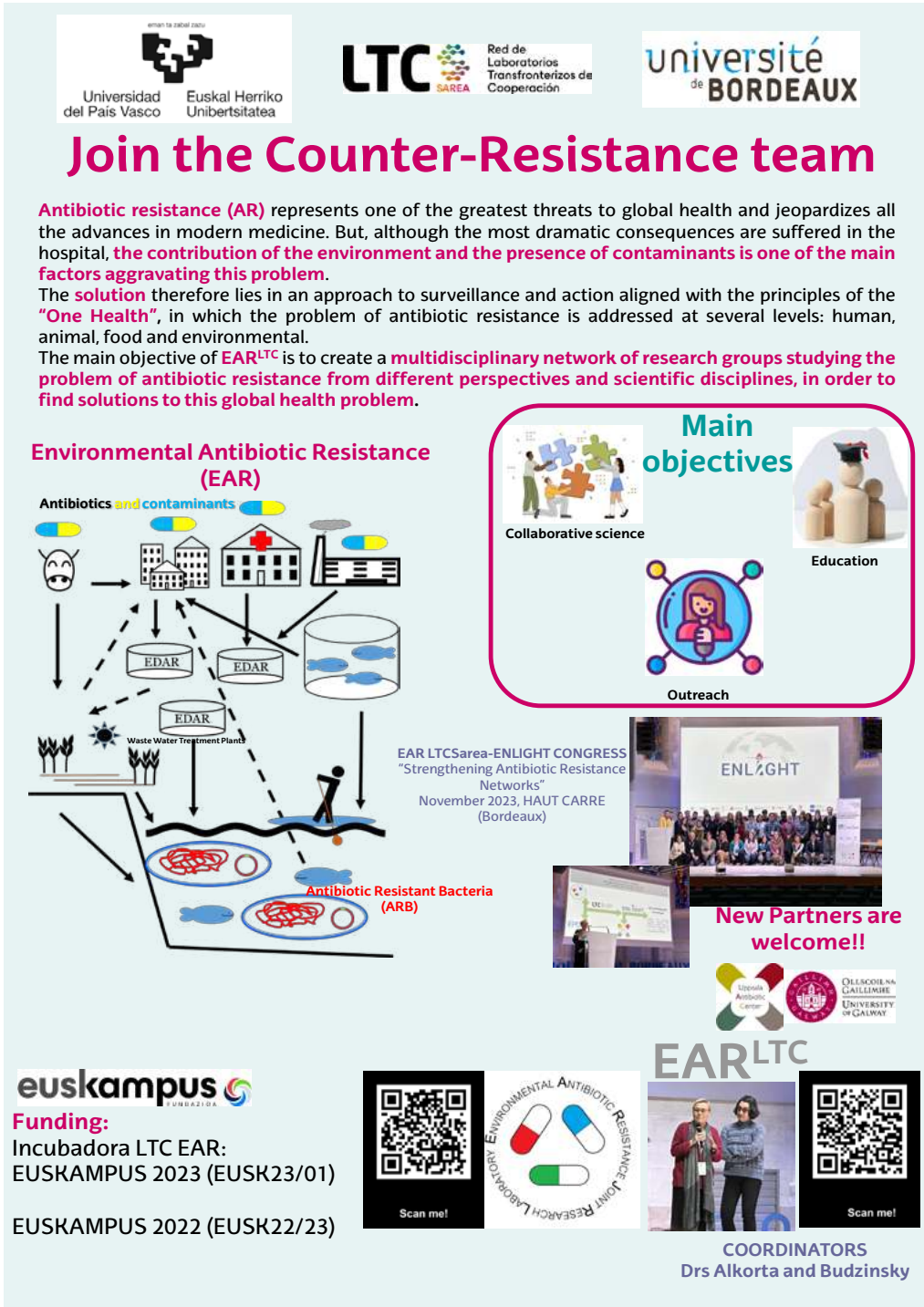

EAR LTC incubator

Join the Counter-Resistance team

Itziar Alkorta[1]

[1] University of the Basque Country and Helene Budzinsly, University of Bordeaux.

HumEVOL LTC incubator

From bones to landscapes: Integrated approaches with virtual tools for the study of Neanderthal origins

Diego López-Onaindia[1]
Kim Genuite[1]
Martin Arriolabengoa[2]
Aurore Issartel[1]
Elle Liagre[1]
Christine Couture-Veschambre[1]
Asier Gómez-Olivencia[2]

[1] PACEA UMR 5199, CNRS, Université de Bordeaux, Ministère de la Culture, Pessac, France.

[2] Dept. Geología, Facultad de Ciencia y Tecnología, Universidad del País Vasco/Euskal Herriko Unibertsitatea, UPV/EHU, Leioa, Spain.

MultiArchSciences LTC Incubator

From Jerez to the Atlantic: first archaeometric approach to Southwestern Andalusian ceramic trade containers production

Saúl Guerrero Rivero[1]
Javier G. Iñañez[1]
Fernando Amores Carredano[2]
Gorka Arana[3]
Rémy Chapoulie[4]

[1] University of the Basque Country / Euskal Herriko Unibertsitatea (UPV/EHU). Department of Geography, Prehistory and Archaeology. Experimental space for innovation in Heritage and Cultural Landscapes (GPAC).

[2] University of Seville, Department of Prehistory and Archaeology.

[3] University of the Basque Country / Euskal Herriko Unibertsitatea (UPV/EHU). IBeA, Faculty of Science and Technology.

[4] Archéosciences Bordeaux: Matéraux, Temps, Images et Sociétés - UMR 6034.

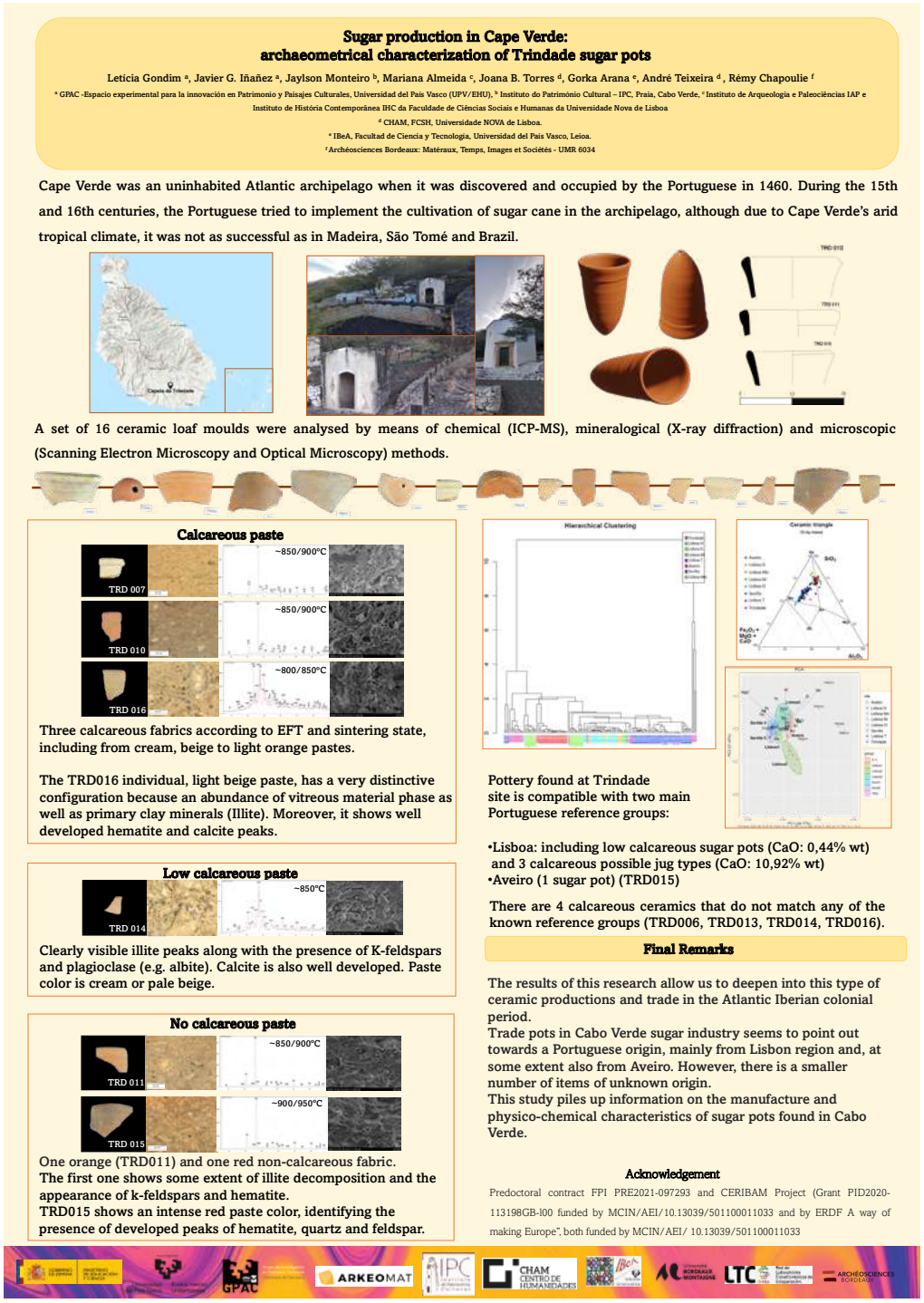

MultiArchSciences LTC Incubator

Sugar Production in Cape Verde: Archaeometrical Characterization of Trindade Sugar Pots

Letícia Gondim[1]
Javier G. Iñañez[1]
Jaylson Monteiro[2]
Mariana Almeida[3]
Joana B. Torres[4]
Gorka Arana[5]
André Teixeira[4]
Rémy Chapoulie[6]

[1] GPAC -Espacio experimental para la innovación en Patrimonio y Paisajes Culturales, Universidad del País Vasco (UPV/EHU).

[2] Instituto do Património Cultural – IPC, Praia, Cabo Verde.

[3] Instituto de Arqueologia e Paleociências IAP e Instituto de História Contemporânea IHC da Faculdade de Ciências Sociais e Humanas da Universidade Nova de Lisboa.

[4] CHAM, FCSH, Universidade NOVA de Lisboa.

[5] IBeA, Facultad de Ciencia y Tecnología, Universidad del País Vasco, Leioa.

[6] Archéosciences Bordeaux: Matériaux, Temps, Images et Sociétés - UMR 6034.

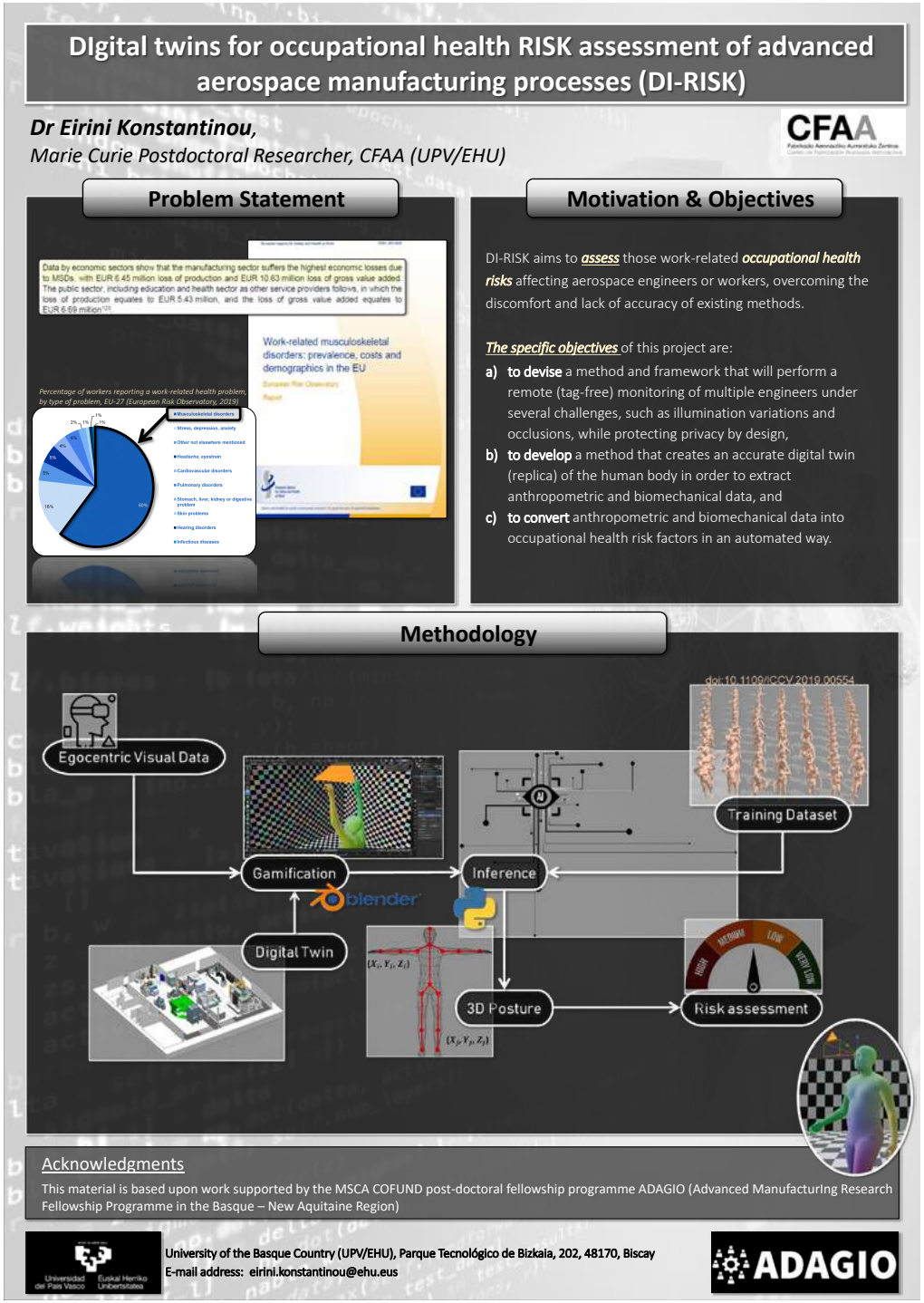

ADAGIO

Digital twins for occupational health RISK assessment of advanced aerospace manufacturing processes (DI-RISK)

Eirini Konstantinou[1,2]

[1] Marie Curie Postdoctoral Researcher, CFAA (UPV/EHU).

POLYMAT

Funded by the European Union

Universidad del País Vasco · Euskal Herriko Unibertsitatea

Discovering new crystallization modes in random copolymers

Ricardo A. Pérez-Camargo[1], Yilong Liao[1], Haritz Sardon[1], Antxon Martínez de Ilarduya[2], Wenxian Hu[3,4], Guoming Liu[3,4], Dujin Wang[3,4], Alejandro J. Müller[1,5].

1 POLYMAT and Department of Polymers and Advanced Materials: Physics, Chemistry, and Technology, Faculty of Chemistry, University of the Basque Country UPV/EHU, Paseo Manuel de Lardizábal, 3, 20018 Donostia-San Sebastián, Spain.
2 Department of Chemical Engineering, Polytechnic University of Catalonia ETSEIB-UPC, Diagonal 647, 08028 Barcelona, Spain. 3Beijing National Laboratory for Molecular Sciences, CAS Key Laboratory of Engineering Plastics, Institute of Chemistry, Chinese Academy of Sciences, Beijing 100190, P. R. China. 4University of Chinese Academy of Sciences, Beijing 100049, P. R. China. 5Ikerbasque, Basque Foundation for Science, Plaza Euskadi 5, 48009 Bilbao, Spain.

• INTRODUCTION •

Random copolymers formed by semi-crystalline parent homopolymers can crystallize in three well-known modes (Scheme 1), depending on the comonomer inclusion/exclusion balance: **isomorphism** (total inclusion), **isodimorphism** (partial inclusion), and **comonomer exclusion** (total exclusion). Isodimorphism and isomorphism have garnered significant attention because of their crystallization across all composition ranges. A model Poly(A)-ran-Poly(B) copolymer can illustrate their differences

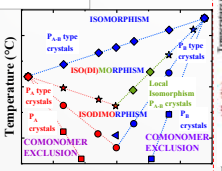

Scheme 1. Crystallization modes [2]

In isomorphic copolymers, the similarity between PA and PB allows co-crystallization in unique P_{A-B} crystals that differ from the parent components, leading to a linear relationship between the melting temperature (T_m) and comonomer content. For isodimorphic crystallization, due to the comonomer exclusion/inclusion balance, PA-type or PB-type crystals are formed, depending on the composition. The partial exclusion of B co-units causes a T_m depression of PA-type crystals as B content increases, and vice-versa, reaching a minimum T_m, where PA- and PB-type crystals can coexist. This pseudo-eutectic behavior extends to other properties such as enthalpies (ΔH) and crystallinities (X_c).[1,2] This work on a series of **linear aliphatic polycarbonates (PC)** based on poly (octamethylene carbonate) (PC8) as a fixed comonomer with a second comonomer, a PC, with different chain lengths: PC6, PC7, and PC12 reported apparent pseudo-eutectic behavior of T_m vs. PC8 content, but for specific compositions, their ΔH and thus X_c deviate from the expected behavior. Wide Angle X-ray scattering revealed the presence of a **new third phase (γ phase)** for these compositions, differing from that of the parent components. Further examination of these compositions' properties reveals isomorphic crystallization features. Therefore, our study discovered a **novel crystallization mode for random copolymers that exhibit mixed isodimorphism for some compositions and isomorphism for others.**

• EXPERIMENTAL PART •

PCn_{CH2}x-*ran*-PCn_{CH2}y with x= PC6, PC7 or PC12 and y= PC8

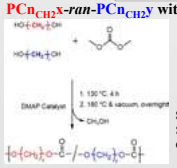

Random copolycarbonates
PC6-*ran*-PC8
PC7-*ran*-PC8
PC12-*ran*-PC8

Scheme 2. Illustration of Aliphatic Copolycarbonates Synthesized via Polycondensation of Diols with Dimethyl Carbonate.

•RESULTS AND DISCUSSION •

a. Thermal transitions showing pseudo-eutectic trend.

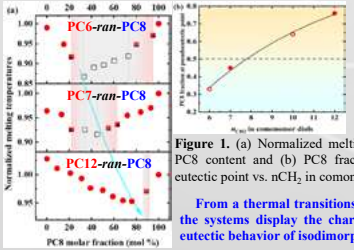

Figure 1. (a) Normalized melting temperatures vs. PC8 content and (b) PC8 fraction at the pseudo-eutectic point vs. nCH_2 in comonomers (diol) [4]

From a thermal transitions point of view, all the systems display the characteristic pseudo-eutectic behavior of isodimorphic copolymers.

The range of compositions with the γ phase and the pseudo-eutectic point position depends on the chain length.

n_{CH2} > 8, p.-eutectic >50%

n_{CH2} < 8, p.-eutectic <50%

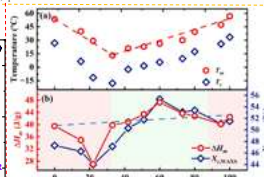

Figure 2. (a) Temperature transitions vs. PC8 content and (b) ΔH_m and X_c vs. PC8 content [3].

Despite the pseudo-eutectic behavior for the first-order thermal transitions, the ΔH_m and X_c show an atypical trend, with higher values than the homopolymers, and even showing a maximum at 60% PC8. This is the first evidence of a new third phase (γ phase)

b. Structural evidence of a third new phase.

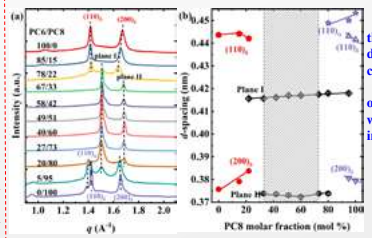

Figure 3. (a) WAXS patterns at -40 °C after cooling (at 20 °C/min) from the melt. (b) *d*-spacing vs PC8 content.[3]

WAXS analysis reveals the γ phase is completely different from the parent components.

Moreover, the *d*-spacing of this phase varies linearly with comonomer content, as in isomorphic copolymers.

c. Isomorphism for specify compositions.

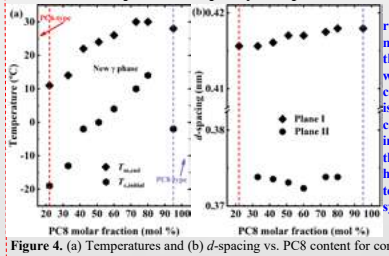

Figure 4. (a) Temperatures and (b) *d*-spacing vs. PC8 content for compositions with the third new phase. [3]

The linear relationship between the melting temperature and the *d*-spacing shown with respect to PC8 content indicates a local isomorphism for those copolymers crystallized in the γ phase, although the copolymer family has been demonstrated to be an isodimorphic system as a whole.

• CONCLUSIONS•

- **The mixed isodimorphic/isomorphic crystallization mode were found in three different copolycarbonates, and it is characterized by a pseudo-eutectic behavior from a first-order thermal transition point of view but displaying a third new phase for specify compositions from a structural point of view.**
- **On the one hand, those compositions exhibiting the third new phase exhibit atypically high X_c values that deviate from the expected pseudo-eutectic behavior. Additionally, the range of compositions in which the new phase is present depends on n_{CH2}.**
- **The formation of the new phase can be related to a conformational distortion of methylene segments that facilitates a resurgence of dipole-dipole interactions compared to the compositions where the new phase is absent (according to FTIR results not shown here).**

ACKNOWLEDGMENTS

- **This project has received funding from the European Union's Horizon 2020 research and innovation programme under the Marie Sklodowska-Curie grant agreement No 101034379**

[1] Pérez-Camargo, R. A. *Eur. Polym. J.* **2018**, 101, 233 [2] Pérez-Camargo, R. A. *Polymer* **2023**, 287, 126412.
[3] Liao, Y. *Macromolecules* **2023**, 56, 8199 [4] Liao, Y. *Macromolecules* (under revision) **2024**.

ADAGIO

Discovering new crystallization modes in random copolymers

Ricardo A. Pérez-Camargo[1]
Yilong Liao[1]
Haritz Sardon[1]
Antxon Martínez de Ilarduya[2]
Wenxian Hu[3,4]
Guoming Liu[3,4]
Dujin Wang[3,4]
Alejandro J. Müller[1,5]

[1] POLYMAT and Department of Polymers and Advanced Materials: Physics, Chemistry, and Technology, Faculty of Chemistry, University of the Basque Country UPV/EHU, Paseo Manuel de Lardizábal, 3, 20018 Donostia-San Sebastián, Spain.

[2] Department of Chemical Engineering, Polytechnic University of Catalonia ETSEIB-UPC, Diagonal 647, 08028 Barcelona, Spain.

[3] Beijing National Laboratory for Molecular Sciences, CAS Key Laboratory of Engineering Plastics, Institute of Chemistry, Chinese Academy of Sciences, Beijing 100190, P. R. China.

[4] University of Chinese Academy of Sciences, Beijing 100049, P. R. China.

[5] Ikerbasque, Basque Foundation for Science, Plaza Euskadi 5, 48009 Bilbao, Spain.

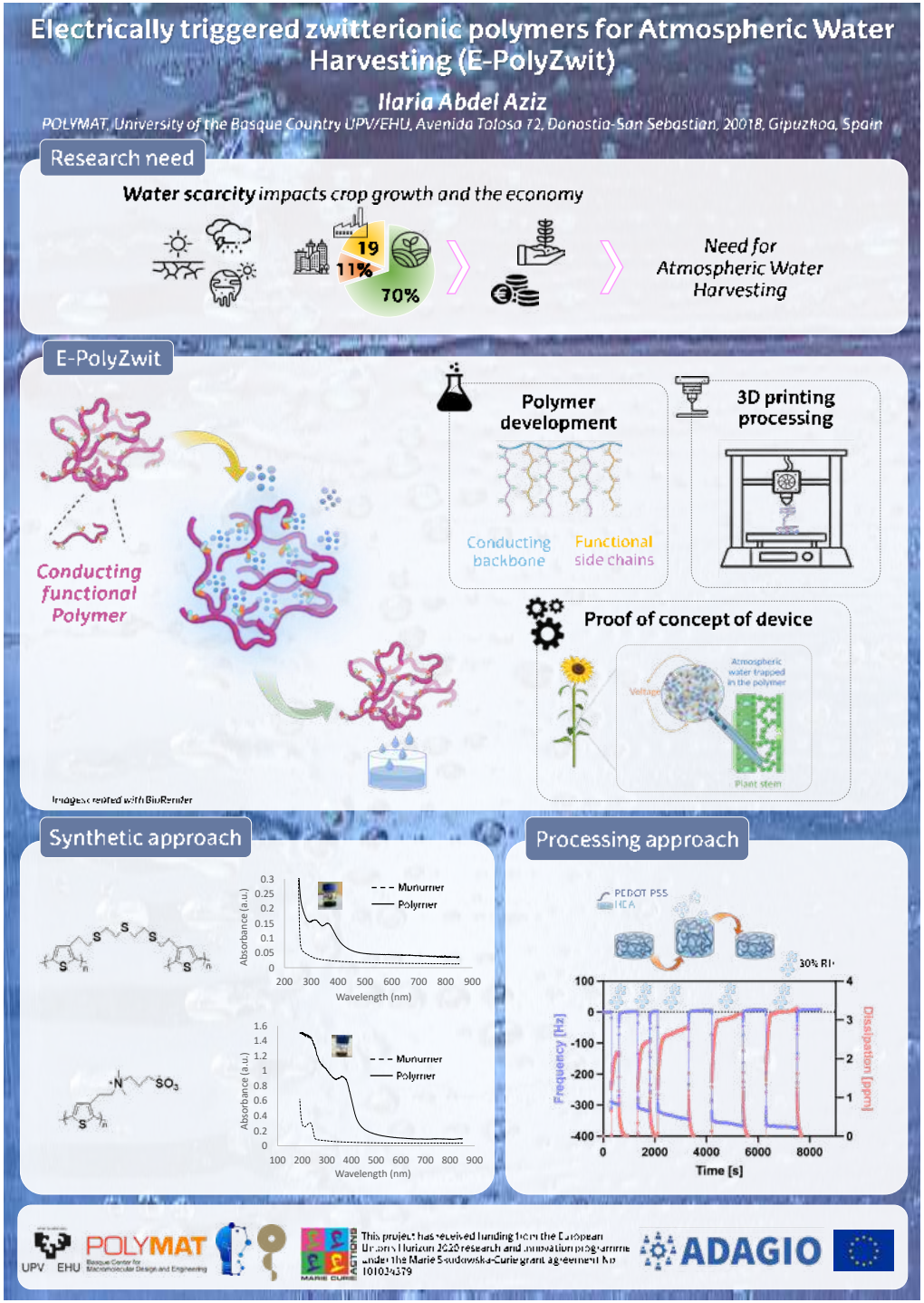

ADAGIO

Electrically triggered zwitterionic polymers for water harvesting (E-PolyZwit)

Ilaria Abdel Aziz[1]
Daniele Mantione[1,2]
Naroa Lopez Larrea[1]
David Mecerreyes[1,2]

[1] POLYMAT, University of the Basque Country UPV/EHU, Avenida Tolosa 72, Donostia-San Sebastian, 20018, Gipuzkoa, Spain.

[2] Ikerbasque, Basque Foundation for Science, 48013 Bilbao, Spain.

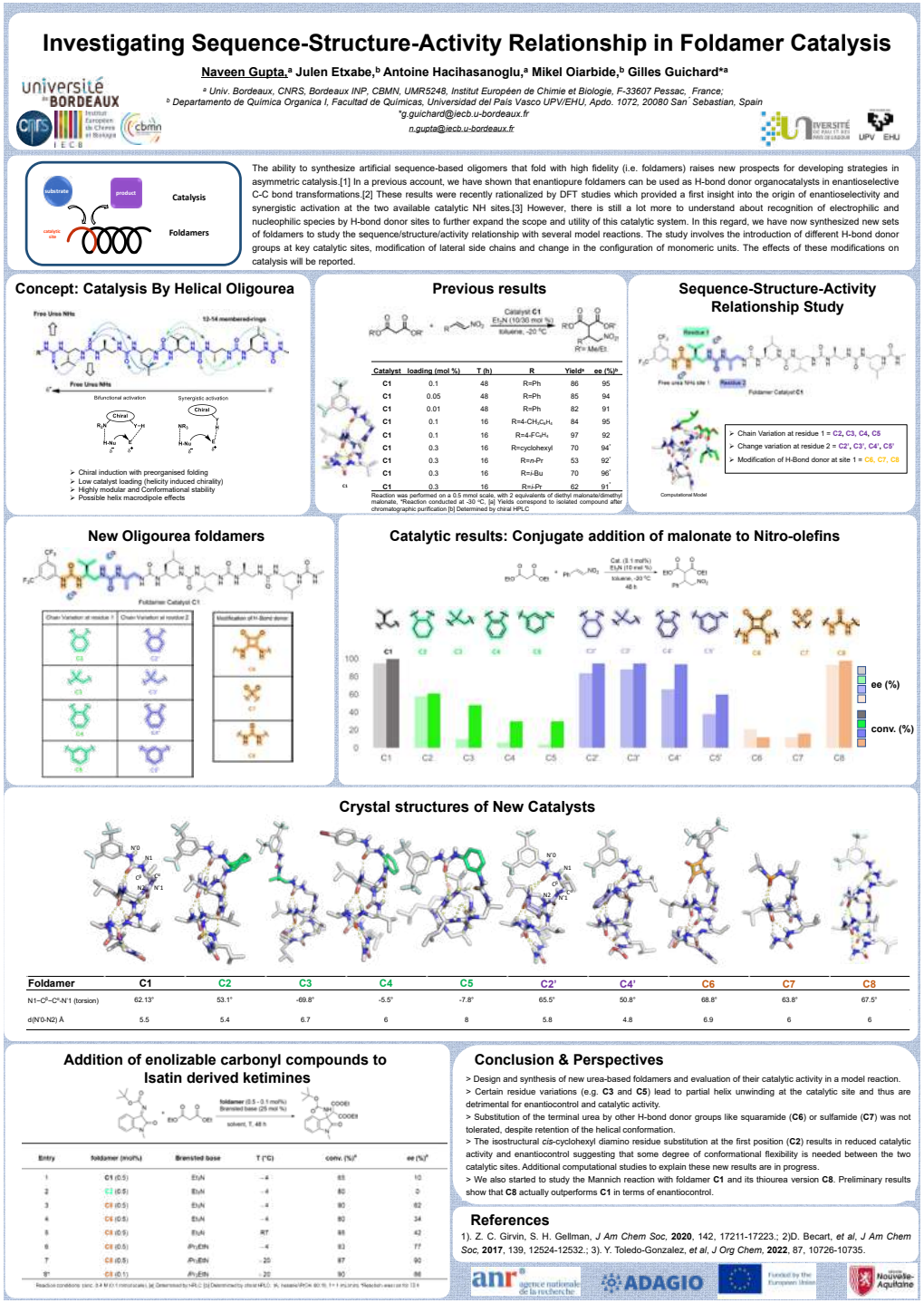

ADAGIO

Investigating Sequence-Structure-Activity Relationship in Foldamer Catalysis

Naveen Gupta[1]
Julen Etxabe[2]
Antoine Hacihasanoglu[1]
Mikel Oiarbide[2]
Gilles Guichard[1]

[1] Univ. Bordeaux, CNRS, Bordeaux INP, CBMN, UMR5248, Institut Européen de Chimie et Biologie, F-33607 Pessac, France.

[2] Departamento de Química Organica I, Facultad de Químicas, Universidad del País Vasco UPV/EHU, Apdo. 1072, 20080 San Sebastian, Spain.

KINETIC MONTE CARLO SIMULATIONS OF MINERAL CARBONATION

Dr. Aleena Alex

MSCA Post-doctoral fellow, University of Basque Country (UPV/EHU)

CARBONATION IN CONCRETE

- Carbonation: degradation (lowering of pH, corrosion); Self healing concrete (SHC), carbon capture utilization and storage (CCUS), carbon curing, cement re-carbonation and calcium carbonate engineering.
- Chemical reaction: $Ca^{+2} + CO_3^{-2} \rightarrow CaCO_3$

Self healing in cement mortar

METHODOLOGY

- Discrete element methods: used for mechanical interactions, fracture, strain etc.

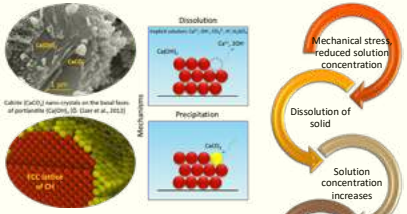

MASKE: A kinetic Monte Carlo simulator

Solid:

- Particles held together by interactions U(r)
- Particles can move everywhere (off-lattice)
- Forces (and stress) arise when particles are not in energy minima
- Dynamics from integration of forces

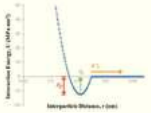

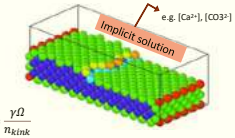

$$U_{ij} = \frac{1}{2}k(r_{ij} - r_0)^2 - \varepsilon_0 \qquad \varepsilon_0 = \frac{\gamma\Omega}{n_{kink}}$$

Corresponding force: $F_{ij} = -\frac{dU_{ij}}{dr_{ij}} = k(r_{ij} - r_0)$

Excess enthalpy ΔH_{ex} in the solid → solid activity ≠ 1 (low U → more stable → low R_{diss})

$$\mathcal{R}_{diss,i} = \frac{k_B T}{h}\frac{c^s}{\gamma^s}\exp\left(-\frac{\Delta G^{\ddagger}_{diss}}{k_B T}\right)\exp\left[\frac{-\Delta U_{diss}(r) - \gamma\Delta\Omega_{diss}}{k_B T}\right]V_M$$

$$\mathcal{R}_{prec,i} = \frac{k_B T}{h}\frac{c^s}{\gamma^s}\exp\left(-\frac{\Delta G^{\ddagger}_{diss}}{k_B T}\right)\beta\, V_M$$

Dissolution rate constant k_{diss}

Saturation index: $\beta = \frac{Q_{in\_sol}}{K_{eq,diss}}$

Molar volume of particle

MOLECULAR SCALE CARBONATION

(a) Initial structure consisting of Calcium silicate hydrate (C-S-H) and Portlandite (CH) and a spherical capillary pore with a seed $CaCO_3$ particle.

(b) Carbonated structure

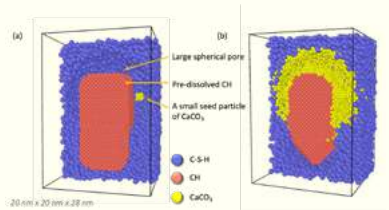

- Effective rates predicted by the molecular scale carbonation simulation were used in macro scale reactive transport and boundary nucleation and growth models and further validated with experimental results.

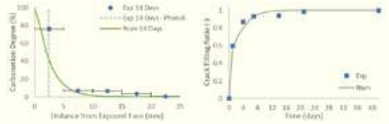

MICRO SCALE CARBONATION

- Autogenous healing of the small crack (1–2-micron width) within 15.75 hours (<1 day) of simulated time.
- The effective rates of:
  - CH dissolution: 1.46×10^{-3} kg/m³/s and
  - $CaCO_3$ precipitation: 1.86×10^{-3} kg/m³/s

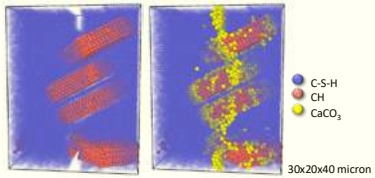

CONCLUSIONS

- Dissolution-precipitation reaction of carbonation in cement paste and microstructure formation simulated using kinetic Monte Carlo theory.
- KMC works at a higher length scale compared to atomistic simulations, each discretized particle representing a molecule. The simulation box sizes can go from nanometer to sub micrometer depending on the computation capacity.
- KMC can sample larger timescales. In KMC time is calculated as inverse of cumulative rate. Thus, depending on the likelihood of dissolution and precipitation, these simulations can sample larger timescales.

REFERENCES

- Coopamootoo, Kumaran, and Enrico Masoero. The Journal of Physical Chemistry C 124.36 (2020): 19603-19615.
- Shvab, Igor, et al. Crystal Growth & Design 17.3 (2017): 1316-1327.
- Alex, Aleena, et al. Cement and Concrete Composites 144 (2023): 105281.

ADAGIO

Kinetic Monte Carlo simulations of mineral carbonation

Aleena Alex[1]

[1] University of Basque Country, UPV/EHU.

ADAGIO

Leveraging sequential step-growth polymerizations to obtain

Lucas Polo Fonseca[1]
Aritz Lamas[1]
Haritz Sardon[1]

[1] POLYMAT, University of the Basque Country (UPV/EHU) Avenida Tolosa 72, 20018 Donostia-San Sebastian, Spain.

Leveraging sequential step-growth polymerizations to obtain hierarchically phase separated materials with UV-curing

Lucas Polo Fonseca [a], Aritz lamas, and Haritz Sardon[a]
[a] POLYMAT, University of the Basque Country (UPV/EHU)
Avenida Tolosa 72, 20018 Donostia-San Sebastian, Spain

Challenges in lamination of PSA

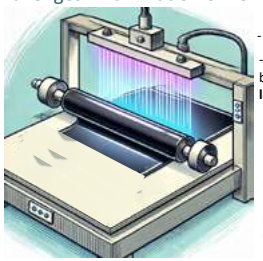

- **Pseudoplastic** resin.
- **Current free-radical polymerization** based **PSAs** need an N_2 **protective layer to avoid O_2 inhibition.**

Increased cost, complexicity, and provides permanent adhesion, with no capacity of easy removal and re-use

Methods, Strategy

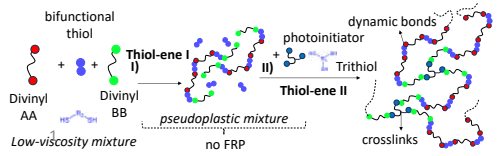

Challenges

- **Potential side-reactions**

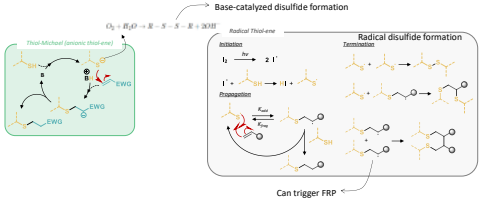

Results

Supressing side reactions

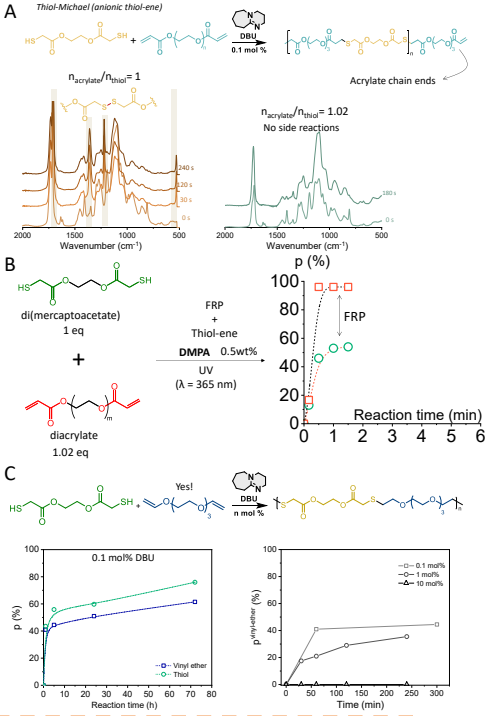

Three formulations, equal composition, distinct polymerization mechanisms

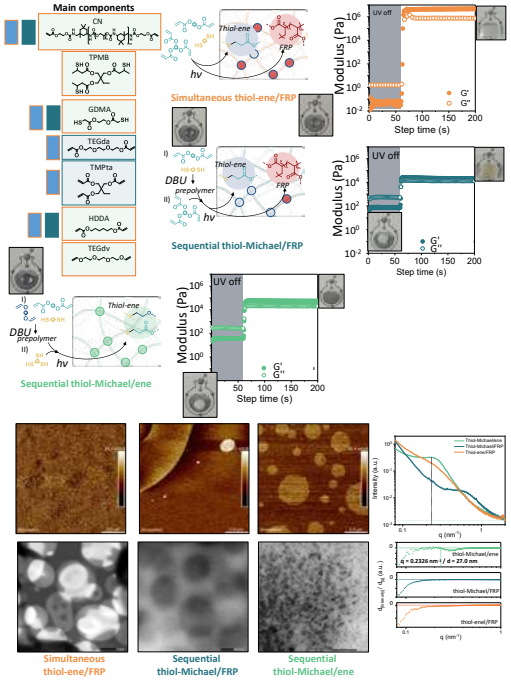

CONCLUSIONS

- Easy two-step sequential protocol that allow hierarchically phase-separated UV-cured resins with supression of side reactions and a full step-growth polymerization mechanism.
- Was applied for PSA manufacturing, future applications include 3D-printing bioMedical devices.

ACKNOWLEDGMENTS

This project has received funding from the European Union's Horizon 2020 research and innovation programme under the Marie Sklodowska-Curie grant agreement No 101034379

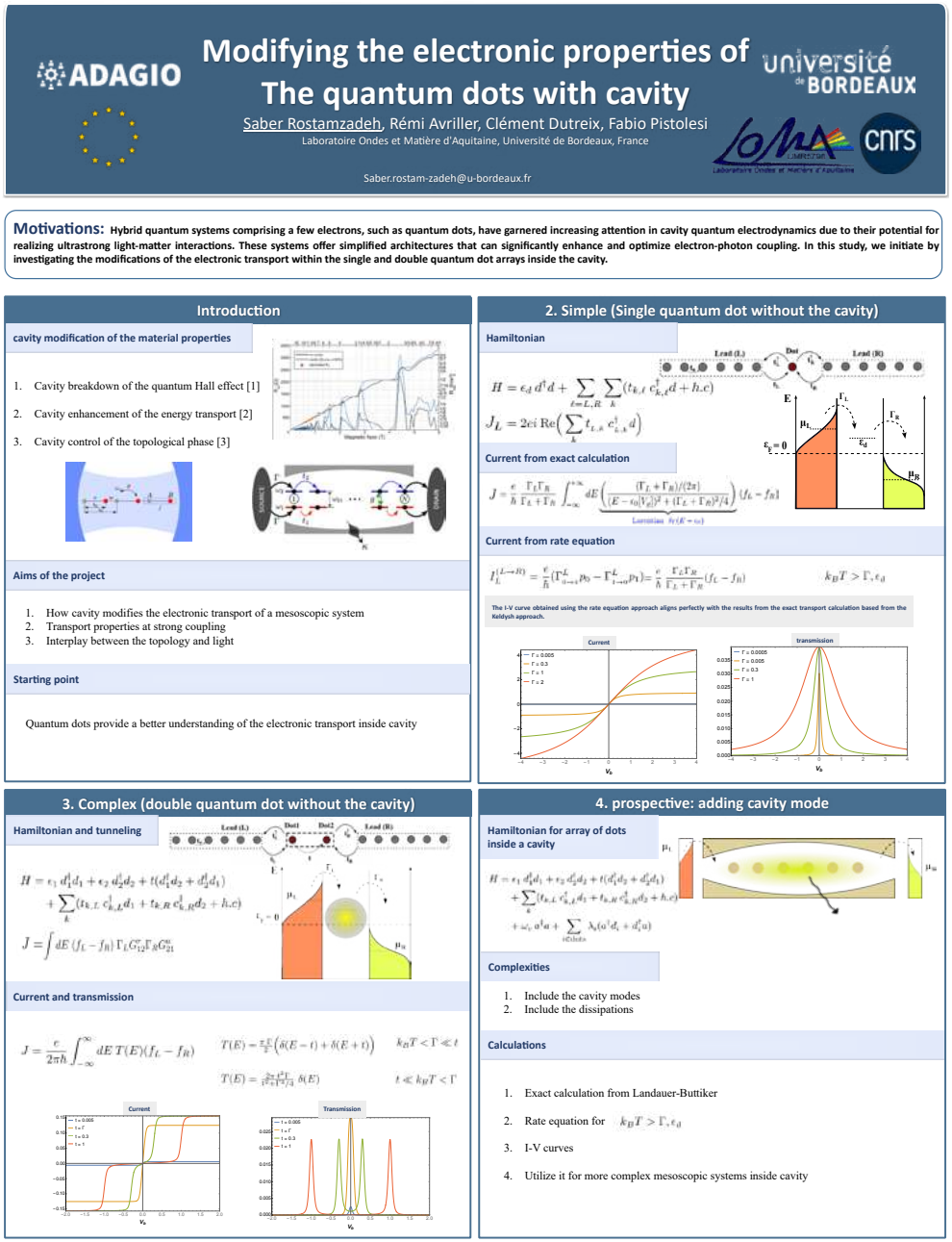

References

1. F. Appugliese, J. Enkner, G. L. Paravicini-Bagliani, M. Beck, C. Reichl, W. Wegscheider, G. Scalari, C. Ciuti, and J. Faist, Science 375, 1030 (2022)
2. D. Hagenmüller, J. Schachenmayer, S. Schütz, C. Genes, and G. Pupillo, Phys. Rev. Lett. 119, 223601 (2017)
3. O. Dmytruk and M. Schiro, Communications Physics 5, 271 (2022)

Acknowledgment

This project has received funding from the European Union's Horizon 2020 research and innovation programme under the Marie Sklodowska-Curie grant agreement No 101034379.

ADAGIO

Modifying the electronic properties of the quantum dots with cavity

Saber Rostamzadeh[1]
Rémi Avriller[1]
Clément Dutreix[1]
Fabio Pistolesi[1]

[1] Laboratoire Ondes et Matière d'Aquitaine, Université de Bordeaux, France.

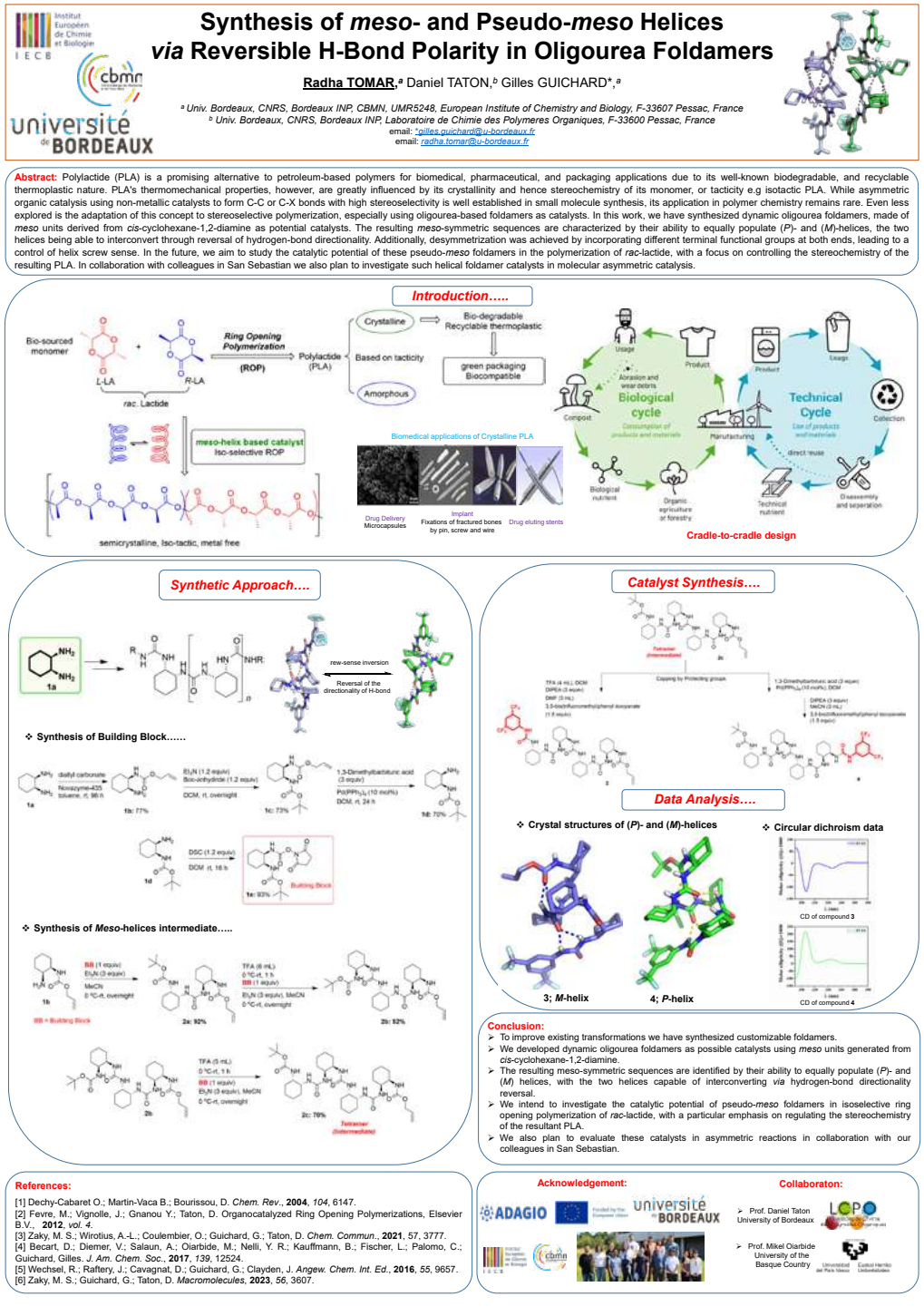

ADAGIO

Synthesis of meso- and Pseudo-meso Helices via Reversible H-Bond Polarity in Oligourea Foldamers

Radha TOMAR[1]
Daniel TATON[2]
Gilles GUICHARD[1]

[1] Univ. Bordeaux, CNRS, Bordeaux INP, CBMN, UMR5248, European Institute of Chemistry and Biology, F-33607 Pessac, France.

[2] Univ. Bordeaux, CNRS, Bordeaux INP, Laboratoire de Chimie des Polymeres Organiques, F-33600 Pessac, France.

1st meeting of the ENLIGHT Interdisciplinary Network on the impact of gender in health

Lucía Gallego[1]
Sandra Sánchez-Urtaza[1]
Laura Alfonso[1]
Elodie Rosanne Santiago[2]
Sofía Villarreal[1]

[1] Faculty of Medicine & Nursing, UPV/EHU.

[2] Faculty of Social and Communication Sciences, UPV/EHU.

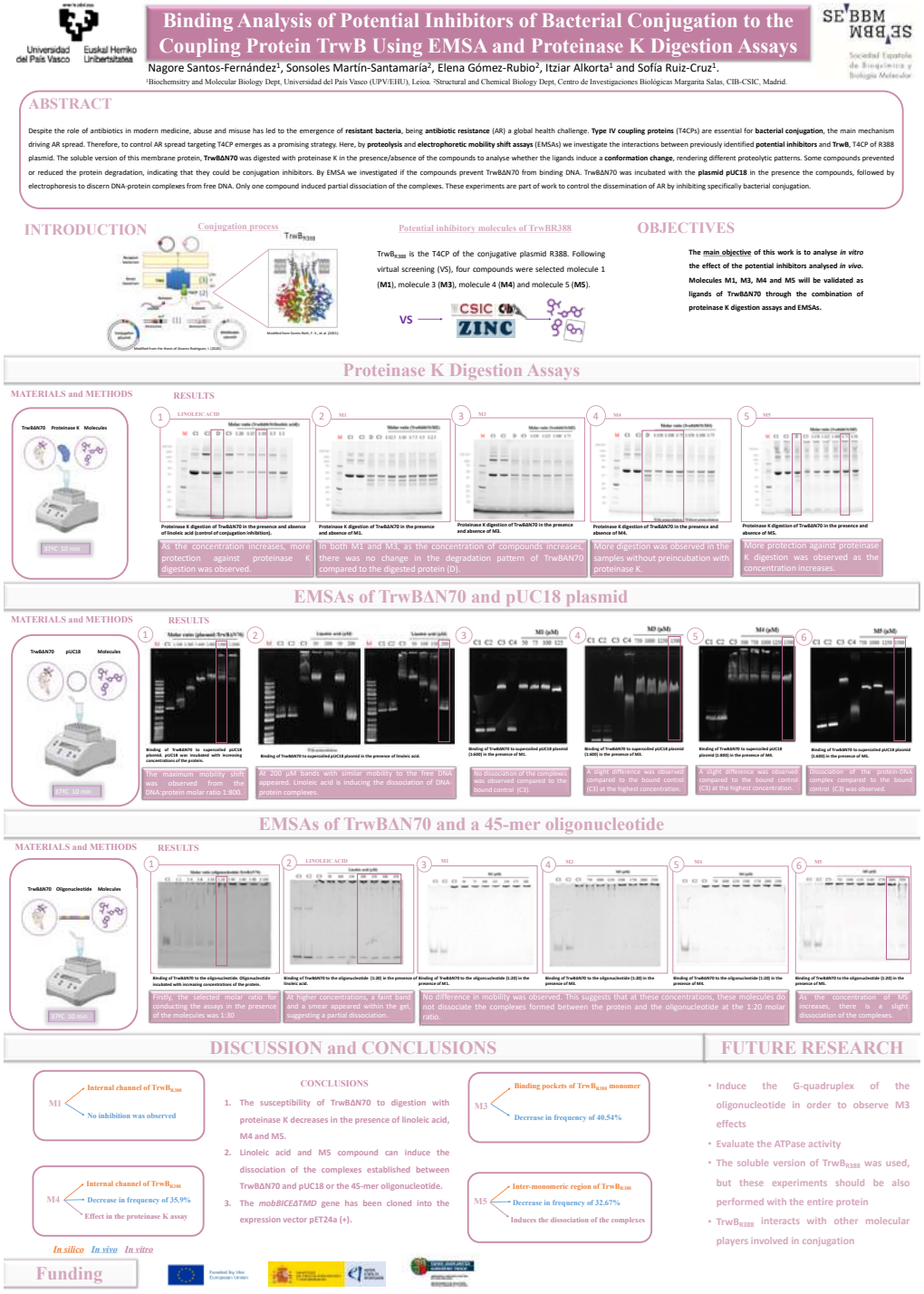

Binding Analysis of Potential Inhibitors of Bacterial Conjugation to the Coupling Protein TrwB Using EMSA and Proteinase K Digestion Assays

Nagore Santos-Fernández[1]
Sonsoles Martín-Santamaría[2]
Elena Gómez-Rubio[2]
Itziar Alkorta[1]
Sofía Ruiz-Cruz[1]

[1] Biochemsitry and Molecular Biology Dept, Universidad del País Vasco (UPV/EHU), Leioa.

[2] Structural and Chemical Biology Dept, Centro de Investigaciones Biológicas Margarita Salas, CIB-CSIC, Madrid.

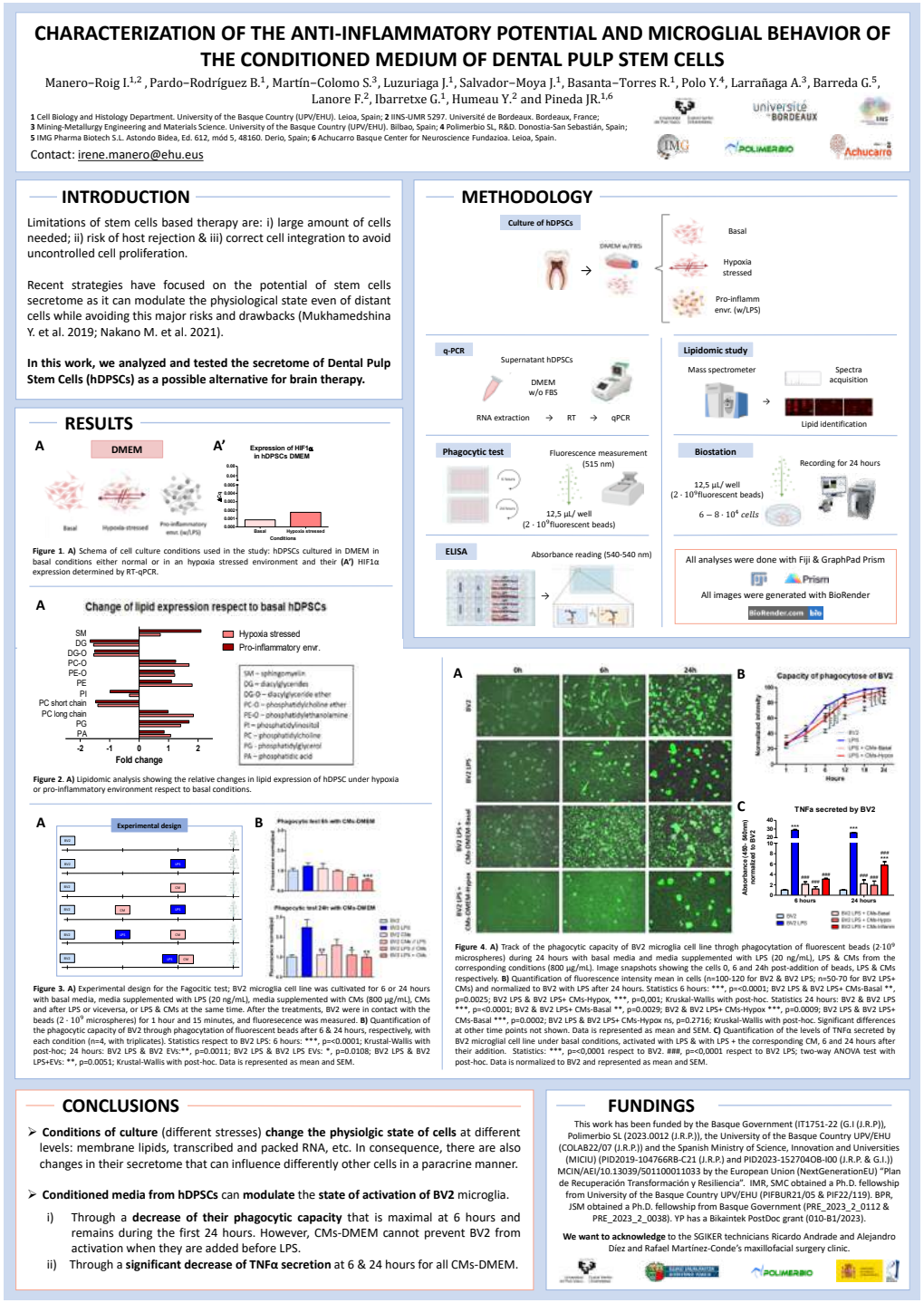

Characterization of the anti-inflammatory potential and microglial behavior of the conditioned medium of Dental Pulp Stem Cells

Manero–Roig I.[1,2]
Pardo–Rodríguez B.[1]
Martín–Colomo S.[3]
Luzuriaga J.[1]
Salvador–Moya J.[1]
Basanta–Torres R.[1]
Polo Y.[4]
Larrañaga A.[3]
Barreda G.[5]
Lanore F.[2]
Ibarretxe G.[1]
Humeau Y.[2]
Pineda JR.[1,6]

[1] Cell Biology and Histology Department. University of the Basque Country (UPV/EHU). Leioa, Spain.

[2] IINS-UMR 5297. Université de Bordeaux. Bordeaux, France.

[3] Mining-Metallurgy Engineering and Materials Science. University of the Basque Country (UPV/EHU). Bilbao, Spain.

[4] Polimerbio SL, R&D. Donostia-San Sebastián, Spain.

[5] IMG Pharma Biotech S.L. Astondo Bidea, Ed. 612, mód 5, 48160. Derio, Spain.

[6] Achucarro Basque Center for Neuroscience Fundazioa. Leioa, Spain.

Conceptual model to evaluate the practices and uses of the fundamentals of Storytelling in the narratives of corporate websites.

Author: Beatriz Donayre Guerrero
Field: Social Communication
Director: Sergio Monge

Abstract

The narratives of corporate websites represent windows to the world of brands and organizations that surround the everyday environment. However, depending on how their content is presented, they can go unnoticed, or on the contrary, they can impact, captivate and show a vital commitment to their audiences and society.

Corporate websites are spaces where the energy of the content can transport the public towards paths of emotions and transformations, just as happens with the stories. But, this does not have to do with using literally a story and presenting it chronologically in some section of the website, but rather with studying and analyzing the theoretical foundations of storytelling and then applying them systematically.

Main objective

This research proposes the development of a conceptual model based on the foundations of storytelling to evaluate and analyze its use on the websites of corporations from the ranking of Great Place to Work companies, that is, organizations with a positive global rating regarding their culture and internal communication, but what about their external communication through their websites? Do they generate content that impacts and transcends?

Results

Two types of approaches: functional and symbolic.

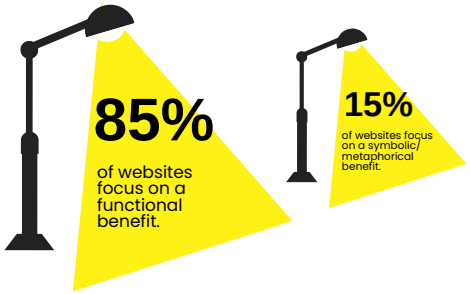

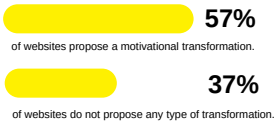

Methodology

Content analysis

Other elements that were included in the conceptual model:

Emotions | Plot | Goals | Arquetypes | Mental Metaphor

Conclusions

The analysis revealed two approaches: the narrative/symbolic perspective and the functional/rational perspective. The first arises from verifying its connection with key elements from the theory of storytelling. And the second one is associated with more conventional and predictable content.

Thus, storytelling, the ancient art of telling, joins the world of communication to propose improvements and changes in corporate narratives, always starting with the question: how to generate transcendence and meaning?, not only for today, but also for the future.

References

Escalas, J. (2004). **Narrative Processing:Building Consumer Connections to Brands**. Journal of Consumer Psychology, 14 (1&2), 168-180.
Moin, S. M.A. (2020). **Brand Storytelling in the Digital Age**. London: Palgrave Macmillan.
Spear, S. (2015). **The Role and Significance of Corporate Stories in Corporate Reputation Management.** (Phd Thesis). University of Portsmouth.

Conceptual model to evaluate the practices and uses of the fundamentals of Storytelling in the narratives of corporate websites

Beatriz Isabel Donayre Guerrero[1]

[1] University of the Basque Country UPV/EHU.

How Contrastive Learning overcomes Domain Shift in classification tasks

Alexander Olza[1]
Roberto Santana[1]
David Soto[2]
Michaël Clément[3]

[1] Intelligent Systems Group, Faculty of Informatics, University of Basque Country (UPV/EHU), Donostia- San Sebastián, Spain.

[2] Basque Center for Cognition, Brain and Language (BCBL), Donostia-San Sebastián, Spain.

[3] Laboratoire Bordelais de Recherche en Informatique (LaBRI), Bordeaux, France.

How Contrastive Learning overcomes Domain Shift in classification tasks

Alexander Olza[1], Roberto Santana[1], David Soto[2], Michaël Clément[3]

1 Intelligent Systems Group, Faculty of Informatics, University of Basque Country (UPV/EHU), Donostia- San Sebastián, Spain
2 Basque Center for Cognition, Brain and Language (BCBL), Donostia- San Sebastián, Spain
3 Laboratoire Bordelais de Recherche en Informatique (LaBRI), Bordeaux, France

Definitions

Domain Shift occurs when the probability distribution of the data used to train a model (source domain - SD) differs from the probability distribution of the testing data (target domain - TD). The goal of modelling is to be accurate in the testing scenario, but a model trained on the source domain is not guaranteed to retain performance in the target domain.

Given a dataset and a notion of similarity between its samples, Contrastive Learning (CL) techniques learn a new representation (the latent space) by bringing related samples closer to each other and maximizing separation to unrelated samples.

Objectives

Define a similarity notion for a binary classification task with two domains, and use CL to reduce the domain shift in the representation.

Defining similarity

- The different classes in the source domain must be apart in the latent space
- Class i from the TD must be close to class i from the SD
- Class i from the TD must be far from class j from the SD

Training & evaluating the representation

Training
- Define a representation function: we have used a MLP.
- Assign a label matrix (Fig. 1) for the data using our similarity notion.
- Translate raw data to the latent space.
- Compute a pairwise similarity of all samples in the latent space, and use a sigmoid to express that as a probability.
- Compute the binary cross-entropy between the pairwise similarity and the label matrix.

Fig. 1: Label matrix

Evaluating
- Baseline: Fit a Logistic Regression (LR) in data from the source domain, in the original feature space. Evaluate it in data from the target domain.
- Evaluation of CL: Use the same instances involved in the baseline, but represent them in the latent space. Fit a LR in the source domain instances and evaluate it in the target domain instances.

Generating synthetic data

Source domain:
Classes 0 and 1 come from two overlapping 400-dimensional gaussian distributions (N=3000).

Target domain:
The relationship between classes 0 and 1 is maintained, but the mean and scale of the gaussians has changed (N=3000).

The 2-dimensional representation using TSNE shows the domain shift (Fig. 2)

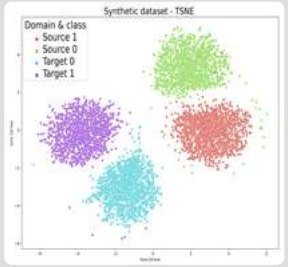

Fig. 2: Visualization of the dataset

Results

Visualization of the latent space

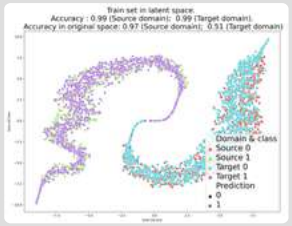

Fig. 3: Latent space representation of instances used for CL training

Fig. 3 shows that the latent space has aquired the desired structure: Source instances from different classes are apart from each other, ensuring a good source classification, and target instances from each class have a similar representation to source instances from their corresponding class, ensuring applicability of the source classifier.

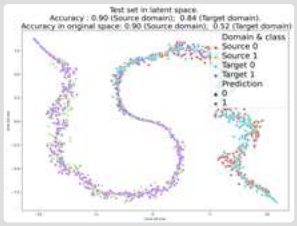

Fig. 4: Latent space representation of instances not used for CL training

Fig. 4 shows that the representation funtion (MLP) generalizes well to unseen samples: The domain shift is reduced, and the unseen instances form separable clusters in terms of class but not domain in the latent space.

Impact on cross-domain classification

Fig. 5 shows that the new representation significantly increases the accuracy of the source classifier when applied to the target domain.

Blue represents the accuracy accross 50 folds of a source classifier applied to the target test set using the original space (the baseline).

Orange represents the accuracy of the source classifier, built and tested on the same data, but using the contrastive latent space.

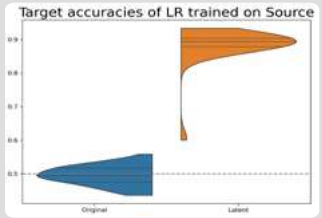

Fig. 5: Classification performance

Conclusions & Future Work

- For the samples used during CL training, the latent space effectively solves the domain shift problem (Fig. 3).
- This generalizes well to unseen samples (Fig. 4).
- Classification results in the target domain improve notably due to the CL representation.
- Moving forward, we will apply this method to real-world scenarios, particularly in the field of Neuroscience.

Contact

alexander.olza@ehu.eus

Acknowledgements

This work has been supported by the Basque Government via the IKUR strategy, project IT1504-22 and the BERC 2022-2025 program, by the Spanish Ministry of Science and Innovation (PID2022-137442NB-I00), by Elkartek (KK-2023/00090), by the Spanish Ministry of Economy and Competitiveness, through the 'Severo Ochoa' Programme for Centres/Units of Excellence (CEX2020-001010-S) and also from project grant PID2019-105494GB-I00.

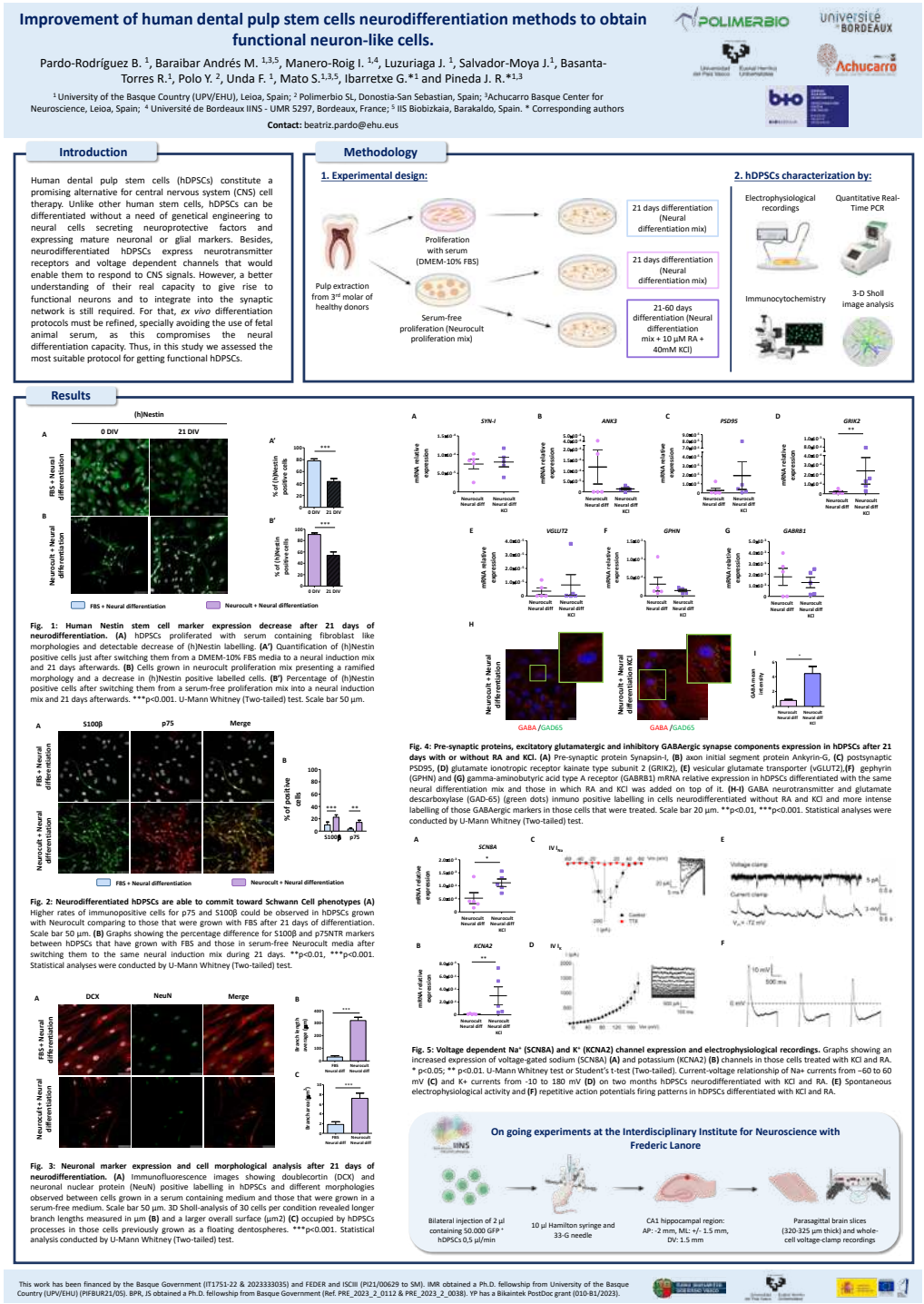

Improvement of human dental pulp stem cells neurodifferentiation methods to obtain functional neuron-like cells

Pardo-Rodríguez B.[1]
Baraibar Andrés M.[1,3,5]
Manero-Roig I.[1,4]
Luzuriaga J.[1]
Salvador-Moya J.[1]
Basanta-Torres R.[1]
Polo Y.[2]
Unda F.[1]
Mato S.[1,3,5]
**Ibarretxe G.*[1]
**Pineda J.R.*[1,3]

[1] University of the Basque Country (UPV/EHU), Leioa, Spain.
[2] Polimerbio SL, Donostia-San Sebastian, Spain.
[3] Achucarro Basque Center for Neuroscience, Leioa, Spain.
[4] Université de Bordeaux IINS - UMR 5297, Bordeaux, France.
[5] IIS Biobizkaia ,Barakaldo, Spain.
*Corresponding authors. These authors contributed equally to this work.

Machine Learning Algorithms for Estimating Mooring Line Tensions of Floating Wind Turbines

Max Kämmerling[1,2]
Vincenzo Nava [1,3]
Javier Del Ser[1,2]

[1] TECNALIA, Basque Research & Technology Alliance (BRTA).
[2] University of the Basque Country (UPV/EHU).
[3] Basque Center for Applied Mathematics (BCAM).

MACHINE LEARNING ALGORITHMS FOR ESTIMATING MOORING LINE TENSIONS OF FLOATING WIND TURBINES

Max Kämmerling[a,c], Vincenzo Nava[a,b], Javier Del Ser[a,c]
(maximilian.kammerling@tecnalia.com)
[a] TECNALIA, Basque Research & Technology Alliance (BRTA), 48160 Derio, Spain
[b] Basque Center for Applied Mathematics (BCAM), 48009 Bilbao, Spain
[c] University of the Basque Country (UPV/EHU), 48013 Bilbao, Spain

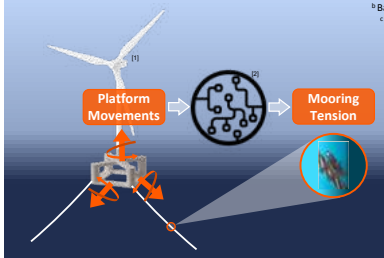

Virtual sensor based on machine learning shows the potential to **replace physical sensor for measuring mooring line tensions** but needs to be further improved for sea states underrepresented in the training data.

[1] Source: Tecnalia Research & Investigation
[2] Oksana Latysheva (2017): Artificial Intelligence. Available online, checked on 22/08/2024

1. Motivation

- Mooring systems are critical subsystems of Floating Offshore Wind Turbines (FOWTs) that require reliable monitoring.
- Direct measurement of mooring tensions is challenging and expensive due to submerged and harsh offshore conditions.
- Indirect estimation of mooring tensions using machine learning is explored in this study as an alternative approach.
- The floater's motions are used as input, as they are easier to measure and offer greater robustness.

2. Use Case

- Measurements were used from a 1/13.6 scaled wave tank model of HarshLab2, a floating laboratory owned by Tecnalia Research & Innovation.
- 15-min runs of 12 different sea states were conducted in a wave tank.
- The floater's motions in six Degrees of Freedom using an optical tracking system and mooring tensions in the three catenary mooring lines using load cells were measured.

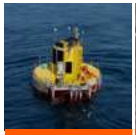

Real scale floating laboratory HarshLab2

Small scale wave tank model of HarshLab2 that provided training data for this study

Chain and load cell of wave tank model's mooring system

3. Machine Learning Model

- A Support Vector Regressor (SVR) with a nonlinear kernel was used.
- The SVR model was trained on data from nine sea states and tested on three held-out sea states.

4. Results

- The model demonstrated strong performance, achieving an R^2 greater than 92% and an average RMSE below 0.9N for all sea states.
- The model's performance diminished for sea conditions not well represented in the training data, showing limited generalization capability.

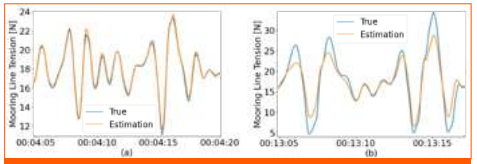

Time series segment of estimations (orange lines) and observed values (blue lines) of mooring line tension of test sea states 62 (a), test sea state 69 (b)

Characteristics of sea states in training and test data and corresponding performance metrics of the SVR model

Run N°	H_s [m, real scale]	T_P [s, real scale]	Dataset	R^2 [%]	RMSE [N]
58	1	5.79	train	98.98	0.1405
59	1	7.72	test	92.18	0.2188
60	1.36	9.65	train	98.45	0.0927
61	1.88	6.87	train	99.44	0.1432
62	1.88	9.15	test	98.48	0.1667
63	1.88	11.44	train	98.44	0.1000
71	2.04	14	train	97.97	0.1016
64	3	7.79	train	99.56	0.1923
65	3	10.39	train	99.22	0.1653
66	3	12.98	train	99.21	0.1672
69-70	4.3	12.29	test	94.01	0.7102
67-68	5.6	9.22	train	97.99	0.8792

5. Future Outlook

- For the remainder of our PhD research the identified generalization problem under unknown sea conditions will be addressed.
- Several other use cases are planned to be investigated, such as wave tank models of FOWTs and, if available, real scale devices installed in offshore conditions.

Microscopic insight on cementitious materials using radiation-scattering techniques

Tomas Stephen Northam de la Fuente[1], Cristina Macia-Castello[1], Guido Goracci[1], Iñigo Galindo[2], Sonia Garcia[2], Santiago Sanz[2], Gustavo Sarmiento[2], Jorge Dolado[1,3] and Felix Fernandez-Alonso[1,3,4]

[1]Materials Physics Center, CSIC-UPV/EHU, Paseo Manuel de Lardizabal 5, 20018 Donostia - San Sebastian, Spain.
[2]SUPRASYS, Avda. Lehendakari Aguirre, 11, 7º, Dpto. 7, 48014 Bilbao, Spain.
[3]Donostia International Physics Center (DIPC), Paseo de Manuel Lardizabal 4, 20018 Donostia - San Sebastian, Spain.
[4]IKERBASQUE, Basque Foundation for Science, Plaza Euskadi 5, 48009 Bilbao, Spain.

Why concrete?

- Cement is the most used synthetic material, with its global production still increasing.

- Great efforts are needed to develop new and more sustainable mortars.

- Despite centuries of studies, basic questions still remain poorly understood.

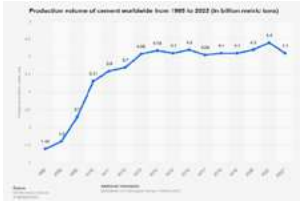

Figure 1: Evolution of global cement production.

Laboratory techniques

- Differential scanning calorimetry (DSC) can be used to study the isotope effect of hydration.

- Figure 2 shows the hydration medium affects on the reaction time of the C_3S.

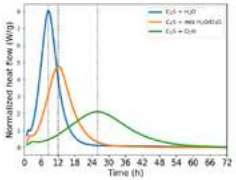

Figure 2: Heat flow evolution of C_3S hydration with different deuteration levels.

- Raman spectroscopy allows the mapping of surfaces of new types of cements.

- This gives information on the main phases composing the material, as shown in figure 3 for a cement that contains portlandite, calcite and a gel phase.

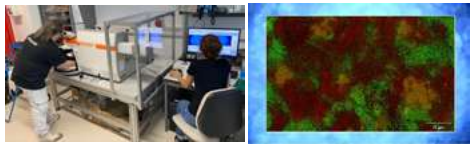

Figure 3: (right) in-Via Reflex Raman by Renishaw (Left) Raman surface mapping of a cement with portlandite (yellow) and calcite (red).

Neutrons (at international facilities)

- Inelastic neutron scattering (INS) can see what Raman can't.

- Figure 4 shows the different lattice and molecular modes of C_3S due to 1 or 2 protons from the hydration.

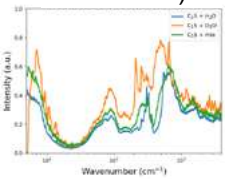

Figure 4: INS spectra of C_3S hydration with different deuteration levels

- Neutron imaging is used to analyze the structure of a material.

- Figure 5 shows the structure of cement foam (CF).

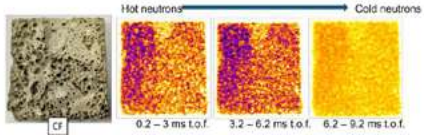

Figure 5: Energy-resolved neutron imaging of CF.

Suprasys (collaboration with industry)

- Development of new equipment for in-situ calorimetry and neutron scattering experiments.

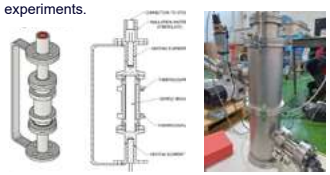

Figure 6. (left) Concept design, (center) technical design and (right) testing and commissioning.

Next steps

- Understand the effects of having different concentrations of portlandite and calcite.

- Obtain information of the structural changes upon deuteration.

- Perform the first measurements with the Suprasys prototype.

References

[1] Fateh Belaïd, Resources, Conservation & Recycling Advances, Volume 15, (2022).
[2] Karen Scrivener *et al.*,, Cement and Concrete Research, Volume 124, (2019).
[3] Guido Goracci *et al.*,, ACS Sustainable Chem. Eng., Volume 12, (2024)

Microscopic insight on cementitious materials using radiation-scattering techniques

Tomas Stephen Northam de la Fuente[1]
Cristina Macia-Castello[1]
Guido Goracci[1]
Iñigo Galindo[2]
Sonia Garcia[2]
Santiago Sanz[2]
Gustavo Sarmiento[2]
Jorge Dolado[1,3]
Felix Fernandez-Alonso[1,3,4]

[1] Materials Physics Center, CSIC-UPV/EHU, Paseo Manuel de Lardizabal 5, 20018 Donostia - San Sebastian, Spain.

[2] SUPRASYS, Avda. Lehendakari Aguirre, 11, 7º, Dpto. 7, 48014 Bilbao, Spain.

[3] Donostia International Physics Center (DIPC), Paseo de Manuel Lardizabal 4, 20018 Donostia - San Sebastian, Spain.

[4] IKERBASQUE, Basque Foundation for Science, Plaza Euskadi 5, 48009 Bilbao, Spain.

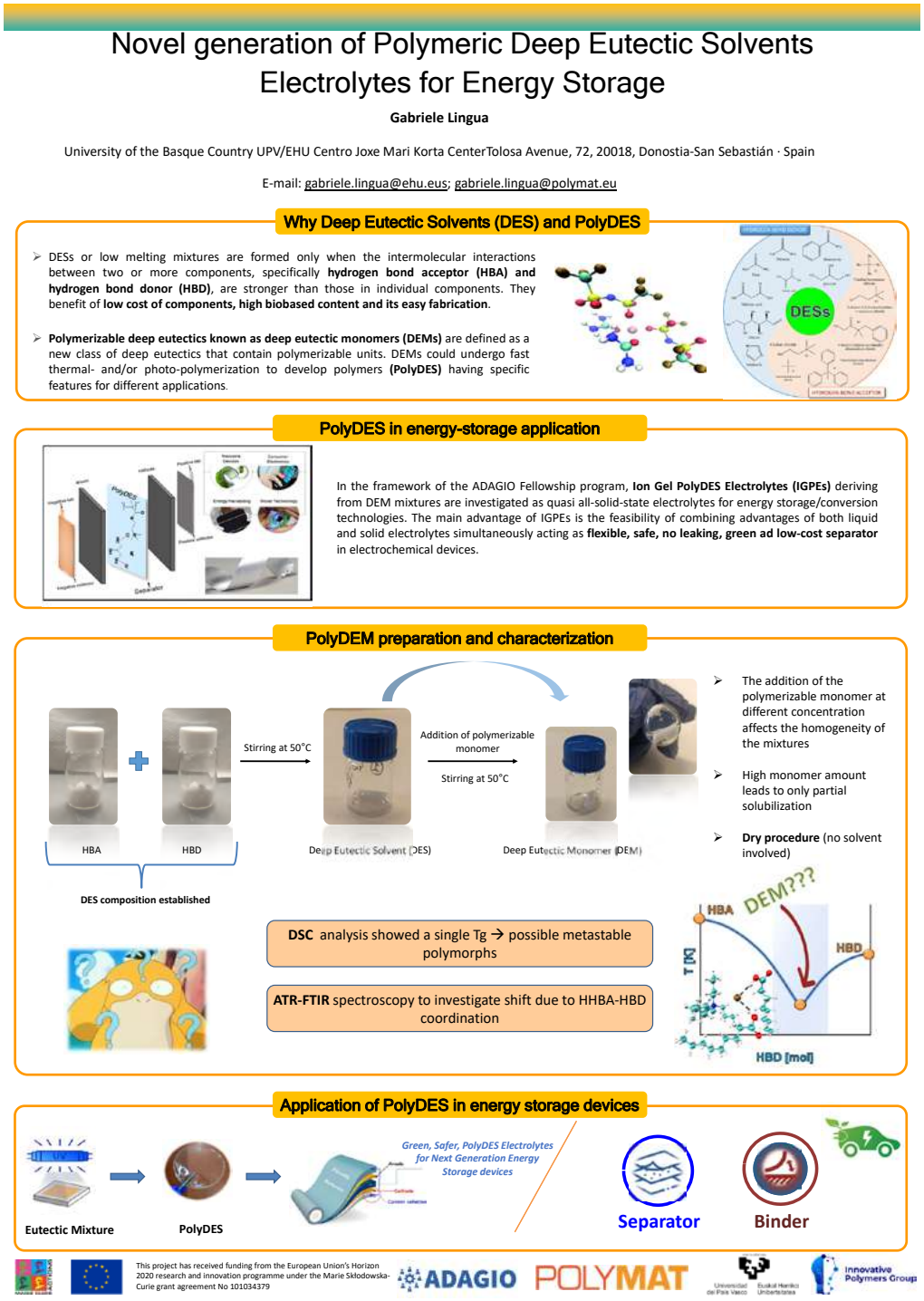

Novel generation of Polymeric Deep Eutectic Solvents Electrolytes for Energy Storage

Gabriele Lingua[1]
Jon Lopez de Lacalle[1]
Matias Picchio[1,2]
David Mecerreyes[1,2]

[1] POLYMATUniversity of the Basque Country UPV/EHUAvenida Tolosa 72, Donostia-San Sebastian, Gipuzkoa 20018, Spain.

[2] IKERBASQUE Basque Foundation for Science María Díaz de Haro 3, Bilbao 48013, Spain.

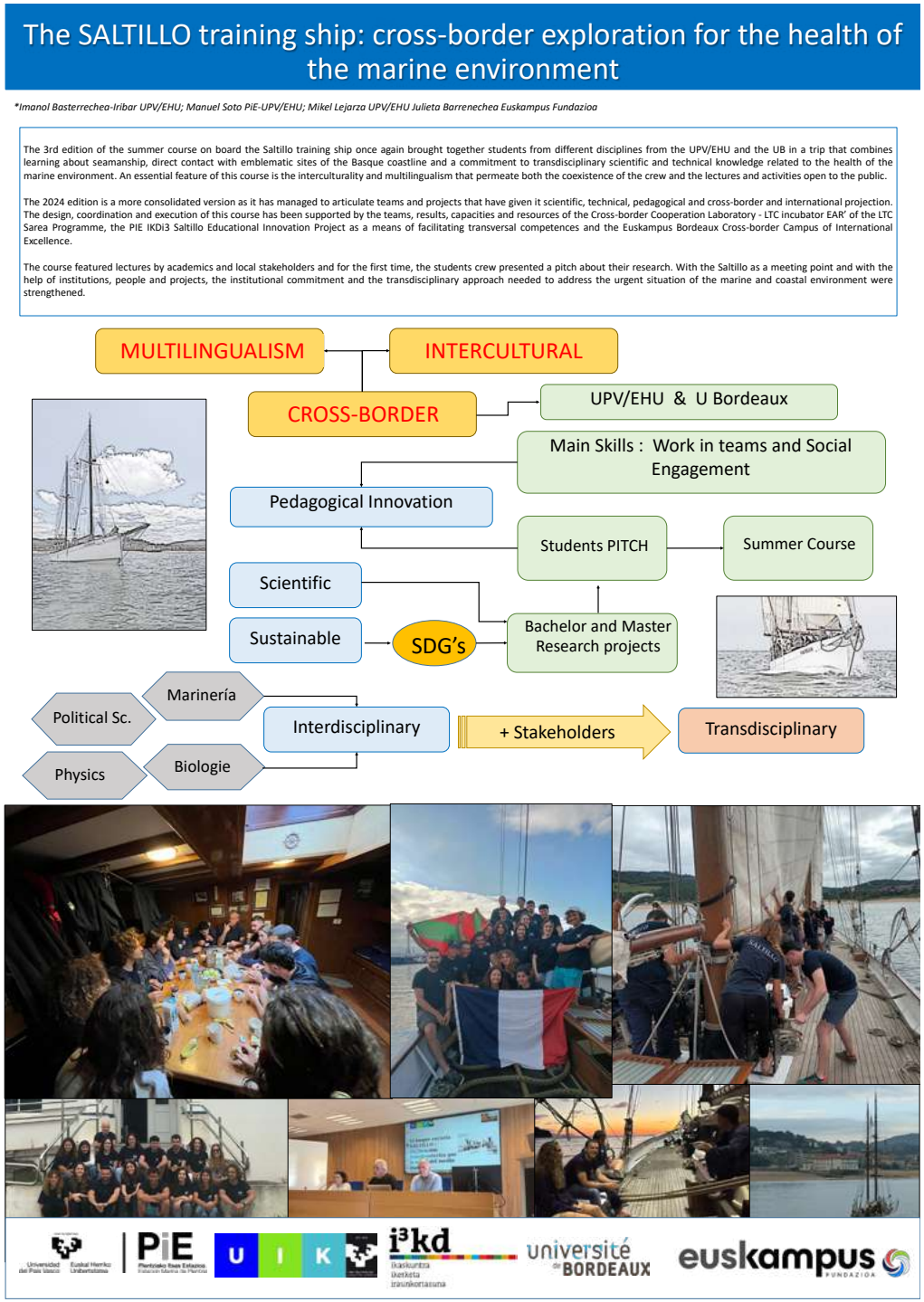

The SALTILLO training ship: cross-border exploration for the health of the marine environment

Imanol Basterretxea-Iribar[1]
Manuel Soto[2]
Mikel Lejarza[1]
Julieta Barrenechea[3]

[1] UPV/EHU.
[2] PiE-UPV/EHU.
[3] Euskampus Fundazioa.

Whole genome sequencing of multidrug resistant *Acinetobacter baumannii* isolates from a hospital from Paraguay

Laura Alfonso[1], Sandra Sánchez-Urtaza[1], Alain Ocampo-Sosa[2], Ruth González[3], Evelyn López[3], Itziar Alkorta[4], Paul G. Higgins[5,6], Lucia Gallego[1]

[1]Laboratory of Antibiotics and Molecular Bacteriology, Department of Immunology, Microbiology and Parasitology, Faculty of Medicine and Nursing, University of the Basque Country, Leioa, Spain. [2]Microbiology Service, University Hospital Marqués de Valdecilla, Valdecilla Health Research Institute (IDIVAL), Santander, Spain. [3]Laboratory of Microbiology, National Hospital of Itauguа, Itaugua, Paraguay. [4] Department of Biochemistry and Molecular Biology, Faculty of Science and Technology, University of the Basque Country, Leioa, Spain. [5] Institute for Medical Microbiology, Immunology and Hygiene, Faculty of Medicine and University Hospital Cologne, University of Cologne, Cologne, Germany. [6]German Center for Infection Research (DZIF), Partner site Bonn-Cologne, Cologne, Germany

BACKGROUND

Acinetobacter baumannii is a pathogen of great clinical importance, capable of causing severe nosocomial infections and acquiring resistance to antimicrobials, specifically carbapenems. Due to the threat to global public health, the World Health Organization classified carbapenem-resistant *A. baumannii* as a priority 1 (critical) pathogen for research and development of new antibiotics. In Latin America, a high rate of carbapenem resistance in *A. baumannii* has been detected, as well as the circulation of some international clones, however, Paraguay is one of the countries with a limited database in this regard. Therefore, the aim of this work was to study multidrug-resistant *Acinetobacter baumannii* clinical isolates from the National Hospital of Itaugua, Paraguay, using molecular biology techniques such as Whole Genome Sequencing (WGS).

MATERIALS AND METHODS

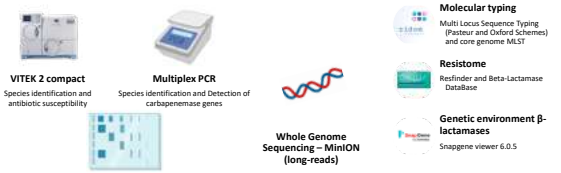

RESULTS

Data analysis from the National Hospital of Itaugua

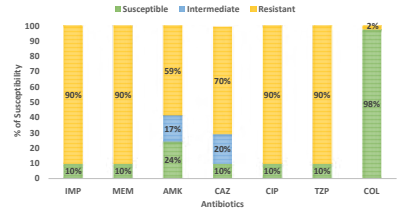

Figure 1. Percentages of antibiotic susceptibility of *A. baumannii* isolates recovered from December 2023 to February 2024. IMP: imipenem, MEM: meropenem, CAZ: ceftazidime, AMK: amikacin, SAM: ampicillin/sulbactam, CIP: ciprofloxacin, GEN: gentamicin.

Virulome analysis of *A. baumannii* isolates from Paraguay

Table 2. Virulence associated genes identified in *Acinetobacter baumannii* isolates.

Adherence, biofilm formation and immune system modulation	*Acinetobacter* Trimeric Autotransporter	*ata*
	Biofilm Controlling Response Regulator	*bfmR, bfmS*
	Efflux pumps AdeFGH	*adeF, adeG, adeH*
	Quorum Sensing	*abaI, abaR*
	Pili csu*	*csuA/B, csuA, csuB, csuC, csuD, csuE*
	Biofilm Associated Protein	*bap*
	Outer Membrane Protein	*ompA*
	Poly-β-1,6-N-acetyl-D-glucosamine	*pgaA, pgaB, pgaC, pgaD*
	Capsule (Capsular type)	PR1, PR2, PR3, PR8: OCL1/KL3 – PR4, PR5, PR6: OCL1/KL81 – PR7: OCL10/KL9
	Lipopolysaccharide	*lpsB, lpxA, lpxB, lpxC, lpxD, lpxL, lpxM*
	Penicillin-Binding Protein G	*pbpG*
Secretion systems	Type II secretion system	*gspC, gspD, gspE1, gspE2, gspF, gspG, gspL, gspM, gspK, gspI, gspH, gspN*
	Type VI secretion system	*tssA, tssB, tssC, tssE, tssF, tssG, tssK, tssH, tssL, tssM, tagX*
Exotoxins	Phospholipases C and D	*plc1, plc2, plcD*
Iron uptake	Acinetobactins	*barA, barB, basA, basB, basC, basD, basF, basG, basH, basI, basJ, bauA, bauB, bauC, bauD, bauE, bauF, entE*

*In the isolated PR6 genes associated with csu pili have not been detected.

Resistome and plasmidome analysis of *A. baumannii* isolates from Paraguay

Table 1. Characteristics of the carbapenem resistant isolates from the National Hospital of Itaugua (Paraguay) regarding the clonal lineage, resistance genes and plasmid profile.

Isolate	International Clone (IC)	ST Pasteur	ST Oxford	β-lactamase genes	Other resistance genes	Plasmids (kb)	Replicon typing-PCR	Replicases (*Acinetobacter* Plasmid Typing Database)
PR1	IC2	ST2	ST1816, ST195	bla_{OXA-65} bla_{OXA-66} bla_{OXA-23} bla_{ADC-25}	*arm(A), aph(6)-Id, aph(3'')-Ib, msr(E), mph(E), tet(B)*	10.4	GR2 (Ac1/Ac2), GR19 (rep135040)	Rep_3 family protein R3-T60
PR2				bla_{OXA-65} bla_{OXA-66} bla_{OXA-23} bla_{ADC-25}	*arm(A), aph(6)-Id, aph(3'')-Ib, msr(E), mph(E), sul1, cat(A)1, tet(B)*	10.3	GR2 (Ac1/Ac2), GR19 (rep135040)	
PR3				bla_{OXA-65} bla_{OXA-66} bla_{OXA-23} bla_{ADC-25}	*arm(A), aph(6)-Id, aph(3'')-Ib, msr(E), mph(E), sul1, cat(A)1, tet(B)*	10.4	GR2 (Ac1/Ac2), GR19 (rep135040)	
PR4				bla_{OXA-65} bla_{OXA-66} bla_{OXA-23} bla_{ADC-25}	*arm(A), aph(6)-Id, aph(3'')-Ib, msr(E), mph(E), sul1, cat(A)1, tet(B)*	10.4 / 2.1	GR2 (Ac1/Ac2), GR19 (rep135040)	
PR5			ST872	bla_{OXA-65} bla_{OXA-66} bla_{OXA-23} bla_{ADC-25}	*arm(A), aph(6)-Id, aph(3'')-Ib, msr(E), mph(E), sul1, cat(A)1, tet(B)*	10.3 / 2	GR2 (Ac1/Ac2), GR19 (rep135040)	
PR6				bla_{OXA-66} bla_{OXA-23} bla_{ADC-25}	*aph(6)-Id, aph(3'')-Ib, sul1, cat(A)1, tet(B)*	10.4 / 2.1	GR2 (Ac1/Ac2), GR19 (rep135040)	-
PR7	IC5	ST79	ST1283	bla_{OXA-65} bla_{OXA-23} bla_{TEM-1A} bla_{ADC-6}	*aph(6)-Id, aph(3'')-Ib, aadA1, aph(3')-VIa, sul2, dfrA1*	13.6	GR4 (Ac4), GR19 (rep135040)	-
PR8	IC2	ST2	ST1816, ST195	bla_{OXA-65} bla_{OXA-23} bla_{ADC-25}	*arm(A), aph(6)-Id, aph(3'')-Ib, msr(E), mph(E), sul1, cat(A)1, tet(B)*	10.9	GR2 (Ac1/Ac2)	Rep_3 family protein R3-T60

Analysis of the homology between strains of the international clone IC2 from Paraguay and Alexandria (Egypt)

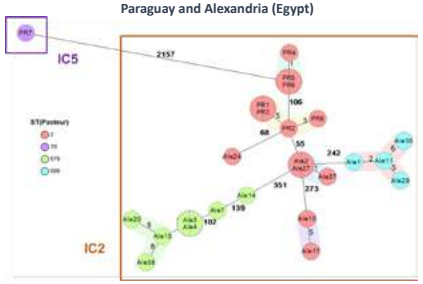

Figure 2. Minimum spanning tree generated with Ridom SeqSphere+ based on a core genome of 2390 alleles using isolates from the National Hospital of Itaugua (Paraguay) and isolates from hospitals in Alexandria (Egypt). The isolates are coloured according to the Pasteur ST and grouped into the international clones to which they belong.

CONCLUSIONS

The presence of multiple resistance genes was demonstrated, including the carbapenemase genes bla_{OXA-65}, bla_{OXA-66} and bla_{OXA-23} in all isolates. Plasmid analysis showed that all strains carried plasmids belonging to replicase groups GR2, GR4 and GR19. Additionally, a large number of virulence genes were detected and most of which stimulate biofilm formation. The isolates were grouped into international clones, finding that most isolates belonged to IC2, an emerging clone in South America, and a single isolate pertaining to IC5, known as the Pan-American clone. This work describes for the first time the circulation of the emerging IC2 clone in Paraguay including a detailed analysis of the resistome, virulome and plasmidome in carbapenem-resistant *A. baumannii* strains.

FUNDING

This work was financially supported by the Department of Education of the Basque Government (Grant N. IT1578-22) and the Ministry of Science and Innovation of the Spanish Government (Grant N. PID2020-116495RB-I00). Dr. Sandra Sánchez-Urtaza is funded by the Basque Government's Postdoctoral Fellowship 2023-2026.

lua.alfonso@gmail.com

Whole genome sequencing of multidrug resistant Acinetobacter baumannii isolates from a hospital from Paraguay

Laura Alfonso[1]
Sandra Sánchez-Urtaza[1]
Alain Ocampo-Sosa[2]
Ruth González3, Evelyn López[3]
Itziar Alkorta[4]
Paul G. Higgins[5,6]
Lucia Gallego[1]

[1] Laboratory of Antibiotics and Molecular Bacteriology, Department of Immunology, Microbiology and Parasitology, Faculty of Medicine and Nursing, University of the Basque Country, Leioa, Spain.

[2] Microbiology Service, University Hospital Marqués de Valdecilla, Valdecilla Health Research Institute (IDIVAL), Santander, Spain.

[3] Laboratory of Microbiology, National Hospital of Itaugua, Itaugua, Paraguay.

[4] Department of Biochemistry and Molecular Biology, Faculty of Science and Technology, University of the Basque Country, Leioa, Spain.

[5] Institute for Medical Microbiology, Immunology and Hygiene, Faculty of Medicine and University Hospital Cologne, University of Cologne, Cologne, Germany.

[6] German Center for Infection Research (DZIF), Partner site Bonn-Cologne, Cologne, Germany.

euskampus FUNDAZIOA